Inaugural dissertation

for

obtaining the doctoral degree

of the Combined Faculty of Mathematics, Engineering and Natural Sciences

of the

Ruprecht - Karls - University

Heidelberg

Presented by

M.Sc. Cornelia Sala

Born in Bremen, Germany

Oral examination: 2nd of April 2025

An interaction network of luminal centrosomal proteins organized by POC1A and POC1B ensures centriolar integrity

Referees: Prof. Dr. Elmar Schiebel

Prof. Dr. Sylvia Erhardt

Table of Content

Summary

The centrosome is a membrane-less organelle and in eukaryotes the main microtubule-organizing center (MTOC). Due to its ability to nucleate and organize microtubules (MT), it plays an important role in cell division, ciliogenesis, cell polarity and cell migration. Therefore, it is not surprising that disfunction of centrosomes has devastating consequences for an organism, leading to various diseases ranging from cancer and ciliopathies to mental and behavioural disorders. The centriole, as the basic structure of the centrosome, is crucial to ensure centrosomal function. Structural defects of centrioles have direct consequences on centrosome function. One factor contributing to the centriolar stability is the inner scaffold, a ring-like substructure in the lumen of the central-to-distal half of the centriole. Based on their localization, POC1B (proteome of centriole 1B), POC5, FAM161A and CCDC15 are suggested inner scaffold components, however, the relationship between these proteins and if other proteins are part of the inner scaffold is still unclear.

Here, I identified POC1A, the human paralogue of POC1B, as a novel inner scaffold component and investigated the function of the two human POC1 proteins within the inner scaffold. Both POC1 proteins are inner centriole proteins with overlapping localization. However, while POC1A resides closer towards the centriole lumen, POC1B is in proximity to the centriole wall. Loss of POC1A or POC1B affects the centriolar localization of inner scaffold components like POC5, FAM161A, Centrin and CCDC15. Based on the results presented in this study, POC1A-POC1B heterodimers organize the complex protein network of the inner scaffold by cross-linking different proteins. This is achieved by the ability to interact with various proteins through different interaction modes mediated by their N-terminal WD40 domain, C-terminal coiled-coil region, or both. Crucial for the inner scaffold is the interaction between POC1A and POC5, and the ability of POC5 to form a tetramer. POC1A-POC1B heterodimers interact with the MT-binding proteins FAM161A and MDM1, which may lead to a positioning of the POC5 tetramer close to the centriolar wall. Disruption of the inner scaffold leads to broken centrioles and mitotic defects, confirming the importance of the inner scaffold in maintaining centriole integrity. In addition, this study shows that combined loss of POC1A and POC1B results in complete disintegration of centrioles, highlighting their role in centriole biogenesis and stability.

Zusammenfassung

Das Zentrosom ist ein membranloses Zellorganell, das in eukaryotischen Zellen eine zentrale Rolle bei der Organisation des Zytoskeletts einnimmt, indem es Mikrotubuli nukleiert und organisiert. Es ist nicht nur wichtig für die Zellteilung und der Ziliogenese, sondern auch für Zellpolarität und Zellmigration. Aufgrund dieser vielseitigen Funktionen ist es daher nicht verwunderlich, dass ein zentrosomaler Defekt zu zahlreichen Krankheiten wie Krebs, Ziliopathien und psychischen Krankheiten führen kann. Die Zentriole, als Fundament des Zentrosoms, hat einen grundlegenden Einfluss auf das Zentrosom: strukturelle Defekte an Zentriolen wirken sich direkt auf die Funktion des Zentrosoms aus. Ein Faktor, der zur Stabilität von Zentriolen beiträgt, ist der „inner scaffold“, eine ring-artige Struktur im Lumen, die sich entlang der zentralen bis distalen Hälfte des Zentriols erstreckt. Basierend auf ihrer Lokalisation werden die Proteine POC1B (proteome of centriole 1B), POC5, FAM161A und CCDC15 als mögliche Komponenten des „inner scaffold“ in Betracht gezogen. Das Zusammenspiel zwischen diesen Proteinen und ob auch andere Proteine Teil des “inner scaffold” sind, ist jedoch noch unklar.

Im Rahmen dieser Studie, identifizierte ich POC1A, ein Paralog von POC1B in menschlichen Zellen, als neue Komponente des “inner scaffold” und untersuchte die Funktion der beiden menschlichen POC1-Proteine innerhalb dieser Struktur. Beide POC1-Proteine sind innere zentrioläre Proteine mit ähnlicher Lokalisation. Während POC1A jedoch näher zum zentriolären Lumen hin lokalisiert ist, befindet sich POC1B in der Nähe der Zentriolwand. Der Verlust von POC1A oder POC1B beeinträchtig die Lokalisation von POC5, FAM161A, Centrin und CCDC15 innerhalb der Zentriole. Ausgehend von den Daten in dieser Studie, organisieren POC1A-POC1B-Heterodimere das komplexe Proteinnetzwerk des „inner scaffold“, indem sie verschiedene Protein miteinander verknüpfen. Dabei interagieren die POC1 Proteine über unterschiedliche Interaktionsmodi, die deren N-terminale WD40-Domäne, die C-terminale Coiled-Coil, oder beide Regionen involviert, mit verschiedenen Proteinen. Sowohl die Interaktion zwischen POC1A und POC5 als auch die Fähigkeit von POC5 ein Tetramer zu bilden, spielen eine entscheidende Rolle für die Funktion des „inner scaffold“. POC1A-POC1B-Heterodimere interagieren mit den MT-bindenden Proteinen FAM161A und MDM1 und positionieren somit vermutlich das POC5-Tetramer nahe der Zentriolwand. Defekte im „inner scaffold“ führen zu strukturell beschädigten Zentriolen und Fehlern während der Mitose, was die große Bedeutung des „inner scaffold“ für die Aufrechterhaltung der Zentriolintegrität bestätigt. Darüber hinaus zeigt diese Studie, dass der kombinierte Verlust von

POC1A und POC1B zum vollständigen Zerfall von Zentriolen führt, was ihre Rolle bei der Biogenese und Stabilität der Zentriolen unterstreicht.

1. Introduction

1.1 The eukaryotic cell cycle

What do all living organisms have in common? It is the simple fact, that all living organisms, no matter how different they might be, are the result of cell division. In unicellular organisms it is the basis of reproduction, while in multicellular organisms it is fundamental for development and reproduction. The details of the cell division process differ from organism to organism. However, the basic principle remains the same: a cell duplicates its content to separate it to the two daughter cells, leading to identical genetical copies of the precursor which in turn repeat the process of duplication and division, hence the name cell cycle[1]. Two major events in the cell cycle are particularly important: the duplication of the genome that happens in the Synthesis-phase (S-phase); and the segregation of the duplicated genetical material to the two daughter cells (mitosis) and the ultimate cell division with cytokinesis (M-phase)[1,2]. The cell cycle of eukaryotic cells usually consists of two additional phases in between of S-phase and M-phase, called gap phases (G1 between mitosis and S-phase and G2 between S-phase and mitosis) that allow the cell to grow and monitor the internal and external environment (Fig. 1)[1,3]. G1, S and G2 phase are also summarized as interphase. The events in the cell cycle are tightly controlled by a cell-cycle control system which includes certain checkpoints to ensure that all environmental factors and conditions are suitable for entering the next phase[1,3]. The first checkpoint is in late G1, called restriction point, which controls entry into a new the cell cycle[1,3]. The second checkpoint is the G2/M transition in late G2, which triggers mitotic entry if certain conditions as successful DNA replication are met[1,3]. At the metaphase-to-anaphase transition in mitosis, the sister-chromatid separation is stimulated and monitored to trigger anaphase and to proceed to cytokinesis[1,3]. Problems or unfavourable conditions during all phases, result in an arrest at the transition points through the control systems. Absence of favourable factors in G1 can lead to quiescence of cells (G0-phase: a reversible resting point).

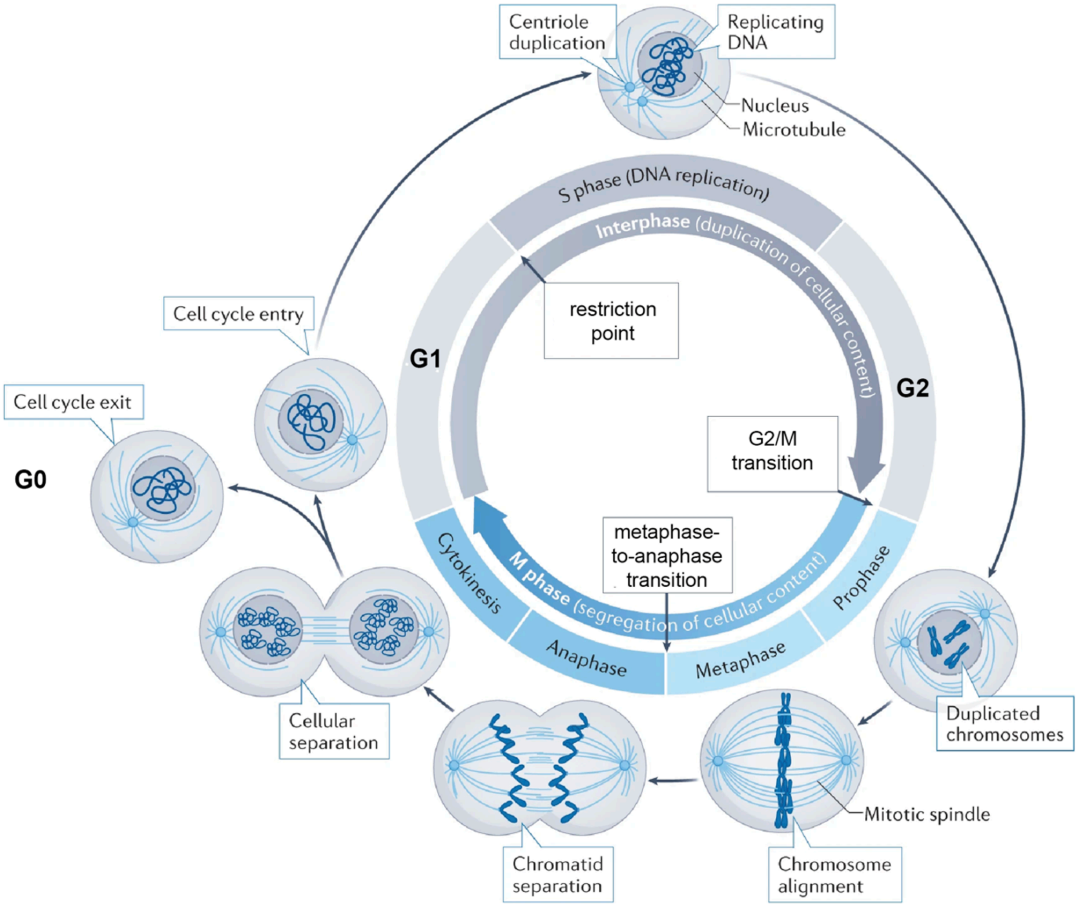

Figure 1: The eukaryotic cell cycle consists of interphase and mitosis
The cell cycle in eukaryotic cells consists of interphase (G1, S and G2) and mitosis (prophase, metaphase, anaphase and cytokinesis). In interphase, genetical and cellular contents are duplicated in preparation for mitosis, in which the chromosomes are segregated, and the cell ultimately divides. Before entering the next phase, the cell-cycle control system monitors at checkpoints if all conditions are suitable for proceeding to the next phase. *Figure modified from (Matthews et al., Nat Rev. Mol Cell Bio, 2022)*[3].

1.1.1 Regulation of the cell cycle

The eukaryotic cell cycle is regulated by a cell-cycle control system made of molecular "switches", monitoring the progression through the cycle[1]. Key components in this control system are members of a family of serine/threonine kinases, called cyclin-dependent kinases (Cdks) and proteins known as cyclins[3,4]. Cdks can only fulfil their kinase activity if bound to cyclins, and whereas Cdk levels usually are constant in the cell, the up- and downregulation of cyclin levels are critical for Cdk-activity[1,2]. In addition to Cdks and cyclins, three additional components help to tightly control the cell cycle: Cdk-activating kinases (CAK), Cdk-inhibitors (CIK) and ubiquitin-ligase complexes[1,5,6]. If a cyclin binds to a Cdk enzyme, the Cdk undergoes a conformational change, leading to a partial active state[1,4]. The fully active state is only achieved when an additional kinase, the CAK, phosphorylates the Cdk at its T loop (Thr 160), which allows access of the protein substrate to the active site of the Cdk[1,5]. Fine-tuning of the

activity of the cyclin-Cdk complex is mediated by a protein kinase, called Wee1 which inhibits Cdk activity[7], and the phosphatase Cdc25 that in turn increases the activity[8]. While activation of Cdks is achieved by CAKs, inhibition is mediated by the CKIs by binding to the cyclin-Cdk complex, leading to inactivation of the Cdk complex[1,5]. Phosphorylation and dephosphorylation are fundamental mechanisms driving the cell cycle control system. Additionally, regulated proteolysis, particularly during mitosis, plays a critical role in ensuring proper cell cycle progression. SKP-CUL1-F-box-protein (SCF) complex and the anaphase-promoting complex/cyclosome (APC/C), both members of the ubiquitin ligase family, are involved in protein degradation by catalysing the ubiquitination of target proteins[1,9]. These ubiquitin ligases function at distinct stages during the cell cycle: SCF ubiquitinylates mostly from late G1 to early M-phase cyclins and CKIs like p27, whereas APC/C ubiquitinates S- and M phase cyclins but acts also at the metaphase-anaphase transition by targeting securin[1,10]. Securin is important to keep sister-chromatid pairs together by blocking the protease separase and by targeting it for protein degradation in metaphase, the separation of chromosomes is triggered and thus the cell proceeds to anaphase[1,10]. The interplay between all these components is important for proper cell cycle progression. At the beginning of a new cell cycle, G1 cells contain low levels of cyclins, mainly through the activity of the APC/C and the proteasome at the end of the previous cell cycle[1,6]. In this stage, the cell either decides to enter a new cell cycle or to remain quiescent at the restriction checkpoint. Levels of G1 cyclins (cyclin D) and G1/S- cyclins (cyclin E) increase during this stage and bind to their Cdk partner to prime the cell for cell cycle entry[1]. Recent studies indicate that the binding of cyclin D to Cdk4/6 facilitates cell cycle entry by preventing the transition from the G1 phase to a quiescent state. In contrast, the binding of cyclin E to Cdk2 promotes the hyperphosphorylation of the retinoblastoma protein (Rb), driving cell cycle progression from G1 to S phase. Rb inhibits E2F-dependent transcription and by phosphorylation of Rb, E2F is released and starts the transcription of various genes, among them cyclin E which drives a positive feedback loop[3,11]. Commitment to enter S-phase and start the replication of DNA is stimulated by the increased levels of S-cyclins (cyclin E) which is the result of the previously increased E2F-dependent transcription and the inactivation of APC/C that primes cyclin A for protein degradation[3]. During S-phase, levels of G1/S-cyclins decrease, while S-cyclins maintain a constant elevated level until mitosis and can bind to Cdk2[1,3,12]

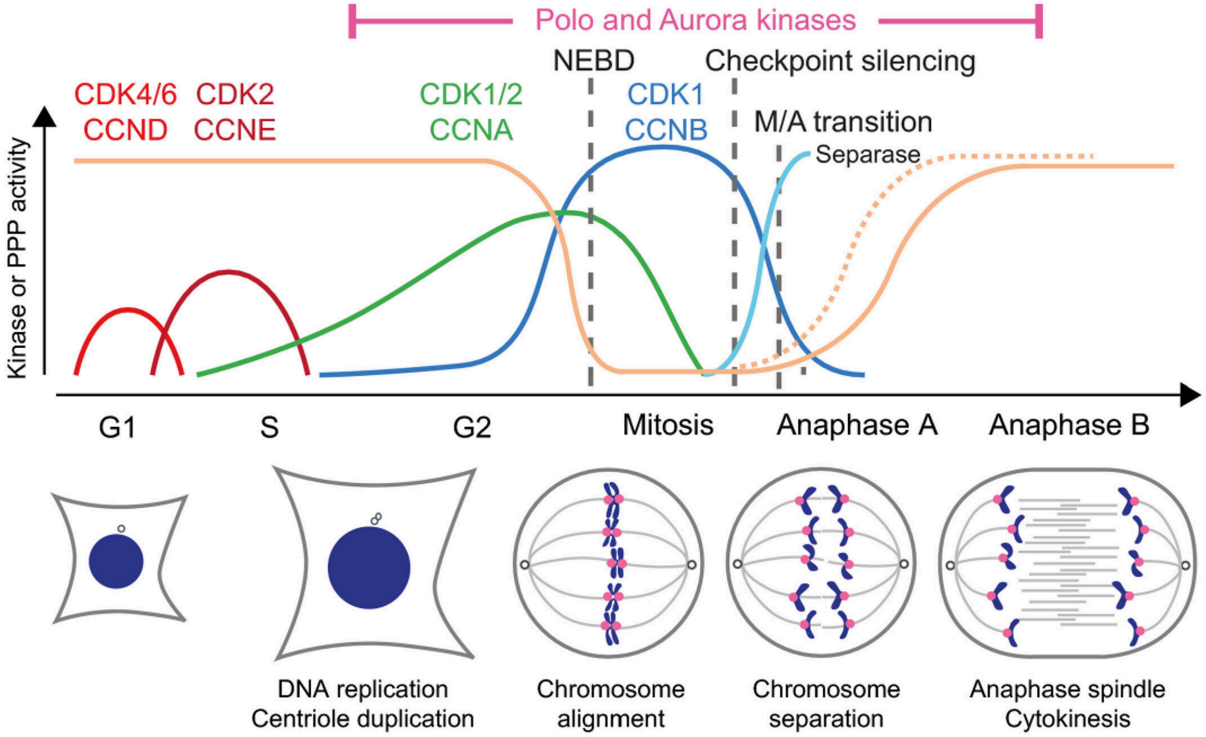

Figure 2: The Cell cycle is controlled by the interplay of cyclins and cyclin-dependent kinases (Cdks)
The formation of cyclin-Cdk complexes drives the progression though the cell cycle. Different classes of cyclins bind to different Cdks. Note that Cdk levels stay constant during the cell cycle, whereas cyclin levels fluctuate between the cell cycle phases. *Figure modified from (Holder et al., FEBS Letters, 2019)*[13].

1.1.2 The cell division

Following the events in S- and G2-phase, the cell prepares for the entry into mitosis. This is accompanied by an increase of M-cyclins (cyclin B) that bind to Cdk1, triggering the start of mitosis, the nuclear envelope breakdown (NEBD) and the proper positioning of the mitotic spindle[1,3,14]. In addition to Cdk1, other kinases as Aurora kinase-A and -B (Aurora A and Aurora B) and Polo-like kinase 1 (Plk1) are involved in the formation of the mitotic spindle and the attachment of the chromatids to the spindle[15–17]. The mitotic spindle plays an important role in mitosis, as it organizes the segregation of the chromosomes to the new daughter cells (Fig. 3). The centrepiece of this dynamic structure are the two centrosomes (see 1.2) that nucleate microtubules (MTs) from the poles of the spindle. The resulting MT array consists of different types of MTs such as kinetochore microtubules (K-MTs, connected to the kinetochores), non-kinetochore MTs (nK-MT) and astral MTs (A-MTs, connected to the cell cortex)[18], that help to position the spindle properly within the cell, as well as positioning the chromatids for the subsequent cell division. The spindle assembly checkpoint (SAC) serves as the final checkpoint in the cell cycle control system. It ensures that all chromosomes are correctly attached to spindle MTs via their kinetochores, providing sufficient time for proper alignment and thereby preventing aneuploidy [19]. Once all kinetochores are properly attached, the SAC activates the

ubiquitin ligase APC/C, leading not only to a degradation of cyclin B and therefore inactivation of Cdk1, but also to metaphase-to-anaphase transition by degrading securin, which in turn releases the enzyme separase that is involved in separating sister chromatids[1,10,19]. The mitotic spindle disassembles, and the cell progresses to cytokinesis, in which the cell division is complete, and the two daughter cells can start a new cell cycle.

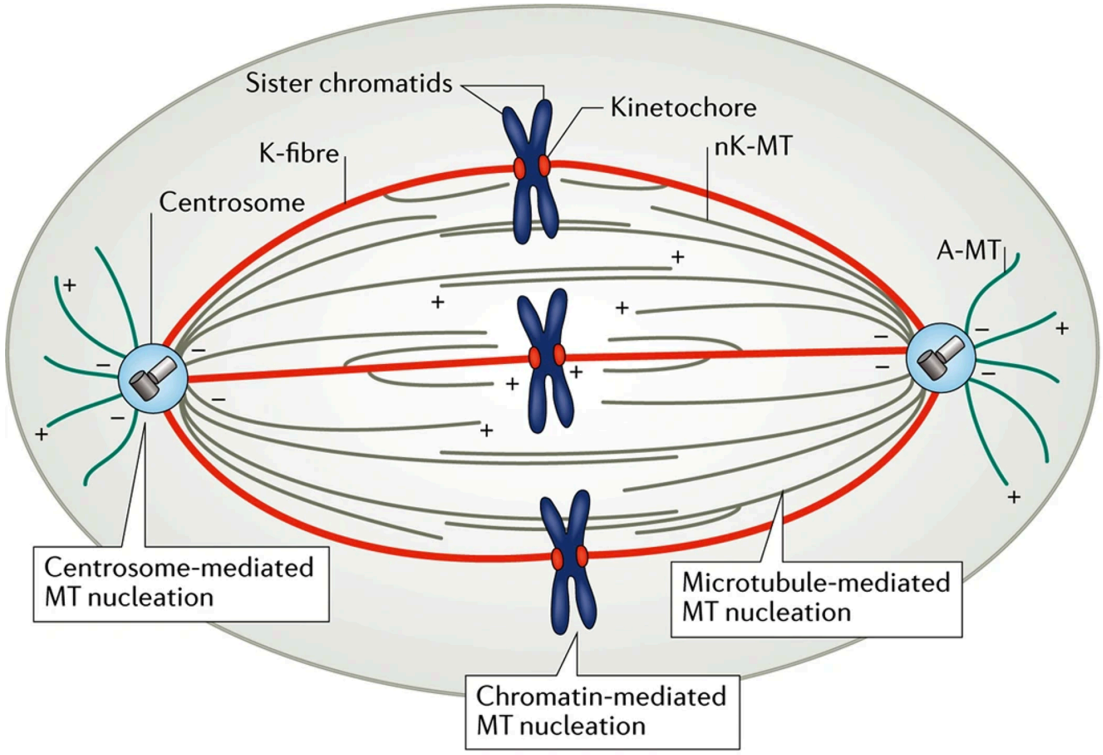

Figure 3: The mitotic spindle
The miotic spindle of mammalian cells as a cartoon, illustrating the different components and the different types of MTs. The two centrosomes at the poles of the mitotic spindle nucleate and organize the MTs. *Figure modified from (Prosser & Pelletier., Nat Rev., 2017)*[18].

1.2 The centrosome

MTs are key for a proper progression through mitosis and the segregation of the genetical content, but what are MTs and how do cells organize these dynamic structures? MTs are cylindrical structures, consisting of α- and β-tubulin that form 13 protofilaments[1,20,21]. Due to the parallel fashion of the protofilaments, MTs display a structural polarity, where one end contains α-tubulin as last subunit (minus end) and the other end β-tubulin (plus-end)[20,22,23]. MTs are highly dynamic, switching at the plus end between growing (by polymerisation of α/β-tubulin) and shrinking[20,24]. In eukaryotic cells, the centrosomes are the main MT-organizing centre (MTOC). These membrane-less organelles, consist of a MT-based cylindrical structure, called centriole, and the surrounding pericentriolar material (PCM)[25–29]. To achieve the MT-

organizing function, MT nucleating factors localize at the centrosome (especially in the PCM), such as protein complexes consisting of γ-tubulin and several other proteins[30–35]. In higher eukaryotes, these protein complexes form the γ-tubulin ring complex (γ-TuRC), which nucleates MTs and caps them at their minus end[20,36–38]. Therefore, centrosomes do not only organize MTs but ensure also MT polarity which is especially important for the mitotic spindle formation[24].

1.2.1 The centrosome cycle

Similar to the cell cycle, also centrosomes have their own cycle, that is in tune with the cell cycle (Fig. 4). Interphase cells contain two centrosomes that are tethered together via a filamentous network, called centrosome linker, and a network of MTs between them[39–42]. In G1, the two centrosomes consist of one centriole each that is surrounded by the PCM[42]. During the transition from G1 to S phase, PCM components like CEP57, CEP63, CEP192, CEP152 are recruited to the centriolar wall[43–45]. This promotes the recruitment of polo-like kinase 4 (PLK4), the master-regulator of centriole duplication, and STIL to a defined region at the proximal end of the centriole[45–51]. Once at the centriole, these proteins trigger the recruitment of other proteins such as SAS6, CEP135, CPAP and γ-TuRC[52–56]. This cascade of recruited proteins leads, like the duplication of DNA in the cell cycle, to the centriole duplication, in which a new centriole (called procentriole) is formed at the proximal region of the pre-existing older (or parental) centriole. The procentriole remains engaged to the parental centriole and continues to elongate during S and G2 phase by the recruitment of different proteins like CEP120, SPICE, Centrobin and POC5[53,54,57–59]. The procentriole, unlike its parental centriole, has not yet converted into a fully functional centrosome that can recruit PCM components and nucleate MTs, and acquires this ability only after entering the next cell cycle. The conversion into a functional centrosome is called centriole-to-centrosome conversion (CCC), a stepwise process that requires not only the recruitment of proteins like CEP295, CEP44 and PPP1R35 during S-phase but also modification and disengagement of the procentriole from its parental centriole through a Plk1-dependent pathway during mitosis[60–63]. This mechanism ensures that a centriole duplicates only once per cell cycle, preventing thereby mitotic defects by inhibiting the formation of more than two fully functional centrosomes[64,65]. In preparation for mitosis, the PCM increases, and the centrosome linker dissolves, resulting in a separation of the centrosomes and their movement to opposite poles in order to form the mitotic spindle[66–68]. With mitotic exit, the procentriole from the previous cell cycle, disengages from its parental centriole and acquires PCM and thus, the ability to nucleate MTs and function as a centrosome[60,69,70]. The centrosome linker is re-

established and the cell starts again the cell cycle with two centrosomes that consist one centriole each.

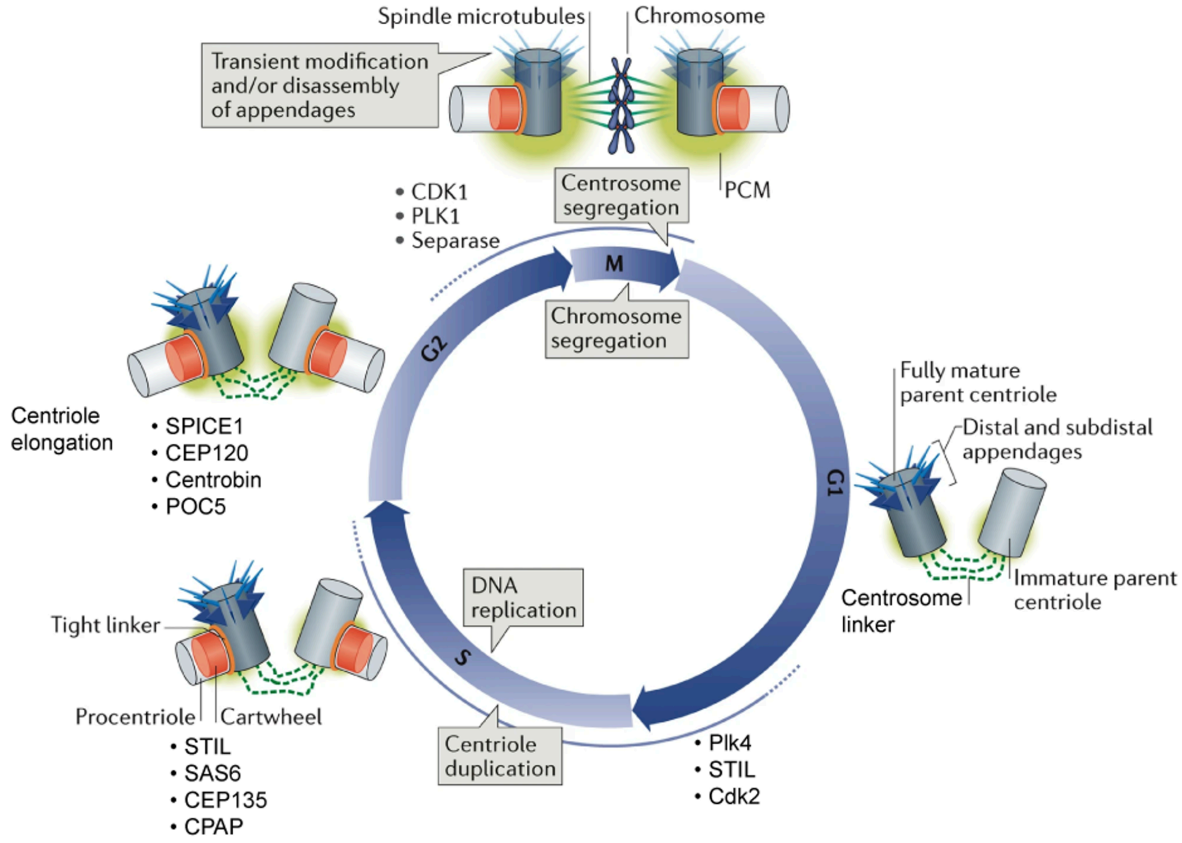

Figure 4: The centrosome cycle is in tune with the cell cycle
During the centrosome cycle, the centrosome duplicates, maturates and separates to start a new cell cycle with two centrosomes. Key proteins involved in these steps are depicted. *Figure modified from (Nigg & Holland., Nat Rev. Mol Cell Biol., 2018)*[65].

1.2.2 The human centriole architecture

The centriole, as the backbone of the centrosome, is a cylindrical structure consisting of nine MT-triplets with a canonical height and diameter in humans of 450-500 nm and 250 nm, respectively[71,72]. Each MT triplet is composed of three lateral connected microtubules called A-, B- and C-tubule. The A-tubule shows the characteristic closed microtubule ring structure composed of 13 protofilaments, whereas the B- and C-tubule are incomplete MTs with 10 protofilaments each[72–74]. For the development of the MT triplets, not only the α/β-tubulin subunits are important, but also two less-studied members of the tubulin superfamily: δ- and ε-tubulin[75,76]. Together with TEDC1 and TEDC2, δ- and ε-tubulin are critical for the formation of the MT triplets and therefore important for centriole biogenesis[77–79]. A striking feature of centrioles is their polarity: they can be divided in a proximal, a central and a distal part, with each region displaying different substructures and protein composition. The proximal region is defined by several substructures like the SAS-6 based cartwheel, pinhead and triplet base[80–82].

The cartwheel, which spans around 100 nm of the centriole lumen, has a nine-fold stacked organization and is based on nine SAS-6 homodimers that form a ring with radial spokes extending to the centriole wall[81,83–85]. Hereby, the pinhead is forming the connection between the radial spokes of the cartwheel and the A-tubule of the centriole wall. In addition, the presence of the A-C linker, that covers about 40% of the centriole, connects adjacent MT triplets via a link between the A- and C-tubule and marks the proximal centriole region[73,81,85]. Potential pinhead proteins are CEP135 and CPAP[86,87] and a recent study suggested CCDC77, MIIP and WDR67 as components of the A-C linker[88]. All these structures are assumed to be important to establish the nine-fold symmetry and to contribute to the stability of centrioles[73,83,88]. Along the longitudinal axis, the aforementioned proximal substructures are gradually lost and replaced by a new structure, called the inner scaffold, that defines the central part of centrioles. The inner scaffold is a stacked ring-like structure in the centriole lumen that extends to the distal part and is attached to the A-B junction of MT triplets[73,85,89]. Due to its high coverage along the centriole (nearly 70%), the inner scaffold is likely to contribute to centriole stability. Based on localization studies, POC1B, POC5, FAM161A (a MT-binding protein), Centrin-2 and CCDC15 have been described as potential inner scaffold components[85,90]. The bridging of the inner scaffold structure with the MT triplets at the A-B junction is assumed to be mediated by the MT-binding protein WDR90[91]. However, the detailed mechanism how these proteins build the inner scaffold structure and if other proteins are involved is still not understood.

At the very distal end of the centriole two structures appear, that not only mark the distal portion but also the maturity status of a centriole. The distal end shows electron-dense structures in the form of tilted blades, called distal appendages (DA), that are radially distributed around the centriole[92]. A recent study showed that the DA are attached to the MT wall and show the same nine-fold symmetry[92]. Identified proteins involved in the formation of DA are ANKRD26, C2CD3, CEP83 and CEP164[92,93]. Just beneath the DA, the subdistal appendages (SA) are localized and extend at 90° angles from the MT wall. In contrast to the DA, the subdistal appendages have a cone-like structure and do not display a nine-fold symmetry[94,95]. The protein composition of this structure includes proteins like ODF2, CEP128, centriolin, Ninein and CEP170[95,96]. The distal and subdistal appendages are only present in the older (matured)

centriole and important for ciliogenesis and the anchoring and organization of MTs[95].

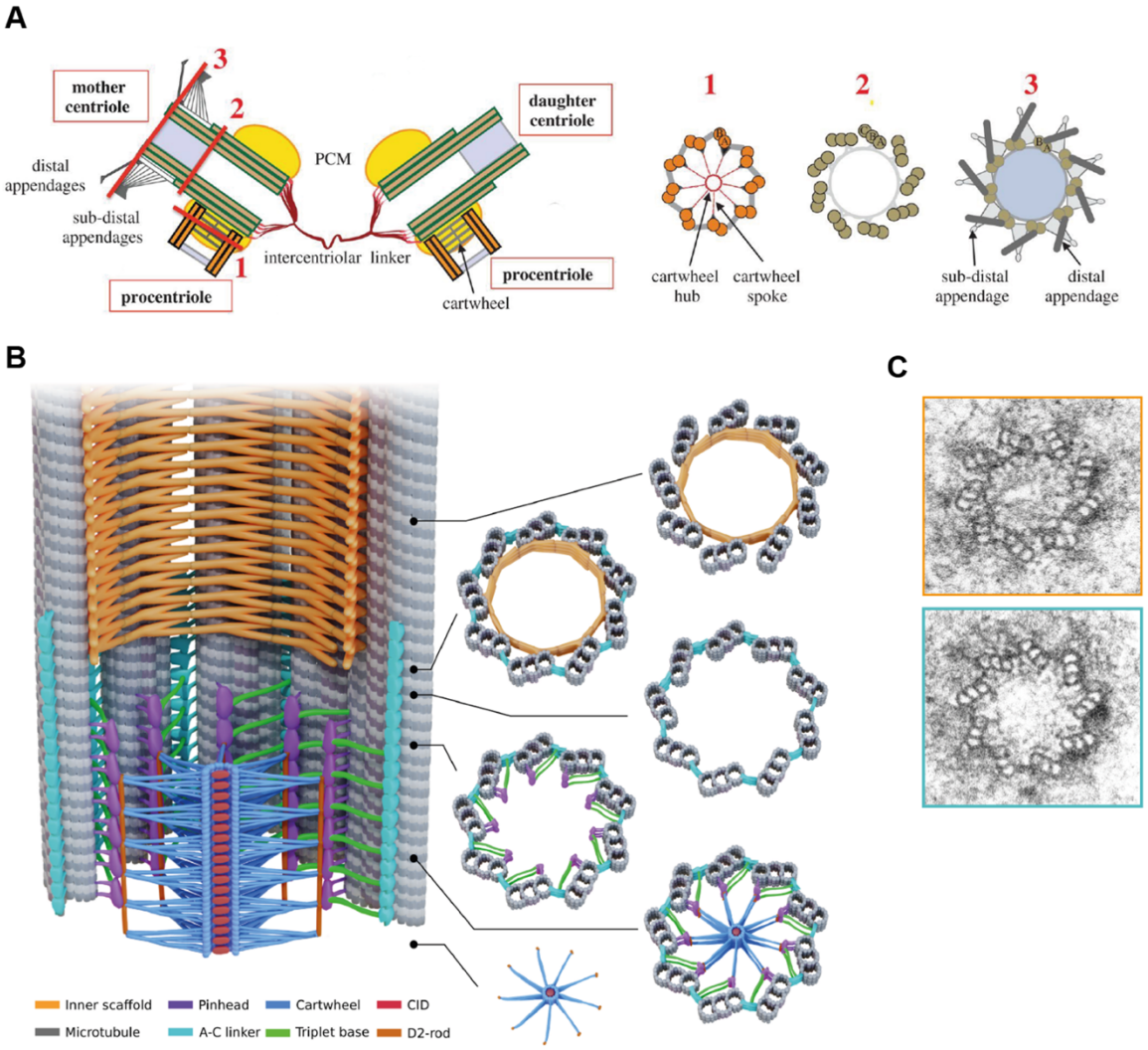

Figure 5: Architecture of human centrioles
(**A**) Cartoon of centrosomes of a S-phase cell. Each centrosome consists of one parental centriole at which at the proximal end the procentriole forms. Only the older centriole (here mother centriole) shows the DA and SDA and is primed to form a cilium. Both centrosomes are connected via the centrosome linker. The red numbers show cross section views. (**B**) Detailed view of the centriolar substructures. At the proximal part the cartwheel, pinhead and A-C linker are present. The inner scaffold (orange) marks the central part of a centriole. (**C**) Electron microscopy images of cross-section centrioles showing the A-C linker (turquoise) and the inner scaffold (orange). *Figure modified from (**A**) (Bornens & Gönczy, 2014, Phil. Trans. Royal Soc. Lond B Biol Sci [97]), (**B**) (Klena et al., 2020, EMBO J [81]), (**C**) Image generated in this study.*

1.2.3 The inner scaffold

Adjacent MT triplets in the central and distal region of centrioles are connected through a circular structure in the lumen, called the inner scaffold. This structure has been observed among different organisms, including mammals, *Paramecium*, *Tetrahymena* and *Chlamydomonas*[85,98–100]. In humans, the inner scaffold covers up to 85% of the centriole length and Cryo-ET analysis of centrioles from *Paramecium* and *Chlamydomonas* revealed a dense helical lattice structure for the inner scaffold[85]. Despite some differences, the inner scaffold is conserved between species with the stem as the link between the MT triplets and the inner scaffold (Fig. 6).

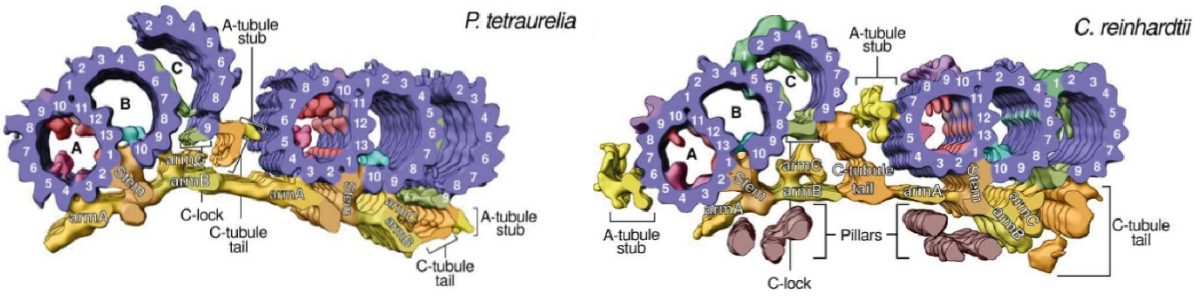

Figure 6: Comparison of the inner scaffold from *Paramecium* and *Chlamydomonas*
Subtomogram averaging from top view centrioles of *Paracemium tetraurelia* and *Chlamydomonas reinhardtii* showing the reconstructed inner scaffold. MT triplets are connected via the stem with the inner scaffold. Between the species, differences how the inner scaffold is built in detail can be observed. *Figure modified from (LeGuennec, 2020, Science Advances[85]).*

An important role for centriole stability has been suggested for the inner scaffold as it can adapt its shape under external forces to maintain the connection of the MT triplets[85]. Localization studies propose the centriolar proteins POC1B (proteome of centriole 1B), POC5, FAM161A, Centrin-2 and CCDC15 as components for the inner scaffold[85,90]. WDR90 is suggested to function as a junction protein between A-B tubules in the stem region to connect the inner scaffold with the MT triplets[91]. All these proteins localize at the central region of the centriole and have been shown to be involved in centriole biogenesis. POC5 is a conserved protein with Centrin-binding regions and is essential for the assembly of the distal half of centrioles: loss of POC5 results in short centrioles[59]. FAM161A, a MT-binding protein and discovered as a cause of a recessive from of retinitis pigmentosa, shares the evolutionary conserved domain UPF0564 with unknown function[101,102]. Due to its MT-binding property, FAM161A may be involved in connecting the inner scaffold with the MT triplets. POC1B is stably incorporated into centrioles where it interacts with the proximal centriole protein CEP44 and loss of it is associated with ciliary defects[63,103,104]. Interestingly, vertebrates have in addition a paralog form of POC1B, called POC1A. siRNA depletion experiments show mild effects when depleting only one of the *POC1* genes, while co-depleting *POC1A* and *POC1B* results in a severe phenotype with

defective mitotic spindle formation[104]. This indicates that both proteins play an important role in centriole biogenesis and a functional overlap between these proteins. However, the exact differentiation between the paralogues remains unclear and a role of POC1A in the context of the inner scaffold has not been described.

1.2.4 Centrosome-associated diseases

Centrosomes, as the main MT-organizing centre of eukaryotic cells, are important for diverse processes in the cell like cell polarity and migration as well as cell adhesion and the formation of the spindle during mitosis[105–107]. Beyond their MT-dependent functions, centrosomes play a crucial role in environmental sensing and actively participate in signalling pathways through the formation of cilia[108,109]. Given the diverse functions of centrosomes, it is not surprising that malfunction of these organelles is associated with various diseases, mainly tumorigenesis, ciliopathies and autosomal recessive primary microcephaly (MCPH)[65,110,111]. Although cells can still divide in the absence of centrosomes, the presence of a centrosome ensures efficient and proper formation and timing of the mitotic spindle[112,113]. Improper spindle formation, and thus mis-segregation of chromosomes by the loss of centrosomal function, leads to prolonged mitosis and ultimately either to cell cycle arrest or apoptosis via the USP28-53BP1-p53-p21 pathway (Fig. 7A, B)[114–116]. Disrupting this pathway, such as through the loss of the tumor suppressor gene *TP53*, allows cells that have lost centrosomes to evade cell cycle arrest and apoptosis. These cells form centrioles through a *de novo* formation or assemble acentrosomal bipolar spindles[114,117]. *De novo* formed centrioles lack tight regulation and are formed without a pre-existing parental centriole, resulting in over-amplification of centrosomes that is a hallmark of cancer[118,119]. In addition to the *de novo* formation, defects during centriole duplication as well as precocious centriole disengagement during G2 phase can lead to supernumerary centrosomes[120,121]. Although not always the primary cause of cancer, overamplified centrosomes can enhance the progression, due to mis-segregation of chromosomes that can in turn either lead to the loss of tumor suppressors or the accumulation of oncogenes[122,123]. Additionally, overamplified centrosomes play a role in metastasis through increased MT nucleation, increasing thereby the activity of the GTPase Rac1 that leads to cell invasion (Fig. 7C)[124,125].

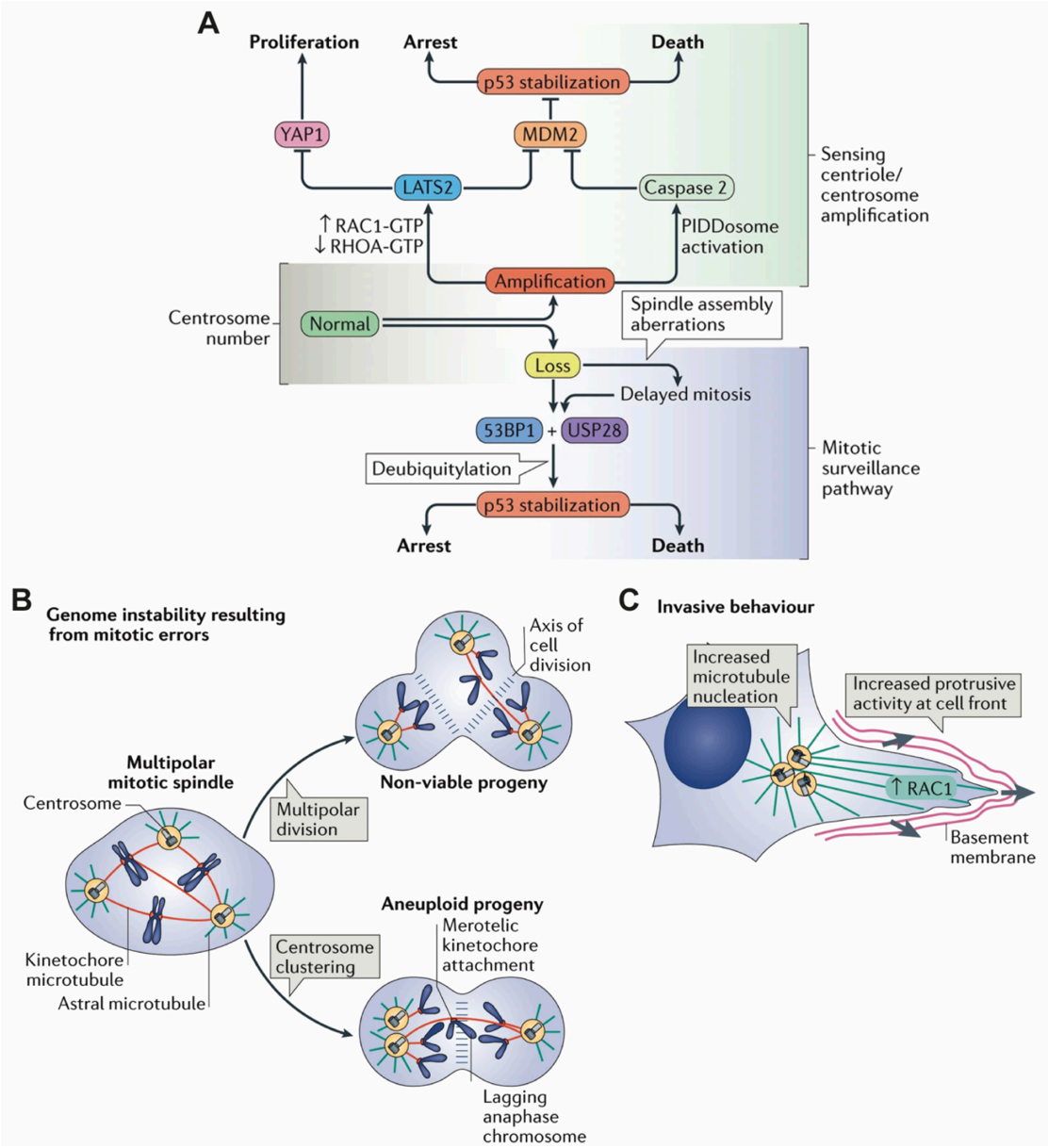

Figure 7: Overamplified centrosomes and cancer
(**A**) Loss or overamplification of centrosomes activate different pathways leading to cell cycle arrest or apoptosis. (**B-C**) Aberrant number of centrosomes affect MT-nucleation activity, thus contributing to mitotic defects cell invasion observed in metastasis. *Figure modified from (Nigg & Holland., Nat Rev. Mol Cell Biol., 2018)*[65].

Not only the number of centrosomes is critical for the centrosome function, but also the overall architecture of the centriole. Mutations in genes encoding for proteins that are considered as inner scaffold components, are related to retinal dystrophies and adolescent idiopathic scoliosis (AIS)[101,126–131]. A mouse study revealed that the inner scaffold is important for the connecting cilium in the photoreceptor cells, explaining why mutations in POC1B, FAM161A or POC5 may cause retinal dystrophies[132].

2. Aim of the study

Centrosomes play a vital role not only in the MT-organization and cell division but also in the formation of cilia and flagella, cell polarity and cell migration. Centrosomal defects are associated with various disease, including cancer, ciliopathies and mental disorders. Centrosomes consist of a MT-based cylindrical structure, called centriole, and the pericentriolar material (PCM), surrounding it. The centriole´s integrity is key for fulfilling the centrosome function. Within the lumen of the centriole, a ring-like substructure called inner scaffold is suggested to contribute to centriole stability.

The aim of this study was the analysis of proteins in the context of centriolar stability with a focus on the inner scaffold. To achieve this, I generated CRISPR/Cas9 knockout cell lines of *POC1A*, *POC1B* and *POC5* and characterized them. Localization studies using ultrastructure Expansion Microscopy (u-ExM) were utilised to map inner centriolar proteins and to analyze a potential mislocalization of these proteins in the respective knockout cell lines and the resulting effect on centriole integrity. Furthermore, the relationship between inner scaffold proteins was investigated in more detail via a combinatorial approach using AlphaFold predictions and co-immunoprecipitation experiments.

3. Results

Parts of the results shown in this thesis were published in Sala et *al*., 2024[133].

Generation and verification of knockout cell lines were performed by Dr. Enrico Salvatore Atorino and me. Protein purification of insect cells was done with the help of Dr. Martin Würtz and the corresponding data acquisition and data analysis were performed by Dr. Martin Würtz and Dr. Annett Neuner. Electron Microscopy was done by Dr. Annett Neuner. AlphaFold-Multimer predictions were performed in collaboration with Dr. Sebastian Eustermann and Dr. Thomas Hoffmann from the European Molecular Biology Laboratory (EMBL). Mass photometry analysis was performed by Dr. Karin Lapouge from EMBL. If not stated differently, I performed all the cell biology experiments and analysis.

3.1 POC1A and POC1B – two different genes, but similar proteins

Several studies identified the basal body- associated protein POC1 (proteome of centriole 1) that is conserved among different species[134–139]. Interestingly, the POC1 protein underwent a gene duplication event in the vertebrate subphylum, leading to two paralogue forms, POC1A and POC1B that are encoded by two different genes[137]. Both paralogues share a similar domain architecture with a seven blade WD40 motif at the N-terminus and a coiled-coil at the C-terminus (Fig. 8A). AlphaFold2 predictions reveal that the WD40 domain as well as the coiled-coil of both proteins is highly ordered, whereas the flexible linker connecting the two domains shows a disordered structure (Fig. 8B). Although both POC1 proteins display a similar domain architecture, there are differences, especially in the linker region, with POC1B´s linker region being longer compared to POC1A´s (Fig. 8A, B). Furthermore, the linker region of POC1B is predicted to have a small, ordered region that forms a beta strand, hereafter called ‘intra’ (Fig. 8B). Conserved residues between POC1A and POC1B are predominantly found in the WD40 domain and the coiled-coil, however, noticeable differences are found in blade 1, 2 and 4 of the WD40 domain as well as in the linker region (Fig. 8C).

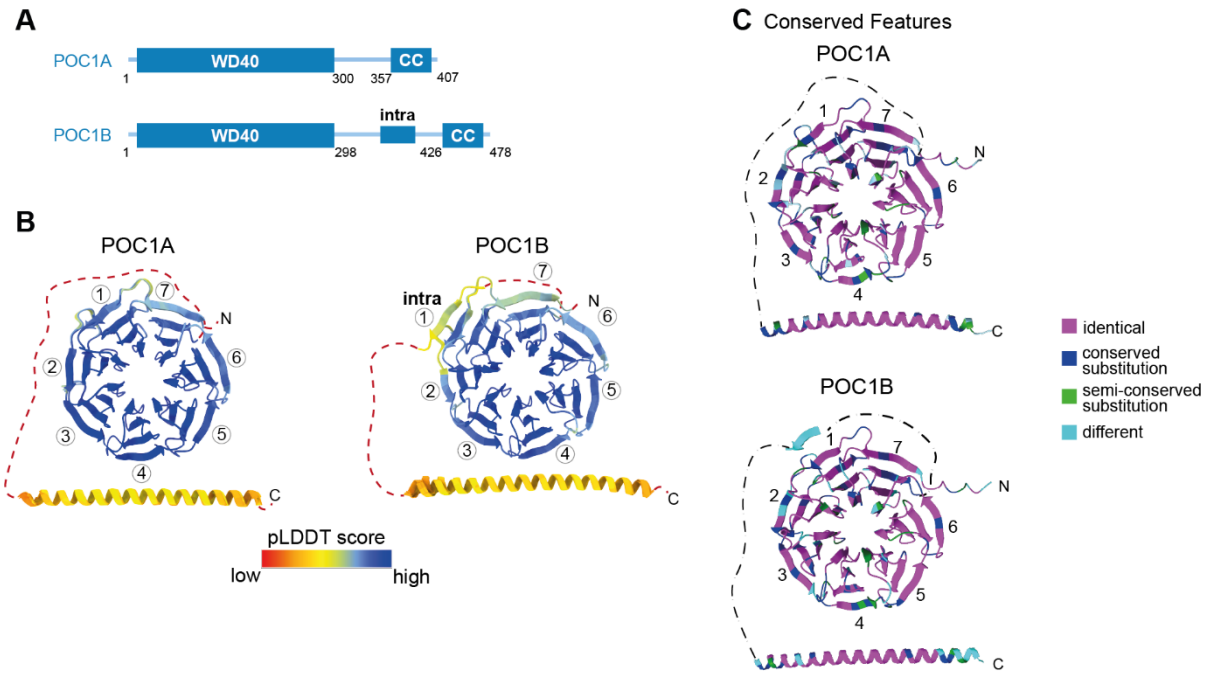

Figure 8: Human POC1A and POC1B display similar domain architecture
(A) Domain architecture of POC1A and POC1B with the WD40 domain at the N-terminus and the coiled-coil (CC) at the C-terminus. (**B**) Ensembles of the 10 best ranked AlphaFold2 predictions. The numbers indicate the blades of the WD40 domain. Colouring based on pLDDT score showing low and high confidence regions. The linker region (dotted line) connecting the WD40 domain and CC has a lower confidence level. (**C**) Representation of the predicted POC1A and POC1B structures showing conserved features in the WD40 domain and CC. *Figure modified and adapted from* (Sala et al., *Nat Comm* 2024)[133].

Studies with the protist *Tetrahymena* indicate POC1 functions as a junction protein that links the B- to A- and C- to B- tubules, thereby playing an important role in centriolar integrity[103,134,140–142]. For the human paralogues POC1A and POC1B, however, the function of these proteins remains unclear, although functional overlaps have been observed. Remarkable, mutations in the *POC1A* and *POC1B* gene give rise to distinct diseases such as SOFT (short stature, onchyodysplasia, facial dysmorphism, and hypotrichosis) syndrome, which is specific for *POC1A*, and autosomal-recessive cone-rod dystrophy in the case of *POC1B*, and are mainly affecting the WD40 domain (Fig. 9)[143–155] . The specific clinical phenotypes indicate separate functions (under certain conditions) for POC1A and POC1B.

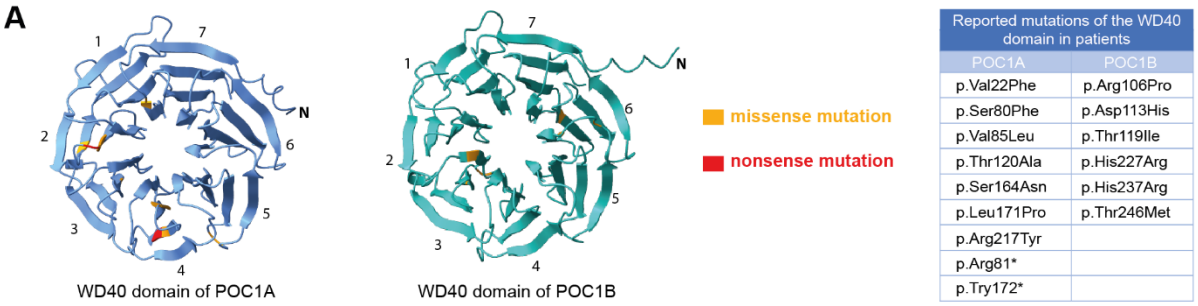

Reported mutations of the WD40 domain in patients	
POC1A	POC1B
p.Val22Phe	p.Arg106Pro
p.Ser80Phe	p.Asp113His
p.Val85Leu	p.Thr119Ile
p.Thr120Ala	p.His227Arg
p.Ser164Asn	p.His237Arg
p.Leu171Pro	p.Thr246Met
p.Arg217Tyr	
p.Arg81*	
p.Try172*	

Figure 9: Mutations in POC1A and POC1B associated with diseases and found in patients
(**A**) Mutations found in patients are frequently located in the WD40 domain coding region of *POC1A* and *POC1B*. Orange indicates missense mutations and red nonsense mutations. In the table the mutations are listed in detail. Figure modified and adapted from (Sala et al., *Nat Comm* 2024)[133].

3.2 POC1A and POC1B are luminal centriolar proteins

In order to gain a deeper understanding, I analyzed the centriolar localization and the time of recruitment of POC1A and POC1B via ultrastructure Expansion Microscopy (u-ExM). Immortalized human retinal epithelial hTERT (RPE1-hTERT; expressing human telomerase reverse transcriptase) cells were stained with antibodies against the respective proteins (Fig. 10A) and α-tubulin (marker for the centriolar wall). Both proteins localized in the lumen of the centrioles and are recruited early in S-phase to procentrioles, suggesting that these proteins are centriolar proteins rather than PCM components (Fig. 10B). Although the proteins overlapped in terms of localization within the centriolar lumen, measuring in depth the length of the respective signals revealed that POC1B extends further to the proximal end of the centriole, covering 76% of a centriole´s length, whereas POC1A showed a more central localization (Fig. 10C, D). The differences in length distribution prompted me to analyze if the diameter of these proteins (or the distance to the centriolar wall) shows differences as well. For this, I analyzed the diameter via u-ExM and focused on top view centrioles stained against the respective antibodies (Fig. 10E). In comparison to POC1A, POC1B showed a larger diameter, suggesting that POC1B is closer to the centriolar wall than POC1A (Fig. 10F). Due to the localization in the central region and the proposed function of POC1B as an inner scaffold component, I mapped the localization of the POC1 proteins in relation to other suggested inner scaffold components like POC5, FAM161A and CCDC15 as well as their distances to the centriolar wall (Fig. 10G-I). MDM1 and CEP44 were included in this analysis, because both proteins have a MT-binding domain and MDM1 localizes along the entire centriole. Furthermore, the proximal end protein CEP44 has been shown to interact with POC1B[63]. The analysis showed a similar localization towards the centriolar lumen for POC1A and POC5, whereas POC1B and CCDC15 extended towards the centriolar wall (Fig. 10I). FAM161A, MDM1 and CEP44 were,

compared to the other proteins, the closest to the centriolar wall, that is in concordance with these proteins having a MT-binding domain. To summarize, POC1A and POC1B are inner luminal centriole proteins that share similar localization with the suggested inner scaffold components POC5, FAM161A and CCDC15 (Fig. 10J).

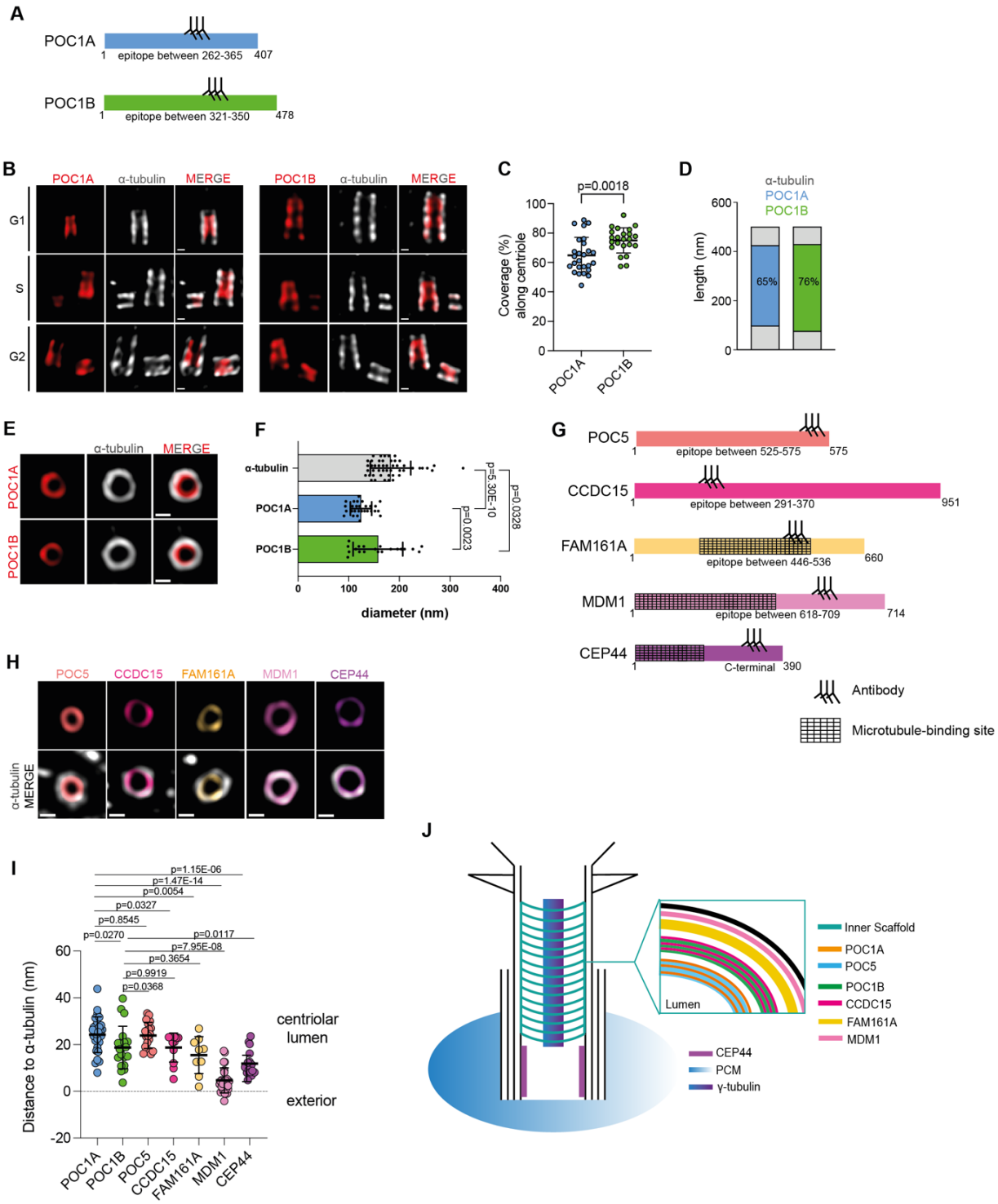

Figure 10: POC1A and POC1B localize in the inner centriolar lumen
(**A**) Region of the epitopes recognized by the antibodies against POC1A and POC1B. The antibodies target the middle/C-terminal part of the proteins. (**B**) U-ExM images of centrioles from cells in different cell phases. Cells were stained against POC1A or POC1B (red) and α-tubulin (grey). Scale bar: 100 nm. (**C**) Coverage of POC1A

and POC1B along the centriole. Analysis derives from cells shown in (**B**). *n*= > 20 centrioles. (**D**) Schematic representation of the centriolar distribution of POC1A and POC1B normalized to a centriole with a length of 500 nm. (**E**) U-ExM of top view centrioles stained against POC1A and POC1B. Scale bar: 100 nm. (**F**) Quantification of the diameter from cells shown in (**E**). *n*= > 20 centrioles. (**G**) Region of the epitopes recognized by the antibodies used in this study against the respective proteins. (**H**) U-ExM of top view centrioles stained against the indicated proteins. Scale bar: 100 nm. (**I**) Quantification of the distance of the respective proteins towards the microtubule wall marked by the α-tubulin signal from cells shown in (**E**, **H**). *n*= > 20 centrioles for control, POC1A, POC1B, POC5 and MDM1. *n*= 12 centrioles (CCDC15), 10 centrioles (FAM161A), 16 centrioles (CEP44). (**J**) Centriolar localization of the inner scaffold proteins depicted in a schematic representation. (**C**, **F**, **I**) Data are presented as mean ± SD. All statistics were derived from two-tail unpaired t-test. *Figure modified and adapted from* (Sala et al., *Nat Comm* 2024)[133].

3.3 Centriolar localization of POC1A and POC1B depends on the full-length protein

POC1A and POC1B share similar protein domains like the N-terminal WD40 and the C-terminal coiled-coil. To identify which part of the proteins is required for centriolar localization, I generated stable RPE1 cell lines expressing different doxycycline (dox) inducible HA-tagged constructs of *POC1A* and *POC1B* subdomains and checked their ability to localize at centrosomes via conventional immunofluorescence (IF) (Fig. 11A, B). In addition to cell lines expressing only the WD40 domain or the C-terminal half of the POC1 proteins, I generated also cell lines that expressed chimeric versions in which the WD40 domain of one POC1 protein is fused with the C-terminal half of its counterpart (hereafter, POC1Ab or POC1Ba). Upon dox-induction, full-length POC1A-HA and full-length POC1B-HA localized at centrosomes as can be assessed by the co-localization with the centrosomal marker γ-tubulin (Fig. 11B). In contrast, the WD40 domains (WD40A and WD40B) as well as the C-terminal half of POC1A and POC1B (C-POC1A and C-POC1B) failed to show a specific centrosomal localization and showed only a diffuse cytoplasmic signal, suggesting that the full-length proteins are required for efficient centrosomal localization. Interestingly, the chimeric versions POC1Ab-HA and POC1Ba-HA localized to the centrosomes, indicating that the POC1 subdomains are interchangeable and that the chimeric proteins may fulfil similar functions as the wild type (WT) proteins.

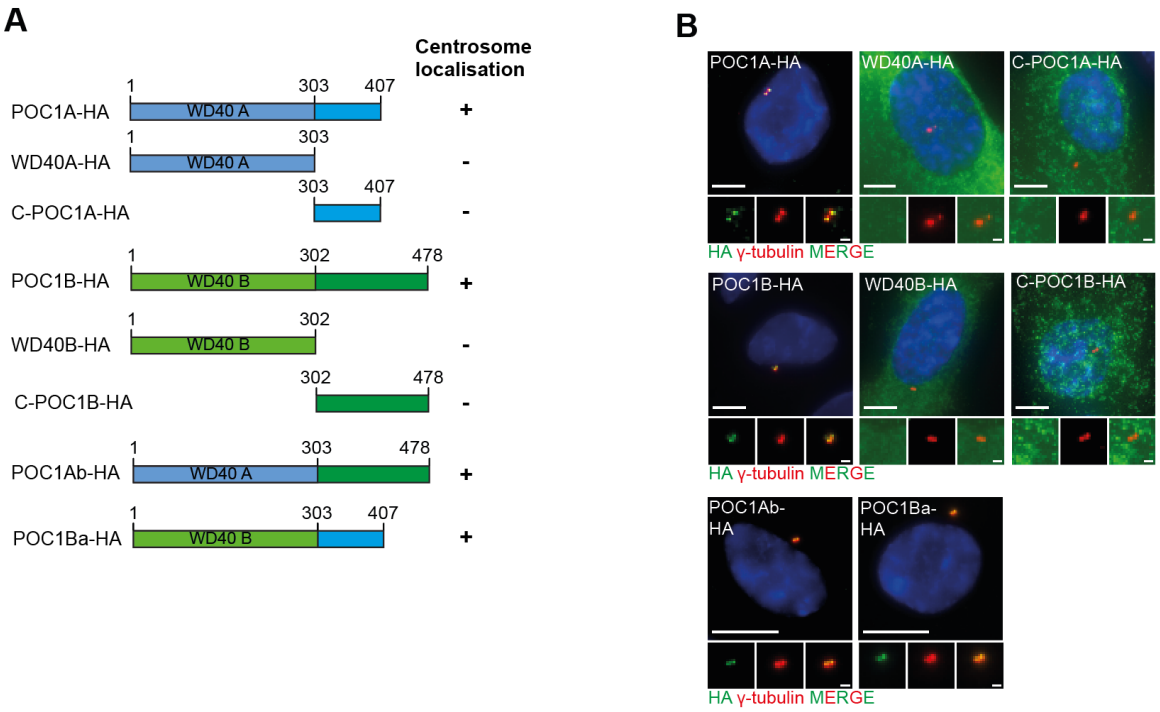

Figure 11: Centriolar localization of POC1 proteins requires the WD40 domain and the coiled-coil region (**A**) Doxycycline (dox)-inducible HA-tagged constructs of POC1A and POC1B tested for their ability to localize at centrosomes. (**B**) Representative IF images of control cells expressing the constructs shown in (**A**). Cells were stained against HA (green) and the centrosomal marker γ-tubulin (red). Scale bars: 5 µm, magnification scale bars: 1 µm. N=3 biologically independent experiments. Data are presented as mean ± SD. Statistics were derived from two-tail unpaired t-test. *Figure modified and adapted from* (Sala et al., *Nat Comm* 2024)[133].

3.4 Generation of *POC1A*$^{-/-}$ and *POC1B*$^{-/-}$ cell lines via CRISPR/Cas9

The next step after determining the localization of POC1A and POC1B, was to identify the function of these proteins. For this, Dr. Atorino generated with CRISPR/Cas9 RPE1 *POC1A*$^{-/-}$ and *POC1B*$^{-/-}$ cell lines using a dual single guide RNA (sgRNA) strategy. The sgRNAs were designed to target exon 2 and exon 7 in the case of POC1A, and intron 4 and exon 10 for POC1B to induce a large deletion (Fig. 12A, C). *TP53* deficient cells are able to proliferate even when centrioles are defective[156,157]. Due to a study showing cell proliferation defects upon *POC1B* depletion[104], the knockout cell lines were generated in a *TP53*$^{-/-}$ background. The knockout cell lines were confirmed initially via genomic sequencing (Fig. 12B, D). To further confirm on protein level if the knockout was successful and to test if the centriolar recruitment of the POC1 proteins depends on each other, I stained control (RPE1 *TP53*$^{-/-}$), *POC1A*$^{-/-}$ and *POC1B*$^{-/-}$ cell lines against POC1A and POC1B and tested for co-localization with γ-tubulin (Fig. 12E). IF, and additionally immunoblot (IB) analysis of whole cell extracts, confirmed the successful knockouts and revealed that the centriolar recruitment of POC1A and POC1B is independent from each other (Fig. 12F-I).

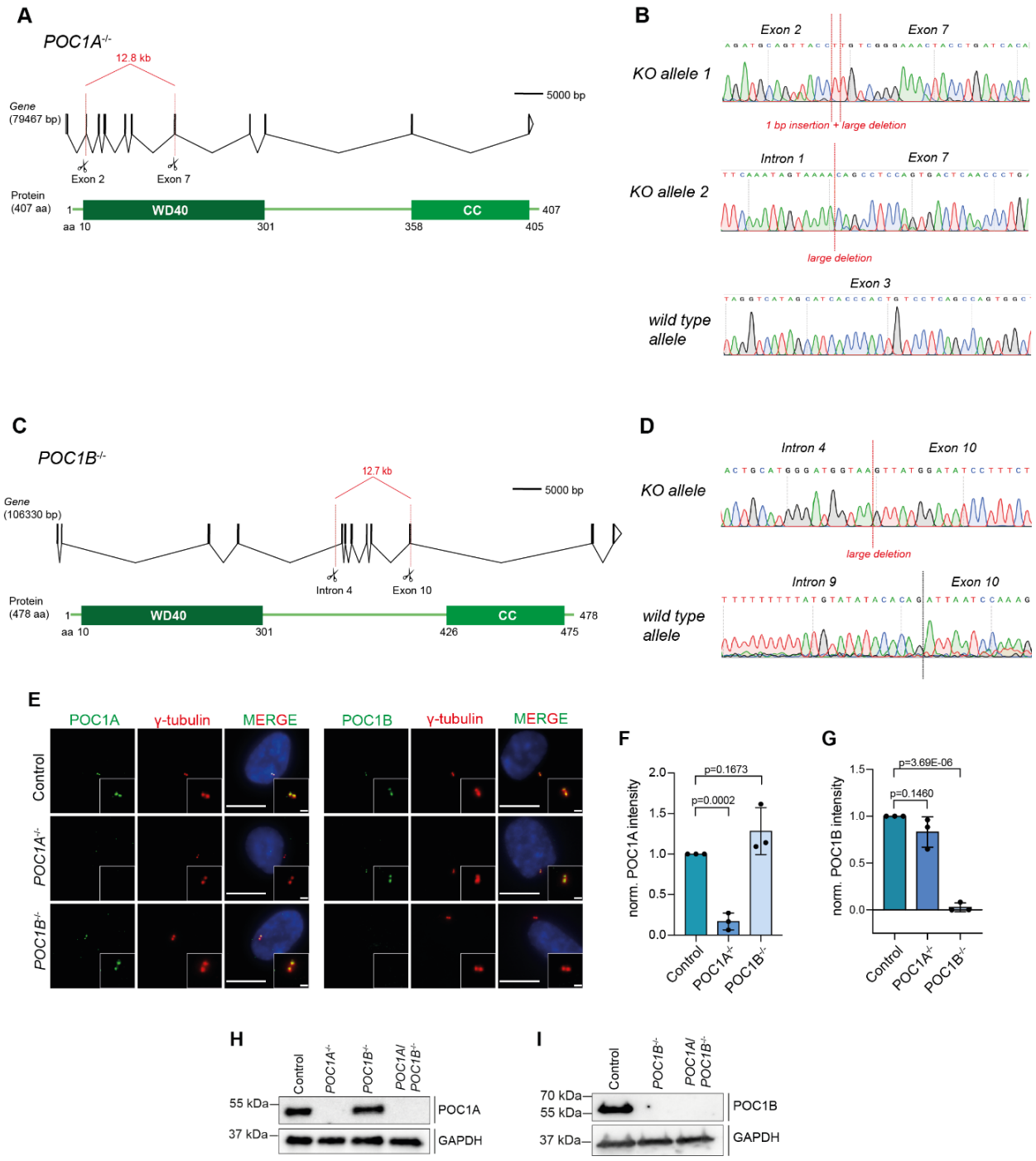

Figure 12: CRISPR/Cas9 generated *POC1* knockout cell lines using the CRISPR/Cas9 dual sgRNA strategy (**A**) Schematic representation of the *POC1A* WT gene and the protein domain architecture. sgRNAs used in this study to generate the knockout target exon 2 and exon 7. (**B**) Chromatograms of the sequenced knockout clone showing an insertion of 1 bp and a large deletion in allele 1 and a large deletion in allele 2. In comparison, in a WT allele with no deletion, exon 3 is following exon 2 and can be sequenced. (**C**) Schematic representation of the *POC1B* WT gene and the protein domain architecture. sgRNAs used in this study to generate the knockout target intron 4 and exon 10. (**D**) Chromatograms of the sequenced knockout clone showing a homozygous genotype with both alleles showing the same large deletion, after which the sequence of exon 10 follows the sequence of intron 4. In comparison, in a WT allele with no deletion, exon 10 is following intron 9. (**E**) Representative IF images of stained *POC1A*$^{-/-}$ and *POC1B*$^{-/-}$ cell lines using antibodies against POC1A or POC1B (green) and γ-tubulin (red). Scale bars: 10 µm, magnification scale bars: 1 µm. (**F**, **G**) Signal intensity measurements of the cells shown in (**E**) to verify the knockout cell lines. Data are presented as mean ± SD. Statistics were derived from two-tail unpaired t-test analysis of N= 3 biologically independent experiments, $n > 150$ cells per cell line for each experiment. (**H**, **I**) Immunoblots of whole cell lysates from knockout and control cell lines. Additionally, a *POC1A/B*$^{-/-}$ double

knockout cell line was included. GAPDH was used as a loading control. *Figure modified and adapted from* (Sala et al., *Nat Comm* 2024)[133].

3.5 Loss of POC1A and POC1B affect the distribution of inner scaffold proteins within the centriole

The functional differences between POC1A and POC1B, if any, are poorly understood. Thus, in order to gain an in-depth understanding and due to the localization of these proteins, the confirmed *POC1A*$^{-/-}$ and *POC1B*$^{-/-}$ cell lines were analyzed for the inner scaffold components POC5, FAM161A and CCDC15 via IF (Fig. 13A). MDM1 was included in this analysis, because preliminary experiments showed a luminal localization along the entire centriolar wall. In the absence of POC1A, POC5 exhibit a drastic reduction of the signal intensity of nearly 80% compared to control cells (Fig. 13A, B). A signal intensity reduction at centrosomes in *POC1A*$^{-/-}$ cells was observed as well for FAM161A (~50% reduction), MDM1 (70%) and CCDC15 (60%) as seen in Fig. 13C-E. Contrary to *POC1A*$^{-/-}$ cells, the absence of POC1B shows no effect on POC5 and FAM161A recruitment to centrioles (Fig. 13A-C). However, MDM1 and CCDC15 are significantly reduced at the centrosomes (Fig. 13D, E).

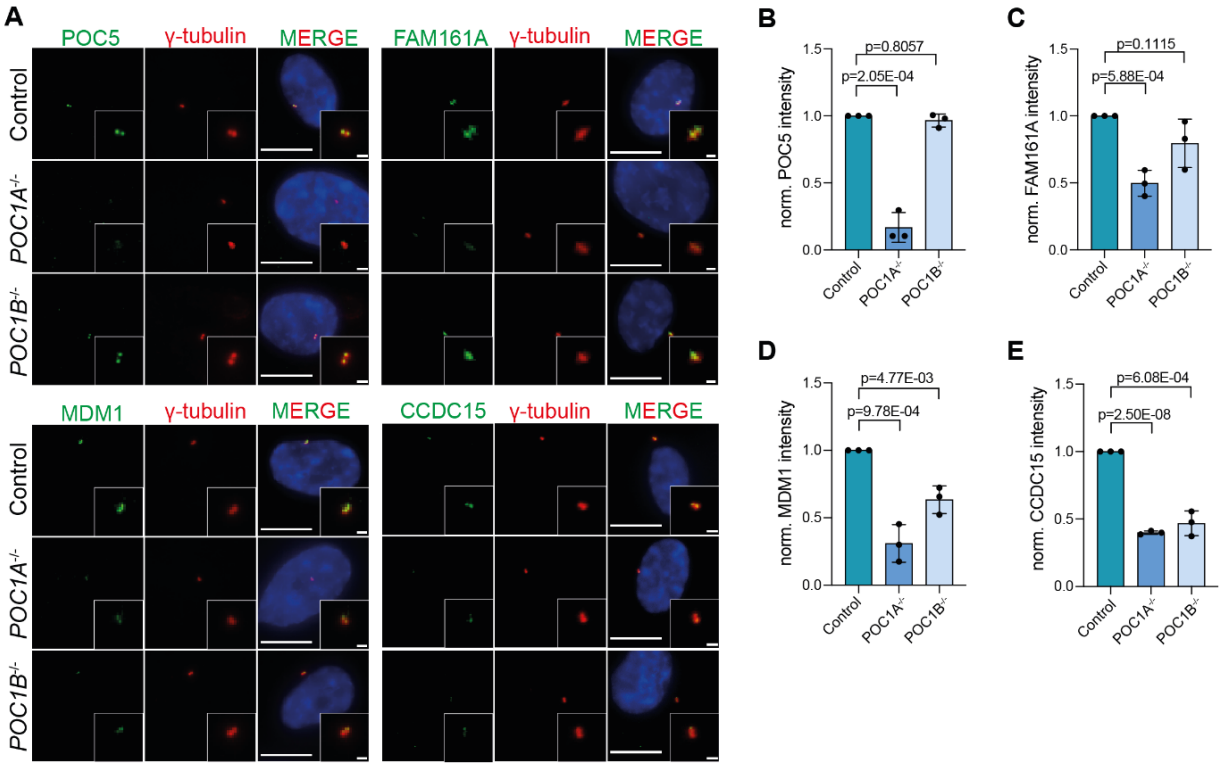

Figure 13: POC1A and POC1B have an impact on inner scaffold proteins
(**A**) Representative IF images of interphase control, *POC1A*$^{-/-}$ and *POC1B*$^{-/-}$ cells stained against the indicated proteins (green) and the centrosomal marker γ-tubulin (red). Scale bars: 10 µm, magnification scale bars: 1 µm. (**B-E**) Signal intensity measurements of the cells shown in (**A**). Data are presented as mean ± SD. Statistics were derived from two-tail unpaired t-test analysis of N= 3 biologically independent experiments, $n > 100$ cells per cell line for each experiment. *Figure modified and adapted from* (Sala et al., *Nat Comm* 2024)[133].

To confirm that the signal reduction of POC5, FAM161A, MDM1 and CCDC15 can be accounted for the loss of POC1A and POC1B, I complemented the knockout cell lines with dox-inducible HA-tagged wildtype versions of *POC1A* and *POC1B*, respectively, and measured the signal intensity of the inner scaffold proteins via IF. Complementation of POC1A restored the centriolar levels of POC5 and CCDC15 to 80% and 90% of the observed levels in control cells (Fig. 14B, C). The same was also the case for *POC1B* complementation: MDM1 and CCDC15 levels were successfully restored at centrioles (80% and 75% of control cells level, respectively) as seen in Fig. 14E and F.

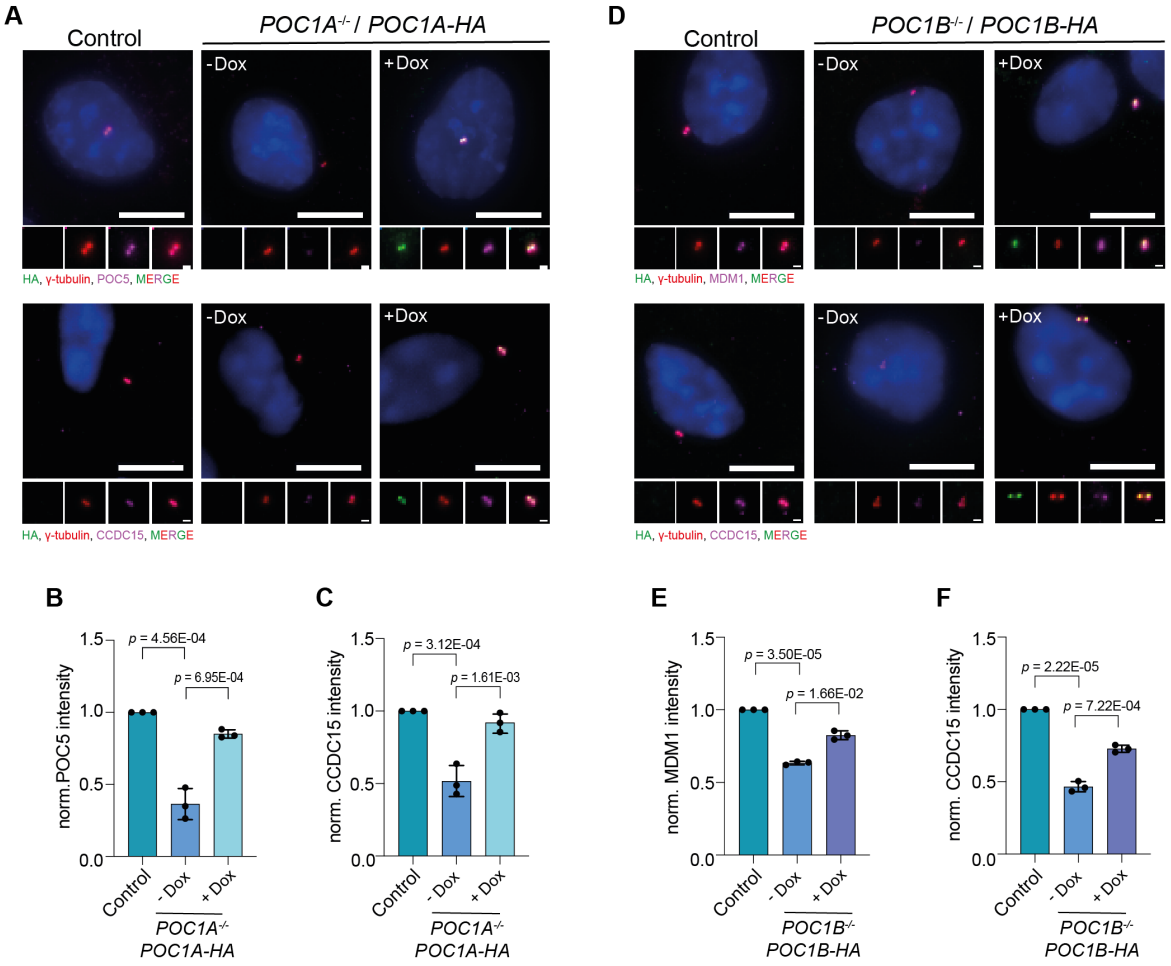

Figure 14: Loss of POC1A and POC1B proteins accounts for the reduction of inner scaffold proteins at the centrosome
(**A**) Representative IF images of interphase *POC1A*$^{-/-}$ cells complemented with dox-inducible HA-tagged *POC1A* construct and stained against HA (green), γ-tubulin (red) and POC5 or CCDC15 (magenta). Scale bars: 10 µm, magnification scale bars: 1 µm. (**B**, **C**) Quantification of the signal intensities of POC5 and CCDC15 at the centrosome. (**D**) Representative IF images of interphase *POC1B*$^{-/-}$ cells complemented with dox-inducible HA-tagged *POC1B* construct and stained against HA (green), γ-tubulin (red) and MDM1 or CCDC15 (magenta). Scale bars: 10 µm, magnification scale bars: 1 µm. (**E**, **F**) Quantification of the signal intensities of MDM1 and CCDC15 at the centrosome. (**B**, **C**, **E**, **F**) Data are presented as mean ± SD. Statistics were derived from two-tail unpaired t-test analysis of N= 3 biologically independent experiments, $n > 100$ cells per cell line for each experiment. *Figure modified and adapted from* (Sala et al., *Nat Comm* 2024)[133].

In addition to conventional IF, I analyzed the effect on inner scaffold proteins upon POC1A and POC1B loss by exploiting the increased resolution that ultrastructure Expansion Microscopy (u-ExM) offers. For this analysis, only longitudinal centrioles showing a near-normal length were considered and the cells were co-stained with antibodies against α-tubulin (centriolar wall marker) and the respective proteins shown in Fig. 15A. Inner scaffold proteins like POC5, FAM161A and CCDC15 displayed a defined localization at the central region of centrioles. Centrin, that is known to interact with POC5[59], showed in addition to the central localization (yellow asterisk) a pool at the tip of the centriole, which corresponds to the Sfi1-dependent pool[158]. Upon loss of POC1A, the distribution of POC5 and FAM161A is altered, and both proteins lose their defined localization at the central part of centrioles (Fig. 15A-C), confirming the results from the conventional IF analysis. In contrast to the *POC1A*$^{-/-}$ cell line, FAM161A is not affected in *POC1B*$^{-/-}$ cells (Fig. 15A, C). However, u-ExM revealed that the POC5 distribution upon POC1B loss is slightly affected, covering now less of the total centriole length compared to control cells (Fig. 15A, B). Similar to POC5, a defined Centrin signal in the central region of centrioles was lost in *POC1A*$^{-/-}$ cells, while the distal tip pool remained unaffected (Fig. 15A, D). In line with the conventional IF analysis shown in Fig. 13, POC1A and POC1B loss affected significantly the distribution of MDM1 and CCDC15 along the centriole (Fig. 15A, E and F). In addition to the inner scaffold proteins, the distribution of γ-tubulin and HAUS4 was checked in the knockout cell lines. Schweizer and colleagues showed that γ-tubulin and HAUS4 (a subunit of the augmin complex) localize within the centriolar lumen and that this localization is dependent on POC5[159]. Together with the inner scaffold, the luminal augmin-γTuRC pool may have a role in stabilizing the centriole. In accordance with these findings, the inner luminal localization of γ-tubulin and HAUS4 is lost in the *POC1A*$^{-/-}$ cell line but remains unaffected in control and *POC1B*$^{-/-}$ cells (Fig 15A, H and G). Taken together, POC1A and POC1B affect the distribution of inner scaffold proteins but show a different impact on specific subsets of proteins, indicating divergent functions of the POC1 proteins.

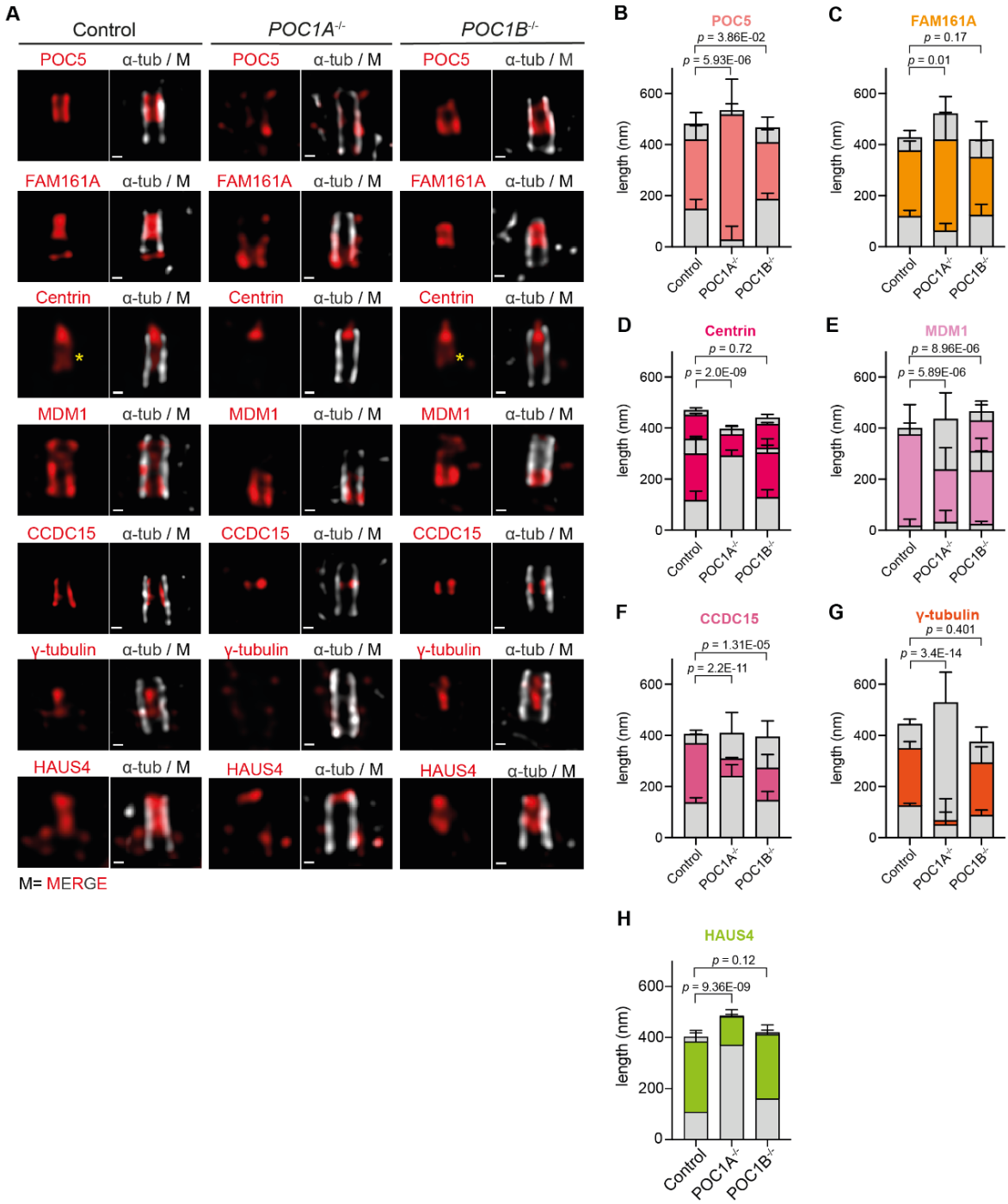

Figure 15: Loss of POC1A and POC1B affect the centriolar localization of inner scaffold proteins
(**A**) U-ExM images of G1 centrioles with near-normal length from control, *POC1A*$^{-/-}$ and *POC1B*$^{-/-}$ cell lines. Cells were stained against the respective proteins (red) and α-tubulin (grey). Scale bar: 100 nm. (**B**-**H**) Quantification of the centrioles shown in (**A**). The distribution of each protein along the centriole was measured in each cell line. Data are presented as mean ± SD. All statistics were derived from two-tail unpaired t-test with n= > 10 centrioles per cell line. *Figure modified and adapted from* (Sala et al., *Nat Comm* 2024)[133].

3.6 Loss of POC1A affects the distribution of proximal end proteins along the centriole

Both POC1 proteins have an impact on the localization of proteins that localize at the central region of centrioles. Due to POC1B´s extension towards the proximal site of centrioles and to its previously published interaction with CEP44, I analyzed proximal proteins such as CEP44, CEP295 and CEP135 in the knockout cell lines to see whether proximal proteins are affected as well. Conventional IF analysis of these proteins did not show any significant effect in the knockout cell lines, except for CEP135 that was slightly reduced in *POC1B*$^{-/-}$ cells (Fig. 16A-F). However, u-ExM analysis of centrioles revealed an altered distribution of CEP135, CEP295 and CEP44. Compared to control cells, POC1A loss resulted in an extended localization of the three proximal proteins towards the distal half of centrioles (Fig. 16G-L). While CEP295 and CEP135 were not significantly altered in *POC1B*$^{-/-}$ cells, CEP44 showed a slight extension towards the distal part (Fig. 16K, L).

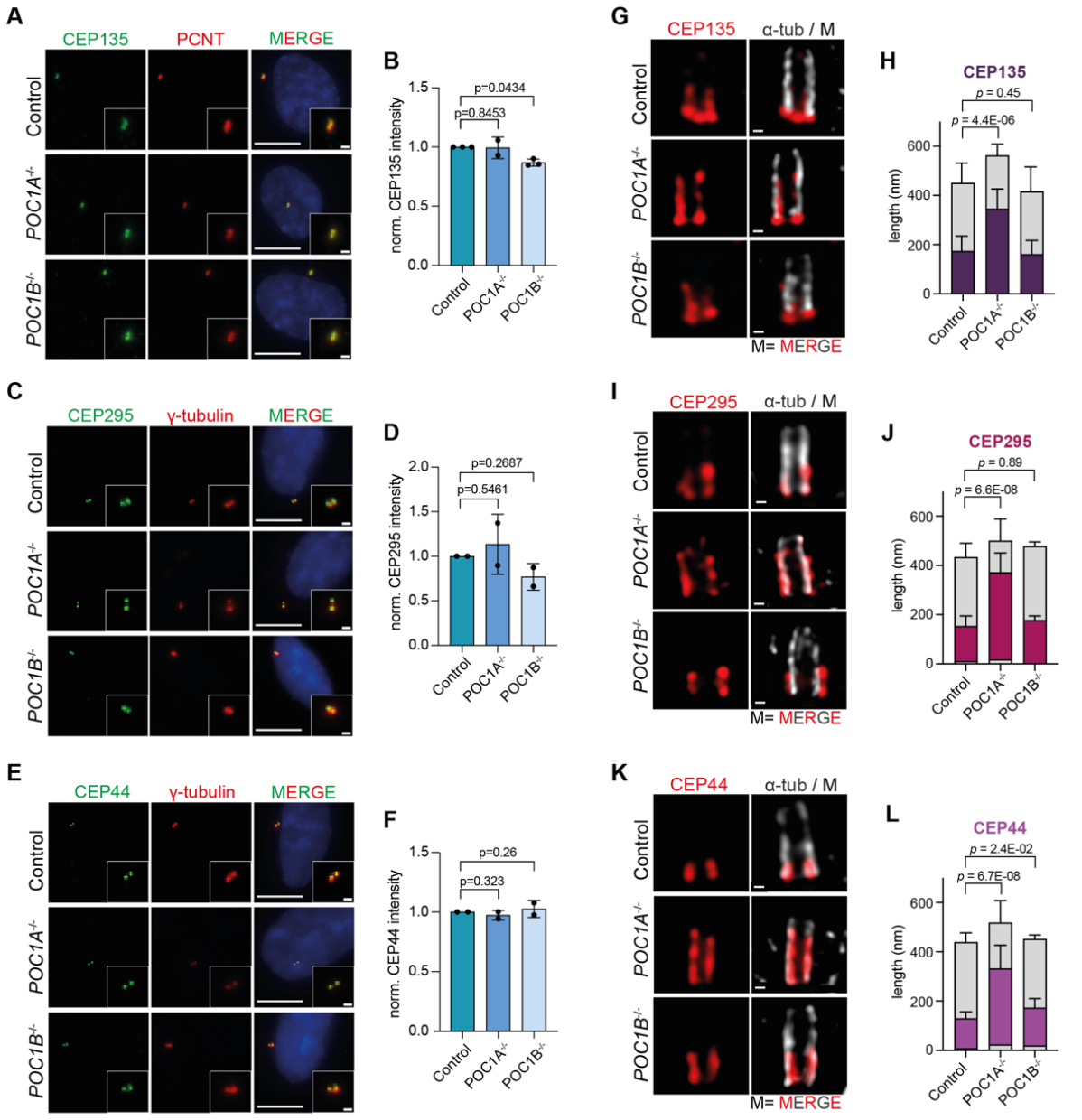

Figure 16: POC1A affects the centriolar distribution of proximal proteins
(**A, C, E**) Representative IF images of interphase control, *POC1A*$^{-/-}$ and *POC1B*$^{-/-}$ cells stained against the indicated proximal proteins (green) and the centrosomal marker γ-tubulin (red). Scale bars: 10 µm, magnification scale bars: 1 µm. (**B**, **D**, **F**) Quantification of the signal intensity from cells shown in (**A**, **C**, **D**). Data are presented as mean ± SD. Statistics were derived from two-tail unpaired *t*-test of N= 3 biologically independent experiments, *n* > 100 cells per cell line for each experiment for CEP135 in Control and *POC1B*$^{-/-}$ cells and N=2 biologically independent experiments, *n* > 100 cells per cell line for each experiment for CEP295 and CEP44; and CEP135 in *POC1A*$^{-/-}$. (**G**, **I**, **K**) U-ExM images of G1 centrioles with near-normal length from control, *POC1A*$^{-/-}$ and *POC1B*$^{-/-}$ cell lines. Cells were stained against the proximal proteins CEP135, CEP295 or CEP44 (red) and α-tubulin (grey). Scale bar: 100 nm. (**H**, **J**, **L**) Quantification of the signal distribution of the respective proteins in each cell line from centrioles shown in (**G**, **I**, **K**). Data are presented as mean ± SD. Statistics were derived from two-tail unpaired t-test with *n*= > 10 centrioles per cell line. *Figure modified and adapted from* (Sala et al., *Nat Comm* 2024)[133].

The extended localization of proximal proteins prompted me to investigate whether the cartwheel structure also shows an extension towards the distal half of centrioles. For this, I analyzed cells stained against SAS-6, a cartwheel component, via u-ExM and grouped the

procentrioles based on their length (Fig. 17A, B). Contrary to CEP44, CEP295 and CEP135, SAS-6 localization is not affected in neither of the two *POC1* knockout cell lines (Fig. 17B). Interestingly, analysing centrioles of RPE1 *POC5*$^{-/-}$ cells (for generation of this knockout see Fig. 19) stained against CEP44, showed a similar phenotype as observed in the *POC1A*$^{-/-}$ cell line (Fig. 17C, D). The *vice-versa* experiment, where POC5 was analyzed in a published RPE1 *CEP44*$^{-/-}$ cell line from our group[63], revealed that loss of a proximal protein affects also the localization of an inner scaffold component and leads to a slight extension towards the proximal site of centrioles (Fig. 17D). These findings suggests that substructures within the centriole may have an influence in terms of restricting and regulating each other's spatial distribution.

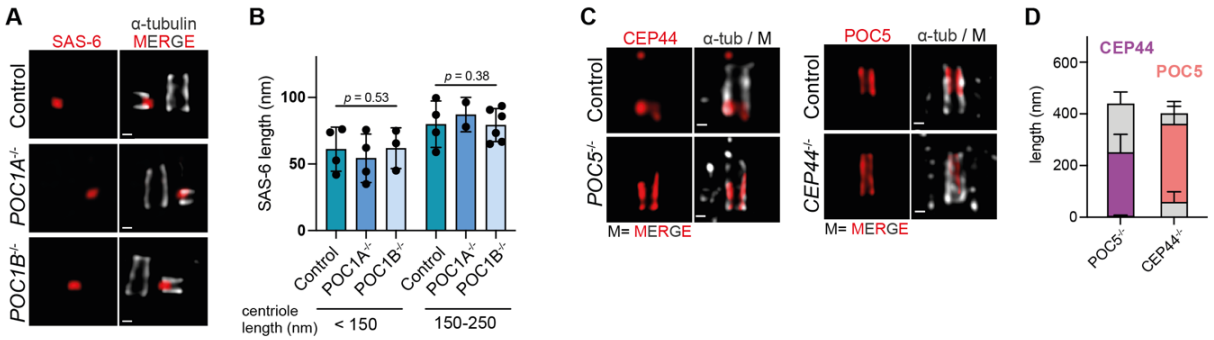

Figure 17: Substructures within the centriole can restrict the distribution of centriolar proteins
(**A**) U-ExM images of procentrioles from control, *POC1A*$^{-/-}$ and *POC1B*$^{-/-}$ cells stained against the cartwheel component SAS-6 (red) and α-tubulin (grey). Scale bar: 100 nm. (**B**) The signal distribution of SAS-6 from the centrioles shown in (**A**) was measured. To avoid artificial differences in signal distribution of SAS-6 due to different procentrioles growth, procentrioles were prior grouped based on their length, estimated by the α-tubulin signal. Statistics were derived from one-way ANOVA. (**C**) U-ExM images of centrioles from control and *POC5*$^{-/-}$ cell lines and stained against CEP44 (red) and α-tubulin (grey). In addition, centrioles from control and *CEP44*$^{-/-}$ cell lines were stained against POC5 (red) and α-tubulin (grey). Scale bar: 100 nm. (**D**) Quantification of the signal distribution of CEP44 and POC5 in the respective knockout cell lines. Error bars represent the SD. N = 9 centrioles (*POC5*$^{-/-}$), 15 centrioles (*CEP44*$^{-/-}$). *Figure modified and adapted from* (Sala et al., *Nat Comm* 2024)[133].

3.7 POC1A interacts with POC5 via the N-terminal WD40 domain

The strong impact on the localization of POC5 upon loss of the POC1A protein, prompted me to investigate whether a potential interaction between POC1A and POC5 occurs within the centriole. Based on my preliminary FLAG-IP experiments, AlphaFold-Multimer predictions were performed in collaboration with Dr. Sebastian Eustermann and Dr. Thomas Hoffmann from EMBL to gain a detailed knowledge about the involved protein domains. AlphaFold-Multimer consistently predicted an interaction of the WD40 domain of POC1A (involving blade 1, 5 and 6) with a C-terminal region of POC5 comprising residues 472-532 (Fig. 18A, upper panel; C). Due to the similarity of the POC1 proteins, predictions were additionally performed for a potential interaction between the WD40 domain of POC1B and POC5, showing similar

results as in the case for POC1A (Fig. 18B, upper panel). Interestingly, including the linker region of POC1B in the predictions, leads to a diminished interaction between the WD40 domain of POC1B and POC5. The linker region, connecting the WD40 domain and the C-terminal coiled-coil, is largely unstructured, but in the case of POC1B it is predicted to form a beta strand at residues 361-365, termed Intra, that interacts potentially with the β-sheet of the WD40 blade 1. Intra competes with the binding of POC5 to blade 1 and thus may lead to a reduced interaction efficiency between POC1B and POC5 (Fig. 18B, lower panel).

To test the predictions and verify them in the cellular context, I performed FLAG-IP experiments with HEK293T cells co-transfected with FLAG-tagged full-length *POC1A* or *POC1B* and different HA-tagged *POC5* constructs (Fig. 18D). In line with the AlphaFold-Multimer predictions, full-length POC5 binds to both POC1 proteins, however, with less efficiency to POC1B than to POC1A (Fig. 18E, lane 5 and 8; F). This indicates that Intra may have an inhibiting effect on the binding between the WD40 domain of POC1B and POC5. Based on the IP experiment, the region in POC5 that mediates the binding to POC1A is located in the C-terminus, verifying the predictions (Fig. 18E, lanes 6 and 7). In addition to identifying the critical region of POC5 for these interactions, I tested which domains of the POC1 proteins are essential for binding. Intriguingly, only the WD40 domain of POC1A showed a strong interaction with POC5, whereas the WD40 of POC1B bound less strongly (Fig. 18G, lanes 5 and 6; H), suggesting that not only Intra is influencing the interaction between POC1B and POC5 but also the WD40 domain. To confirm that also the WD40 domain of POC1B impacts the interaction between full-length POC1B and POC5, I tested the chimeric versions *POC1Ab*-FLAG and *POC1Ba*-FLAG (where the subdomains of one POC1 protein were swapped with its paralogue, see Fig. 11A) by co-expressing them with *POC5*-HA. POC1Ab, that has the WD40 domain of POC1A fused to the C-terminal half of POC1B, was less efficiently binding to POC5 compared to POC1A, indicating that Intra of POC1B indeed negatively impacts the interaction (Fig. 18G, lanes 3 and 7). POC1Ba, although binding with a higher efficiency to POC5 than POC1Ab and POC1B (Fig. 18G, lanes 4, 7 and 8, I), behaved not like POC1A, confirming that also the WD40 domain of POC1B impacts the binding to POC5 (Fig. 18G, lanes 3 and 8). Cells expressing only FLAG-tagged version of the C-terminal domain of *POC1A* and *POC1B* could not co-immunoprecipitated POC5, confirming the WD40 domain as the binding region (Fig. 18J). Lastly, I tested the effect of the POC5 mutant POC5$^{\Delta 472\text{-}532}$-HA that lacks the predicted POC1-interacting-region (amino acid residues 472-532) on the POC1-POC5 interaction. Upon loss of the predicted POC1-interacting-region, POC5 could not be

immunoprecipitated with POC1A or POC1B, confirming the predicted binding site in POC5 (Fig. 18K).

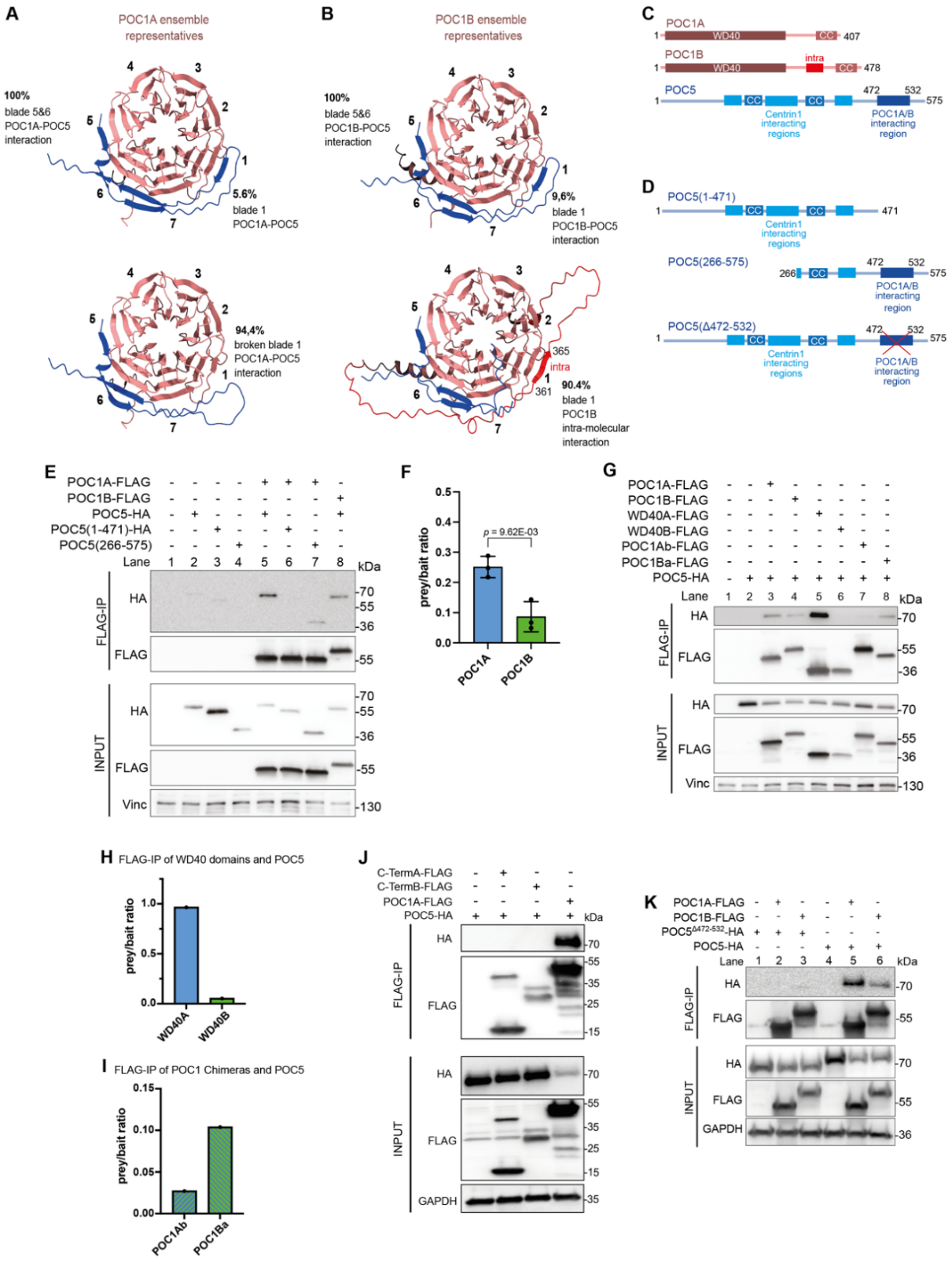

Figure 18: The N-terminal WD40 domain mediates the interaction between POC1A and the inner scaffold protein POC5

(**A, B**) AlphaFold-Multimer predictions of an interaction between the WD40 domains from POC1A and POC1B (salmon) with a C-terminal region of POC5 (blue). POC5 is predicted to contact surfaces on blade 5 and 6, and to

a lesser extent, on blade 1 of the WD40 domain. The lower panel of (**A**, **B**) focuses on blade 1 and shows how the interaction with POC5 is lost, if blade 1 is broken in the case of POC1A or blocked by an additional beta-strand (termed Intra) that is formed by the linker region in POC1B. The percentages indicate the frequencies of the predicted ensembles. (C) Domain architecture of POC1A, POC1B, and POC5. POC5 contains several Centrin-binding regions and is predicted to have a POC1-binding region at residues 472-532. (**D**) Different generated HA-tagged *POC5* constructs used for immunoprecipitation (IP) experiments. (**E**) Representative FLAG-IP from HEK293T cells expressing HA-tagged subdomains of *POC5* and FLAG-tagged full-length *POC1A* or *POC1B*. Vinculin was used as an input control. (**F**) Quantification of FLAG-IP as shown in (**E**). The binding efficiency between the POC1 proteins and POC5 was measured. POC5 binds with a higher efficiency to POC1A than to POC1B. Due to variable expression levels, the signal intensity of the prey band from the IP sample was normalized to the signal intensity of the bait band and the ratio was used as an indicator for the binding efficiency. Data are presented as mean ± SD. (**G**) Representative FLAG-IP from HEK293T cells expressing HA-tagged full-length *POC5* and different FLAG-tagged *POC1A* or *POC1B* constructs, including the chimeric versions *POC1Ab* and *POC1Ba*. Vinculin was used as an input control. (**H**, **I**) Quantification of the binding efficiency between the WD40 domains of the POC1 proteins and POC5 and between the chimeric POC1 versions and POC5. Quantification derives from one representative IP experiment out of N=3 biologically independent experiments. (**J**) Representative FLAG-IP from HEK293T cells expressing FLAG-tagged C-terminal domains of *POC1A* or *POC1B* and HA-tagged full-length *POC5*. As a positive control, FLAG-tagged full-length *POC1A* was included as well. GAPDH was used as an input control. N=3 biologically independent experiments. (**K**) Representative FLAG-IP from HEK293T cells expressing HA-tagged full-length *POC5* or the mutant version $POC5^{\Delta 472\text{-}532}$ lacking the predicted POC1-binding site and FLAG-tagged *POC1A* or *POC1B*. N=2 biologically independent experiments. *Figure modified and adapted from* (Sala et al., *Nat Comm* 2024)[133].

3.8 Loss of *POC5* resembles the $POC1A^{-/-}$ phenotype

The loss of POC1A affects the distribution of inner scaffold components like POC5, FAM161A and Centrin, as well as the localization of the inner luminal pool of γ-tubulin and HAUS4. To see, if loss of other inner scaffold proteins leads to a similar phenotype, I generated a RPE1 $POC5^{-/-}$ cell line in a $TP53^{-/-}$ background via CRISPR/Cas9 (Fig. 19A). POC5 was chosen due to the strong interaction with POC1A. Genomic sequencing, IF and IB analysis verified the successful knockout (Fig. 19B-E). The $POC5^{-/-}$ cell line, like $POC1A^{-/-}$ cells, showed a significant reduction of FAM161A at the centrosomes (Fig. 19A, B). Additionally, the signal intensity of γ-tubulin was also reduced (Fig. 19A, C). To investigate in detail the centriolar localization of different proteins, I performed u-ExM and checked Centrin, MDM1, CCDC15 and γ-tubulin in expanded $POC5^{-/-}$ cells (Fig. 19D). Similar to $POC1A^{-/-}$ cells, only the distal tip pool of Centrin remained unaffected, while the central localization reflecting the POC5-centrin complex[59,158] was lost. A similar impact was also observed for CCDC15 and γ-tubulin but not for MDM1, that showed the same localization observed in control cells. The loss of the inner luminal pool of γ-tubulin is in concordance with the findings in a publication from Schweizer et al., where they showed the localization of γ-tubulin in the centriolar lumen is dependent on the POC5-Augmin interaction[159]. To determine if POC1A and POC1B are as well affected, I also analyzed both proteins in the $POC5^{-/-}$ cell line. Both proteins showed a localization like in the WT control cell line (Fig. 19E), suggesting that POC1A and POC1B function upstream of POC5.

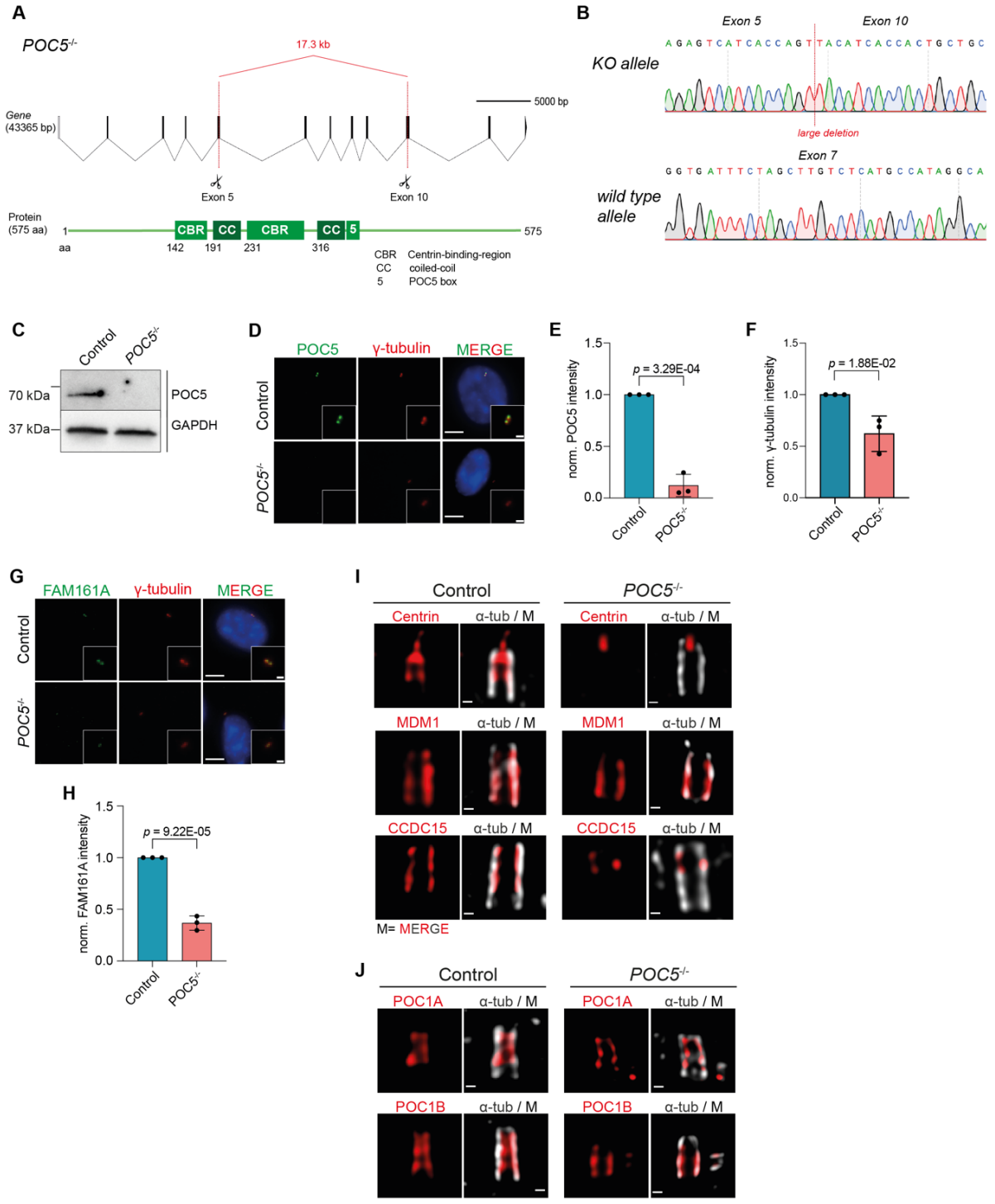

Figure 19: CRISPR/Cas9 generated *POC5* knockout cell line using the CRISPR/Cas9 dual sgRNA strategy
(**A**) Schematic representation of the *POC5* WT gene and the protein domain architecture. sgRNAs used in this study to generate the knockout target exon 5 and exon 10. (**B**) Chromatograms of the sequenced knockout clone showing a homozygous genotype with a large deletion after exon 5. In comparison, in a WT allele with no deletion, exon 7 can be sequenced. (**C**) Immunoblots of whole cell lysates from knockout and control cell line. GAPDH was used as a loading control. (**D**) Representative IF images of control and *POC5*$^{-/-}$ cells stained against POC5 (green) and γ-tubulin (red). Scale bars: 10 µm, magnification scale bars: 1 µm. (**E**, **F**) Signal intensity measurements of the cells shown in (**D**). (**G**) Representative IF images of control and *POC5*$^{-/-}$ cells stained against FAM161A (green) and γ-tubulin (red). Scale bars: 10 µm, magnification scale bars: 1 µm. (**H**) Signal intensity measurements of the cells shown in (**G**). (**I**, **J**) U-ExM images of centrioles stained against the indicated proteins (red) and α-tubulin (grey). Localization of POC1A, POC1B and MDM1 is unaffected in *POC5*$^{-/-}$ cells. Similar to the *POC1* knockouts, CCDC15 is also affected in *POC5*$^{-/-}$ cells. Scale bar: 100 nm. (**E**, **F**, **H**) Data are presented

as mean ± SD. Statistics were derived from two-tail unpaired t-test analysis of N= 3 biologically independent experiments, $n > 100$ cells per cell line for each experiment. *Figure modified and adapted from* (Sala et al., *Nat Comm* 2024)[133].

3.9 POC5´s POC1-binding-region is important for centrosomal localization

The predicted POC1-binding-region at the C-terminus of POC5 is important to mediate the interaction with POC1A. In order to test how deletion of this binding site affects the function of POC5 within the cellular context, I checked via IF for the centrosomal localization in *POC5*$^{-/-}$ cells expressing a dox-inducible HA-tagged POC5 mutant, lacking the POC1-binding-region (*POC5*$^{\Delta 472\text{-}532}$). The mutant failed to efficiently localize at centrosomes when induced at low dox concentrations (20 ng/ml), but the percentage of cells showing centrosomal localization increased, when forced to overexpression with a higher dox concentration (1000 ng/ml, Fig. 20A-C). In contrast, WT POC5 localized efficiently to centrosomes, even at low dox levels (1 ng/ml, Fig. 20A-C). The deletion of the POC1-binding-region not only affected the centrosomal localization but also had an impact on the recruitment of the inner luminal pool of γ-tubulin. Contrary to WT POC5, POC5$^{\Delta 472\text{-}532}$ was not able to rescue the phenotype in *POC5*$^{-/-}$, despite being overexpressed at high dox concentrations and therefore localizing at centrosomes (Fig. 20D, E). The data suggests that the POC1-binding site in POC5 is important for the proper centriolar localization of POC5 and the recruitment of the inner luminal pool of γ -tubulin.

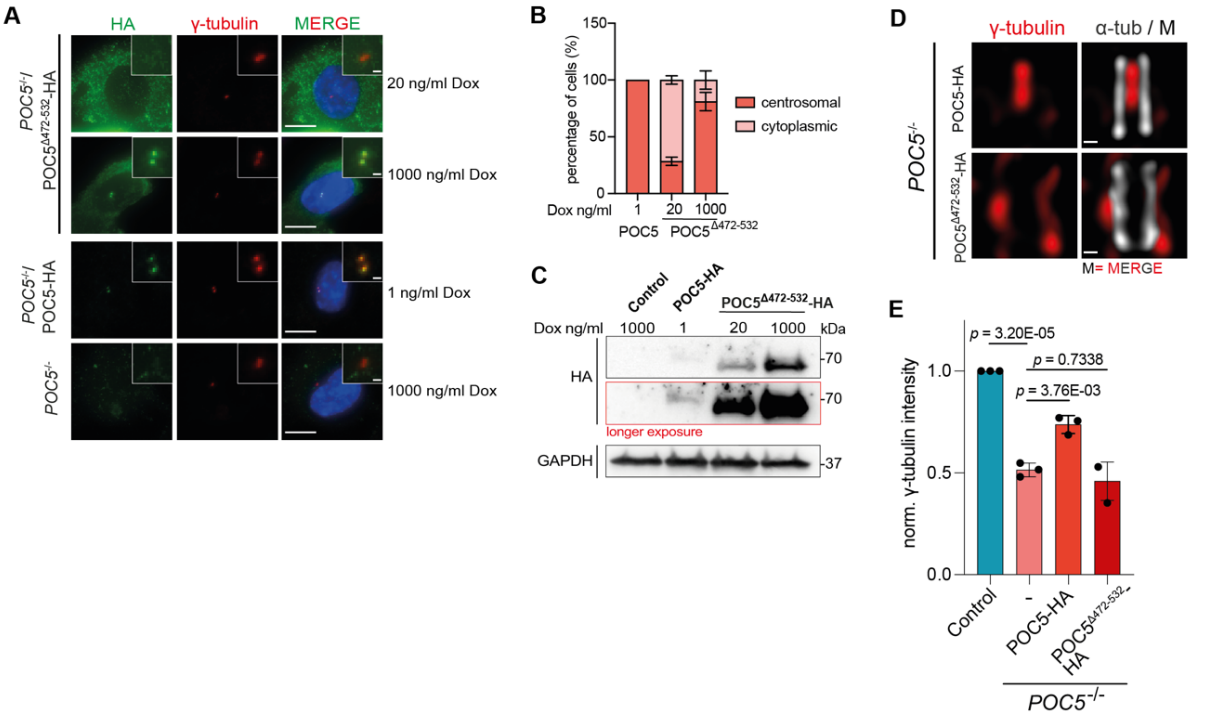

Figure 20: Centrosomal localization of POC5 is mainly facilitated by the POC1-binding region
(**A**) RPE1 *POC5*$^{-/-}$ cells expressing either HA-tagged full-length *POC5* or *POC5*$^{\Delta 472\text{-}532}$ were checked for centrosomal localization by IF. Cells were stained against HA (green) and γ-tubulin (red). Scale bars: 5 µm, magnification scale bars: 1 µm. (**B**) Quantification of (**A**). Percentage of interphase cells showing centrosomal and

cytoplasmatic POC5 localization. Data are presented as mean ± SD. N=2 biologically independent experiments, *n* > 110 cells per cell line for each experiment. (**C**) Immunoblot of whole cell lysates from the cell lines shown in (**A**). The lower HA-immunoblot is a longer exposer of the upper one. GAPDH is used as a loading control. N=2 biologically independent experiments. (**D**) U-ExM images from intact centrioles of RPE1 *POC5*$^{-/-}$ cells expressing either full-length *POC5* or *POC5*$^{\Delta 472\text{-}532}$ and stained against α-tubulin (grey) and γ-tubulin (red), M= merged channels. POC5$^{\Delta 472\text{-}532}$ cannot rescue the luminal γ-tubulin localization. Scale bars: 100 nm. N=3 biologically independent experiments. (**E**) Complementation of *POC5*$^{-/-}$ cells with WT *POC5* can restore γ-tubulin signal at centrosomes. In contrast, expression of *POC5*$^{\Delta 475\text{-}532}$ lacking the POC1 binding site is insufficient for γ-tubulin recruitment. Data are presented as mean ± SD. All statistics were derived from two-tail unpaired *t*-test analysis of N= 3 biologically independent experiments, *n* > 100 cells per cell line for each experiment. *Figure modified and adapted from* (Sala et al., *Nat Comm* 2024)[133].

3.10 POC1 proteins engage in distinct binding mechanisms with various interaction partners

Centrioles of *POC1A*$^{-/-}$ and *POC1B*$^{-/-}$ cells showed an altered localization of MDM1 and FAM161A, suggesting that these proteins are potential interaction partners. In collaboration with Dr. Sebastian Eustermann and Dr. Thomas Hoffmann, AlphaFold-Multimer predictions were performed, to test this possibility and to pinpoint which domains might be involved in the interaction. MDM1 is a 714 amino acid long protein predicted to have large unstructured regions interrupted by short helices (Fig. 21A, B). A strong interaction is predicted to involve the coiled-coil of both POC1 proteins and a short helix at the C-terminus of MDM1 (Fig. 21C). To confirm these predictions, I conducted FLAG-IP experiments in HEK293 cells co-transfected with subdomains of FLAG-tagged *POC1A* or *POC1B* and HA-tagged *MDM1*. Full-length POC1A and POC1B, as well as the C-terminal region of both proteins were able to pull down MDM1 (Fig. 21D, compare lanes 3, 4, 6 and 7). In contrast, no interaction with the WD40 domains of both POC1 was observed (Fig. 21D, lanes 5 and 8).

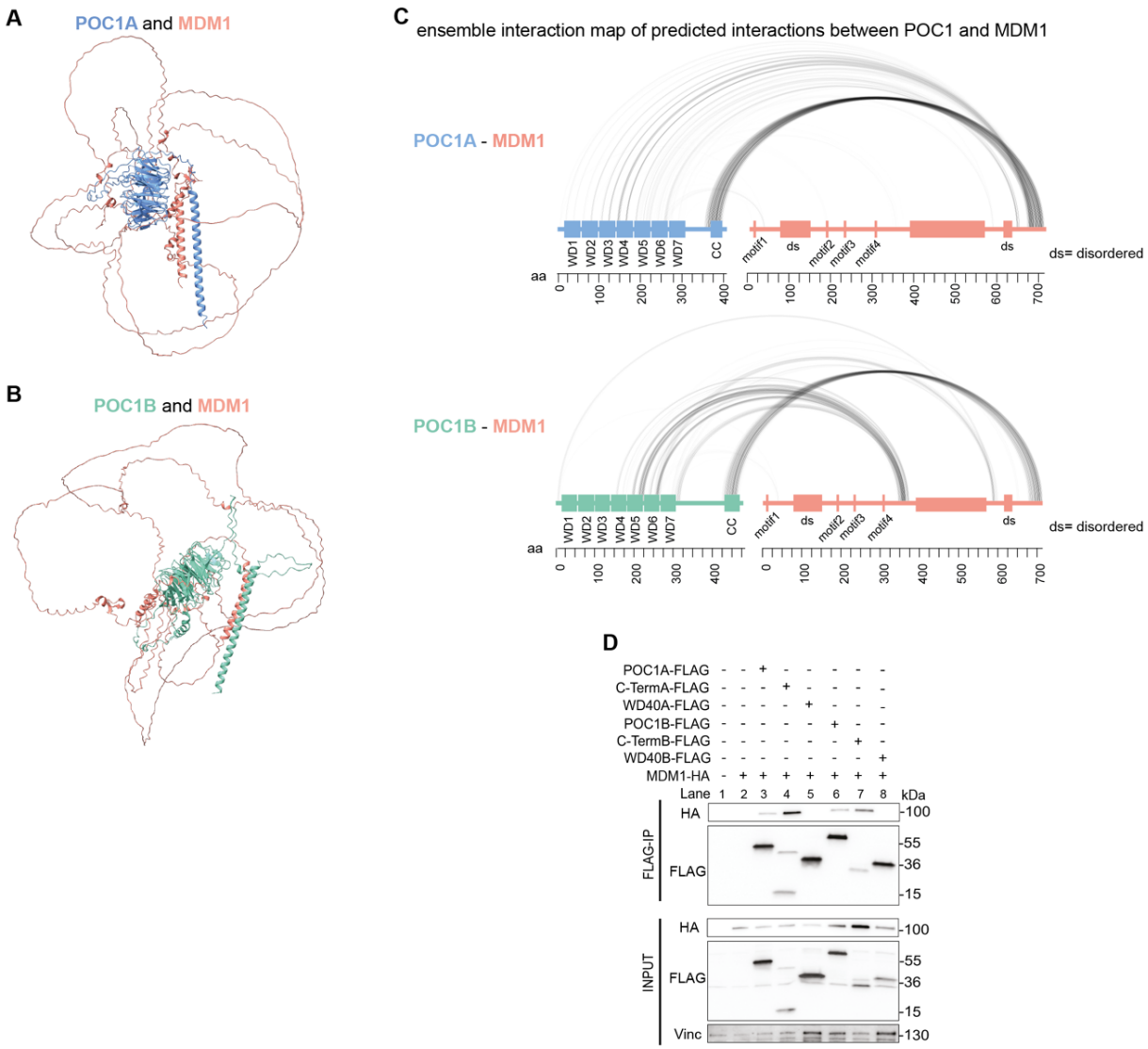

Figure 21: Predicted AlphaFold-Multimer interactions between MDM1 and the POC1 proteins
(**A**, **B**) AlphaFold-Multimer predictions between POC1A (blue) or POC1B (green) and MDM1 (salmon) showing an interaction between the C-termini of both proteins. (**C**) Ensemble interaction map of an interaction between POC1A (light blue) or POC1B (green) and MDM1 (salmon) based on AlphaFold-Multimer predictions. Thicker and darker lines indicate interactions that are predicted to be more robust. The most robust interactions are predicted to involve the coiled-coil regions of both POC1A and POC1B and a C-terminal segment of MDM1. Abbreviation: aa: amino acids. (**D**) Representative FLAG IP from HEK293T cells expressing FLAG-tagged full-length or subdomains of either *POC1A* or *POC1B* together with HA-tagged *MDM1*. Vinculin was used as input control. N=3 biologically independent experiments. *Figure modified and adapted from* (Sala et al., *Nat Comm* 2024)[133].

AlphaFold-Multimer predictions of the POC1 proteins and FAM161A showed interactions involving the WD40 domains as well as the C-terminal coiled-coil (Fig. 22A-C). Subsequent IP experiments confirmed that FAM161A only co-immunoprecipitated efficiently with full-length POC1A and POC1B (Fig. 22D, E). Taken together, these findings show, that POC1A and POC1B display different interaction modes involving the WD40 domain and the C-terminal coiled-coil, leading to binding with different proteins.

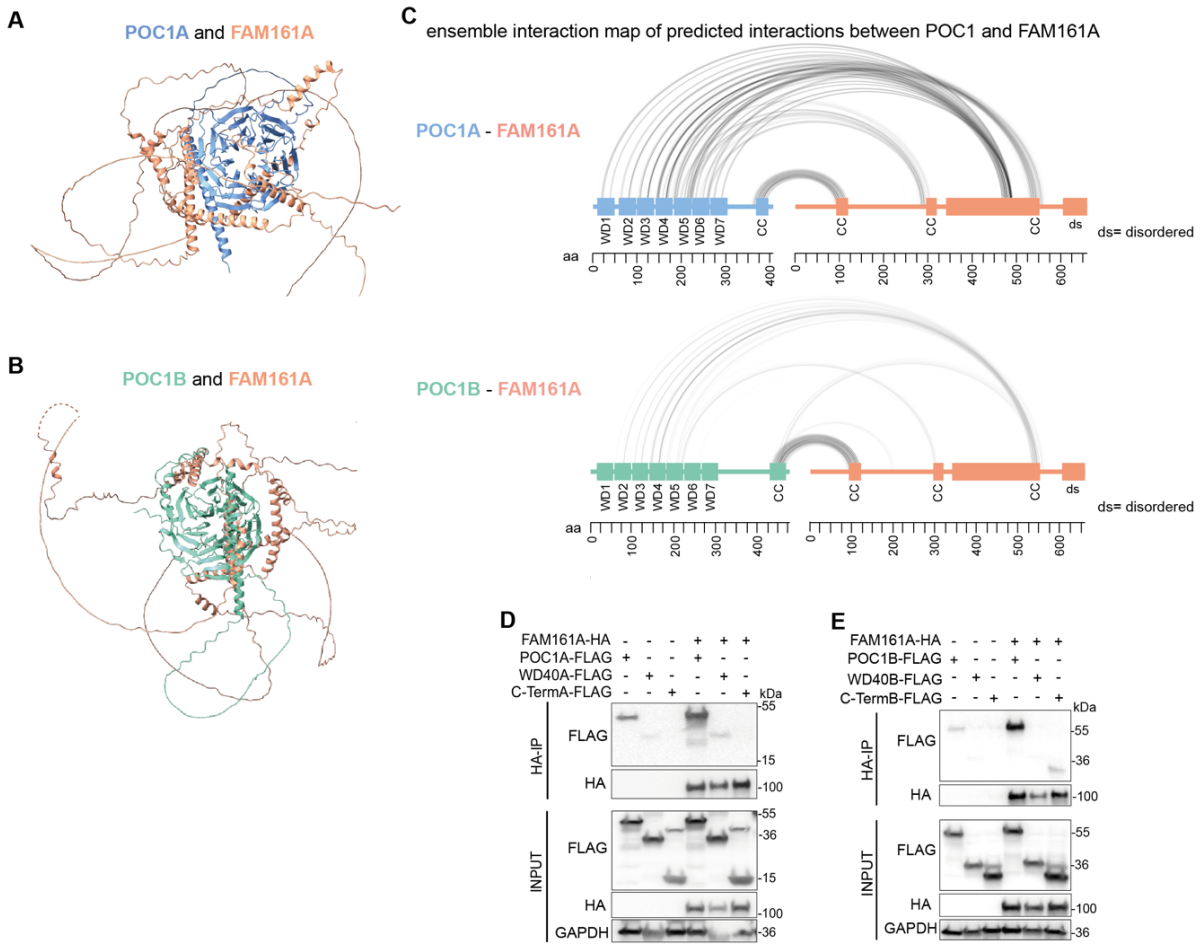

Figure 22: Predicted AlphaFold-Multimer interactions between FAM161A and the POC1 proteins
(**A**, **B**) AlphaFold-Multimer predictions of the interactions between POC1A (blue) or POC1B (green) and FAM161A (salmon) showing an interaction involving the WD40 domain as well as the coiled-coil regions of both POC1 proteins. (**C**) Ensemble interaction map of an interaction between POC1A (light blue) or POC1B (green) and MDM1 (salmon) based on AlphaFold-Multimer predictions. Thicker and darker lines indicate interactions that are predicted to be more robust. The most robust interactions are predicted to involve the WD40 domain and the coiled-coil regions of both POC1A and POC1B. Abbreviation: aa: amino acids. (**D**) Representative HA IP from HEK293T cells expressing HA-tagged *FAM161A* and FLAG-tagged full-length or subdomains of *POC1A*. GAPDH was used as input control. N=3 biologically independent experiments. (**E**) Representative HA IP from HEK293T cells expressing HA-tagged *FAM161A* and FLAG-tagged full-length or subdomains of *POC1B*. GAPDH was used as input control. N=3 biologically independent experiments. *Figure modified and adapted from* (Sala et al., *Nat Comm* 2024)[133].

3.11 POC1A and POC1B form Homo- and Heterodimers via their coiled-coil regions

POC1A and POC1B not only show a similar centriolar localization, but they also share a subset of interaction partners, and their loss affects inner scaffold components. These observations suggest that POC1A and POC1B play a role in the inner scaffold, but what might be the specific function of these proteins within this structure? One possibility is that POC1A and POC1B interact with each other, forming a platform to crosslink other proteins and to build a protein network in the centriolar lumen. Based on preliminary IP experiments, I observed that POC1A and POC1B indeed co-immunoprecipitated each other (Fig. 23). In order to gain a more detailed

insight which domains are involved in this interaction, AlphaFold-Multimer predictions were utilised. The C-terminal coiled-coil regions of POC1A and POC1B were predicted to interact strongly with each other (Fig. 23A, B) and the same outcome is observed for POC1A-POC1A (Fig. 23C) and POC1B-POC1B (Fig. 23D) interactions. Interestingly, interactions were not only predicted between the coiled-coil regions, but also, to a lesser extent, between WD40 domains. In addition, in the POC1B-POC1B homodimer, the WD40 domain is predicted to interact with the Intra region (Fig. 23D). To test these predictions, I conducted FLAG-IP experiments in HEK293T cells. The immunoprecipitation confirmed an interaction between full-length POC1A and POC1B (Fig. 23E; lanes 3 and 13), POC1A and POC1A (lane 10) and POC1B and POC1B (lane 6), that are mediated by the C-terminal coiled-coil region of both proteins (Fig. 23E, lanes 8 and 15; and Fig. 23F). The WD40 domains, at least in the cellular context, were not sufficient enough to mediate an interaction (Fig. 23E, lanes 4, 7, 11 and 14). To further validate the interaction with POC1A and POC1B with another approach, I subsequently tested their proximity within centrioles via Fluorescence Lifetime Imaging Microscopy (FLIM)-Förster resonance energy transfer (FRET). With this approach it is possible to detect when energy from an excited fluorophore (donor) is transferred to a non-excited fluorophore (acceptor) due to their proximity. For this, I co-transfected HEK293T cells with a POC1A-mNeonGreen (donor) and POC1B-mScarlet-I (acceptor) construct. If the two proteins are in close proximity (usually ranging between 2-10 nm), the life time of the donor (in this case POC1A-mNeonGreen) will be reduced in the presence of the acceptor (POC1B-mScarlet-I) compared to cells expressing only the donor construct. In Fig. 23G an example of the microscope software´s analysing tool is shown: in the phasor plot, that shows the FRET trajectory, signals with a longer lifetime appear on the left side, while signals with a shorter lifetime are shown on the right side. FLIM-FRET of living HEK293T co-transfected with POC1A-mNeonGreen and POC1B-mScarlet-I revealed a reduction in lifetime for the donor, when the acceptor is present (Fig. 23H) and also a high FRET efficiency (Fig. 23I). These observations coming from different approaches indicate that POC1A and POC1B form heterodimers mediated by an interaction via their C-terminal coiled-coil regions.

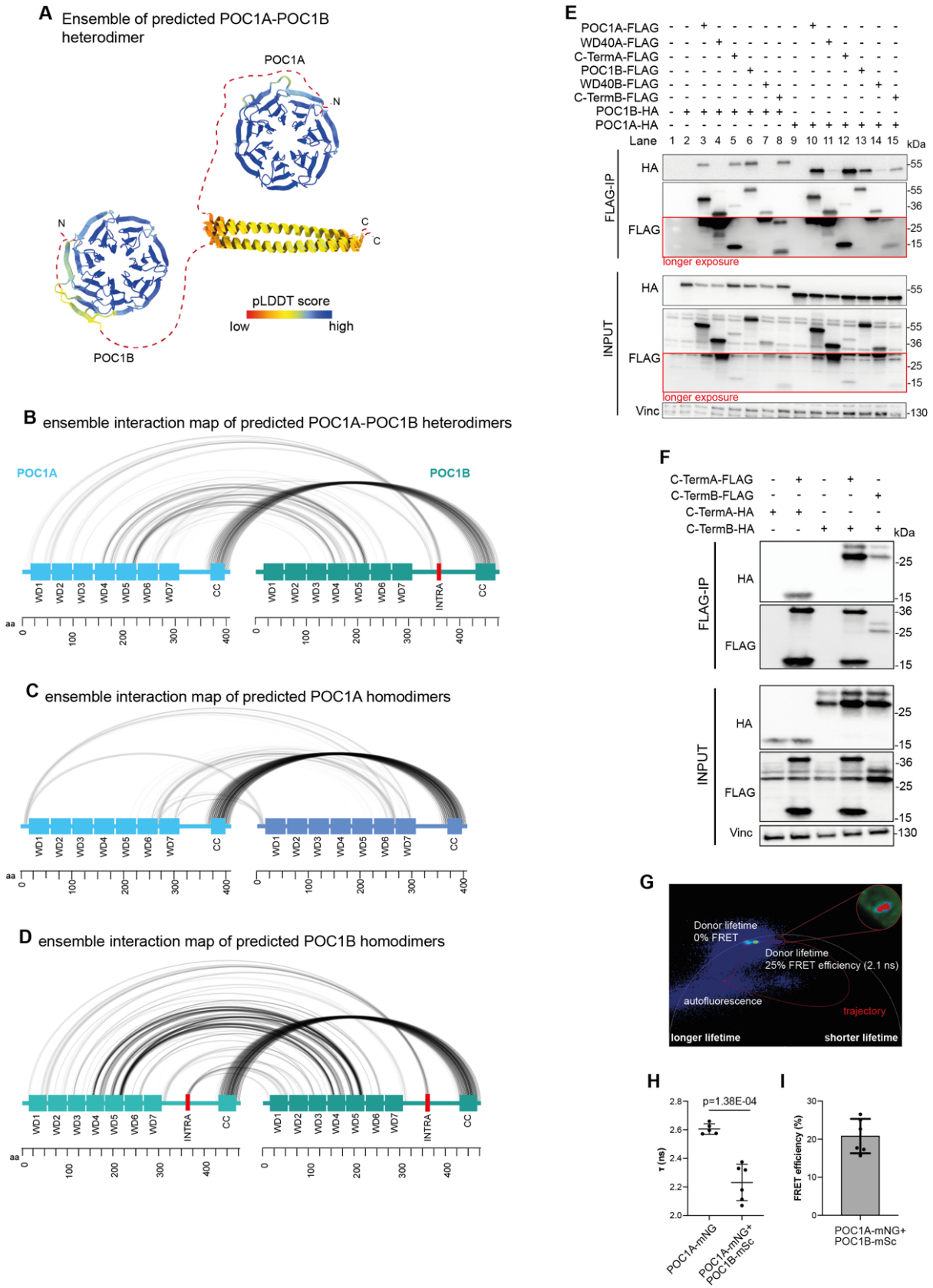

Figure 23: The coiled-coil mediates homo- and heterodimer formation between the POC1 proteins
(**A**) Ensembles of the 10 best ranked AlphaFold-Multimer POC1A-POC1B heterodimer predictions. Colouring based on pLDDT score, showing regions with high and low confidence. The interaction is mediated by the C-terminal coiled-coil of both POC1 proteins. (**B**, **C**, **D**) Ensemble interaction map of a POC1A-POC1B heterodimer (**B**), a POC1A homodimer (**C**) and a POC1B homodimer (**D**). Thicker and darker lines indicate interactions that are predicted to be more robust. The most robust interactions are predicted to involve the coiled-coil regions in all

three cases. aa: amino acids. (**E**) Representative FLAG IP from HEK293T cells expressing FLAG-tagged full-length or subdomains of either *POC1A* or *POC1B* together with HA-tagged full-length *POC1A* or *POC1B* to test for an interaction between these proteins. Vinculin is input control. N=3 biologically independent experiments. (**F**) FLAG-IP of HEK293 cells expressing FLAG and HA-tagged C-terminal domains of *POC1A* or *POC1B* to verify that interactions are mediated by the C-terminus as predicted. Vinculin was used as a loading control. (**G**) Representative image of the FLIM-FRET trajectory from a measurement of one cell co-transfected with POC1A-mNeonGreen (donor) and POC1B-mScarlet-I (acceptor). Signals with a shorter lifetime are depicted on the right side of the phasor plot, which corresponds to a quenching of the donor signal in the presence of the acceptor. The inset shows the centrosomes and in red are the signals marked that can be found on the right side of the phasor plot. (**H**) Quantification of the fluorescence lifetime of the Donor from the representative experiment shown in (**G**) (N=2 biologically independent experiments, with n> 5 living cells per condition in each experiment). Data are presented as mean ± SD. Statistics for the representative experiment were derived from two-tail unpaired *t*-test. (**I**) FRET efficiency of the representative experiment shown in (**H**). Data are presented as mean ± SD. *Figure modified and adapted from* (Sala et al., *Nat Comm* 2024)[133].

3.12 Induced dimerization of the WD40 domain and the C-terminal coiled-coil region restores centrosomal localization of POC1A and POC1B

In previous experiments, I showed that the subdomains of POC1A and POC1B alone are not sufficient to be recruited to centrosomes, indicating that the fusion of both domains is necessary to establish centriolar localization (see Fig. 11). To test this model, I utilized an inducible GFP:GBP dimerization system in living cells (Fig. 24A). For this, I generated different constructs of POC1A and POC1B subdomains tagged either with EGFP or with the GFP-binding protein (GBP, a 13 kDa soluble protein) and mScarlet-I (as a reporter) (Fig. 24B). Upon induction, the subdomains dimerize mediated by the binding of GBP to EGFP and then the centrosomal localization was checked (Fig. 24A). Cells were analyzed using IF to determine whether the dimerized subdomains localize to the centrosome based on co-localization with the centrosomal marker γ-tubulin (Fig. 24C). Consistent, with my previous findings, cells expressing either the EGFP-tagged WD40 domain or the GBP-tagged coiled-coil region alone of both POC1 proteins do not show a signal at the centrosome (Fig. 24C-i-v and xv, xvi). However, cells co-expressing the EGFP-tagged WD40 domain and the GBP-tagged coiled-coil region, showed a centrosomal localization (Fig. 24C- vii, ix). The expression of the domains is interchangeable, as expression of the WD40 domain of one POC1 protein and the coiled-coil region of its counterpart resulted also in a centrosomal localization (Fig. 24C-vii, viii). Interestingly, the dimerization of two WD40 domains (Fig. 24C-xii-xiv) did not facilitate a centrosomal localization as well as dimerization of two WD40 domains containing the linker region (Fig. 24C-xvii-xx). All in all, the data indicates that the centrosomal localization of the POC1 proteins requires the fusion of the WD40 domain and the coiled-coil region.

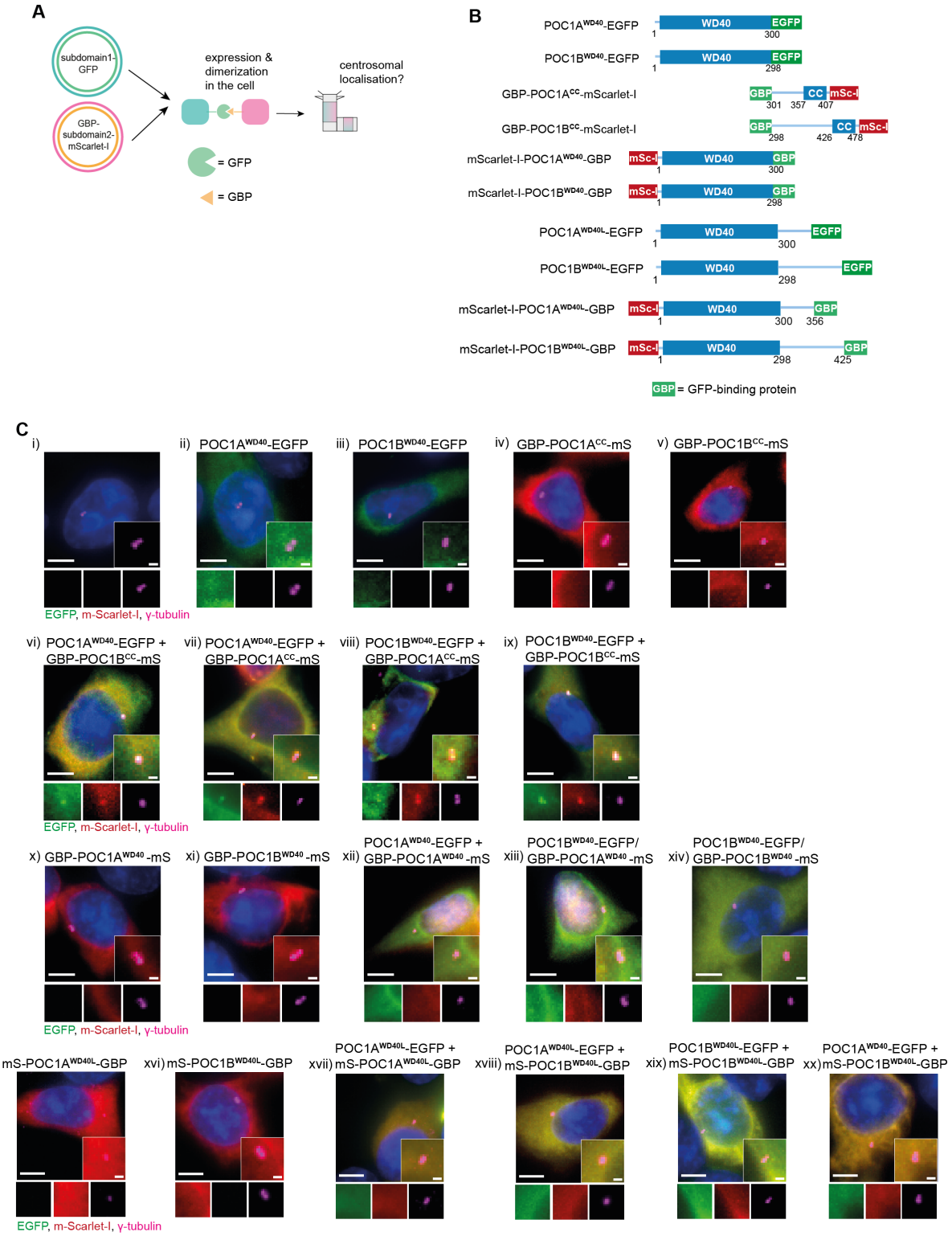

Figure 24: POC1´s WD40 domain and C-terminal coiled-coil together are necessary for centrosomal localization

(**A**) Experimental set-up for the GFP-binder dimerization in which subdomains of POC1 proteins were fused either with GFP or with GBP (mScarlet-I functions as a reporter). Upon expression, the subdomains should dimerize within the cell via the strong affinity of the GBP for GFP. Centrosomal localization upon dimerization was checked via IF. (**B**) Constructs used for the GFP-GBP dimerization experiment within the cell. (**C**) IF of HEK293T cells transfected with the generated constructs shown in (**B**). Centrosomal localization of the EGFP-tagged (green) and m-Scarlet-I-tagged (red) proteins was analyzed using γ-tubulin (magenta). Scale bars: 10 µm, magnification scale bars: 1 µm. N=3 biologically independent experiments. *Figure modified and adapted from* (Sala et al., *Nat Comm* 2024)[133].

3.13 Loss of POC1A and POC1B proteins leads to structurally defective centrioles

The differences in the impact on luminal centriole proteins after loss of POC1A and POC1B, reflects a complex organization pattern within centrioles. I next asked whether disturbing the protein composition affects the overall centriole structure. To answer this question, centrioles of *POC1A*$^{-/-}$, *POC1B*$^{-/-}$ and *POC5*$^{-/-}$ cells were analyzed with electron microscopy (EM). Longitudinal sections of control cells showed centrioles with an intact microtubule wall and with distal and subdistal appendages (green and yellow arrowheads) (Fig. 25A). Cross-sections of centrioles from the proximal region showed the canonical nine-fold radial organization of the microtubule triplets that are connected via the A-C linker (indigo arrowhead) and in the distal part, the appearance of an inner luminal ring, the inner scaffold (orange arrow). In contrast, *POC1A*$^{-/-}$, *POC1B*$^{-/-}$ and *POC5*$^{-/-}$ showed a defective microtubule wall with entire MT triplets missing in the proximal and distal region (magenta arrowheads). The same outcome was also observed via u-ExM (Fig. 25A). Strikingly, the most proximal region of the centrioles appeared to be intact in all knockout cells, therefore the length at which structural defects are occurring was measured (Fig. 25B). In control cells, centrioles were 400 nm long and structurally intact. However, in *POC1A*$^{-/-}$ and *POC5*$^{-/-}$ cells, centriolar defects typically occurred at an average length of 200 nm, whereas defects in *POC1B*$^{-/-}$ cells extended even further proximally at a length of 175 nm. Thus, the impact on the protein composition within the centriole upon loss of the proteins POC1A, POC1B and POC5, leads ultimately to instable and defective centrioles.

The observed defects in the centriolar wall prompted me to check PCM components like γ-tubulin, PCNT and CEP192 in *POC1A*$^{-/-}$ and *POC1B*$^{-/-}$ cells via IF. The signal intensity of these proteins was significantly reduced in the knockout cell lines compared to control cells (Fig. 25C-E). Interestingly, γ-tubulin was not only decreased in *POC1A*$^{-/-}$ (as expected due to the loss of the inner luminal pool), but also in *POC1B*$^{-/-}$ (Fig. 25C). U-ExM analysis of *POC1B*$^{-/-}$ revealed that the distribution of the inner luminal pool of γ-tubulin is not affected in those cells (Fig. 15). This indicates that either γ-tubulin is reduced inside centrioles but the length distribution is unaffected or that the PCM pool is affected upon loss of POC1B.

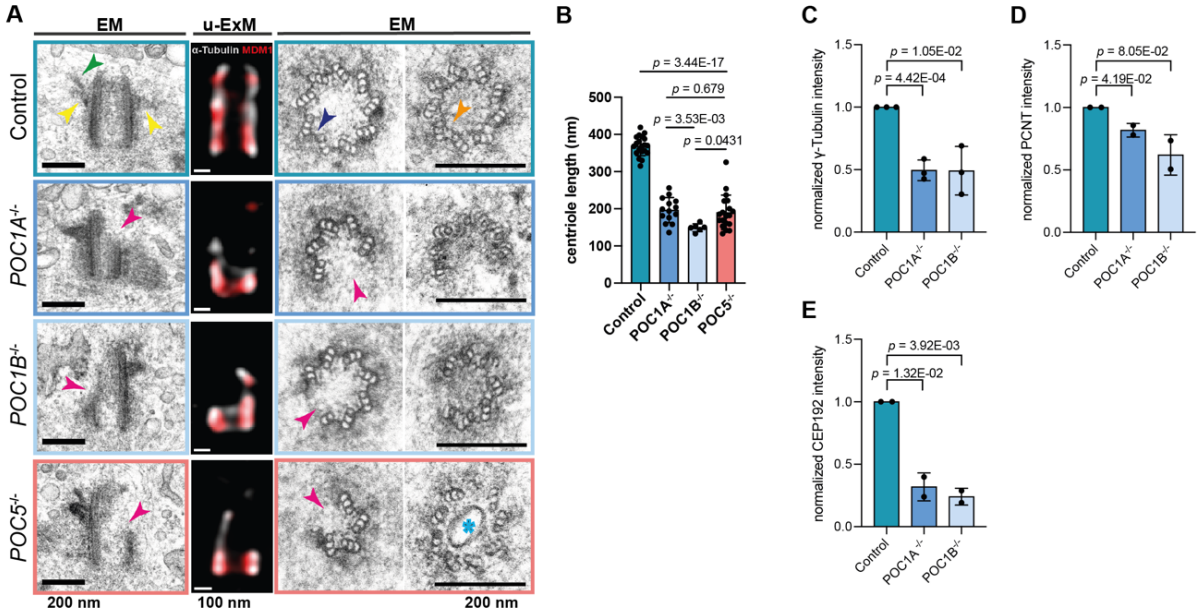

Figure 25: Loss of inner scaffold proteins leads to structurally defect centrioles
(**A**) Longitudinal view and cross-sections of G1 centrioles from control, *POC1A*$^{-/-}$, *POC1B*$^{-/-}$ and *POC5*$^{-/-}$ cells analyzed via EM. All knockout cell lines show broken centrioles with missing MT triplets (magenta arrows). However, the most proximal region appears to be intact (indigo arrow). Cross-sections of *POC1A*$^{-/-}$ and *POC5*$^{-/-}$ cells show deformation or loss of the inner scaffold structure in the distal half of the centrioles (blue asterisk). The phenotype observed in EM corresponds to u-ExM data. Scale bars: 200 nm (EM) and 100 nm (u-ExM). (**B**) Quantification of (**A**). Longitudinal centrioles were analyzed and the length at which a defect occurs was measured. Data are presented as mean ± SD. Statistics were derived from two-tail unpaired *t*-test. (**C, D, E**) Quantification of signal intensities from γ-tubulin and the PCM components PCNT and CEP192. Data are presented as mean ± SD. All statistics were derived from two-tail unpaired *t*-test analysis of N= 3 biologically independent experiments, *n* > 100 cells per cell line for each experiment. *(***A** *and* **B***) modified and adapted from* (Sala et al., *Nat Comm* 2024)[133].

3.14 Structural defects lead to functional defects of centrosomes in *POC1A*$^{-/-}$ and *POC1B*$^{-/-}$ cells

Centrioles of *POC1A*$^{-/-}$ and *POC1B*$^{-/-}$ lose their structural integrity, leading to broken and short centrioles. These structural defects may impact the overall biogenesis and function of centrosomes. To test this hypothesis, I analyzed the *POC1*$^{-/-}$ cell lines for aberrations in centrosome and centriole numbers. The phenotype observed in both knockout cell lines was a significant increase of up to 40% of cells showing more than two centrosomes compared to control cells (Fig. 26A). Additionally, I counted the centriole number based on the distal tip protein CEP97 in G1 and G2 cells and observed an increase of *POC1A*$^{-/-}$ and *POC1B*$^{-/-}$ cells showing more than two centrioles in G1 and more than four centrioles in G2 (Fig. 26B, C). This might indicate defective centrosome biogenesis, which at the end triggers the *de novo* centriole assembly. Although the loss of *POC1A* and *POC1B* in *POC1A*$^{-/-}$ and *POC1B*$^{-/-}$ cells disrupts the structural integrity of centrioles and affects centrosome biogenesis, the phenotype is not severe enough to prevent centriole formation entirely. This led me to ask what the consequences are if both *POC1* genes are none-functional. For this, I analyzed *POC1A*$^{-/-}$/*POC1B*$^{-/-}$ double

knockout cells (hereafter, *POC1A*/*B*$^{-/-}$ cells). Surprisingly, most interphase cells of *POC1A*/*B*$^{-/-}$ cells lost centrosomal Centrin and γ-tubulin signals (Fig. 26D). In contrast to the control and the single knockout cell lines, only roughly 8% of *POC1A*/*B*$^{-/-}$ showed co-localization of γ-tubulin and PCNT, indicating loss of centrosomes in most cells (Fig. 26E).

To confirm this observation, siRNA experiments in the single knockouts were conducted in which *POC1B* was depleted in the *POC1A*$^{-/-}$ cell line and *vice versa* (Fig. 26F). *POC1* single knockouts treated with the control siRNA showed in the majority of the cells two or more γ-tubulin foci. This number dropped to only 40-50% after *POC1A* (in *POC1B*$^{-/-}$ cells) or *POC1B* (in *POC1A*$^{-/-}$ cells) depletion (Fig. 26G). In addition, a reduction in centriole number was observed after depletion of *POC1A* (in *POC1B*$^{-/-}$ cells) or *POC1B* (in *POC1A*$^{-/-}$ cells) compared to the control siRNA (Fig. 26H). Due to the fact, that loss of *POC1A* and *POC1B* primary impact the central to distal region of centrioles, whereas the proximal region appears to be intact (Fig. 25), I stained *POC1A*/*B*$^{-/-}$ cells for CEP44, a proximal centriole marker. Compared to control cells, nearly 98% of *POC1A*/*B*$^{-/-}$ cells showed no co-localization of CEP44 and PCNT, indicating that centrioles are also affected in the proximal region (Fig. Fig 26I, J). The loss of centrosomal signal observed in the *POC1A*/*B*$^{-/-}$ cell line resembles the phenotype of *CEP295*$^{-/-}$ cells that do not show any centrosomal signal[160]. However, in these cells an increase of centrioles was detected in prolonged S-phase arrested cells, indicating that centrioles keep repeatedly form[160]. Therefore, I analyzed *POC1A*/*B*$^{-/-}$ cells in specific cell phases to see if the same case applies after simultaneous loss of *POC1A* and *POC1B*. During the progression of the cell cycle, the percentage of cells showing a co-localization of γ-tubulin and CEP97 was gradually increasing, especially in G2, suggesting that the formation of centrioles via *de novo* assembly is not affected *per se* but the stability of the centrioles is diminished (Fig. 26K). In line with these findings, EM analysis of *POC1A*/*B*$^{-/-}$ cells showed in rare cases only remnants of centrioles (Fig. 26L).

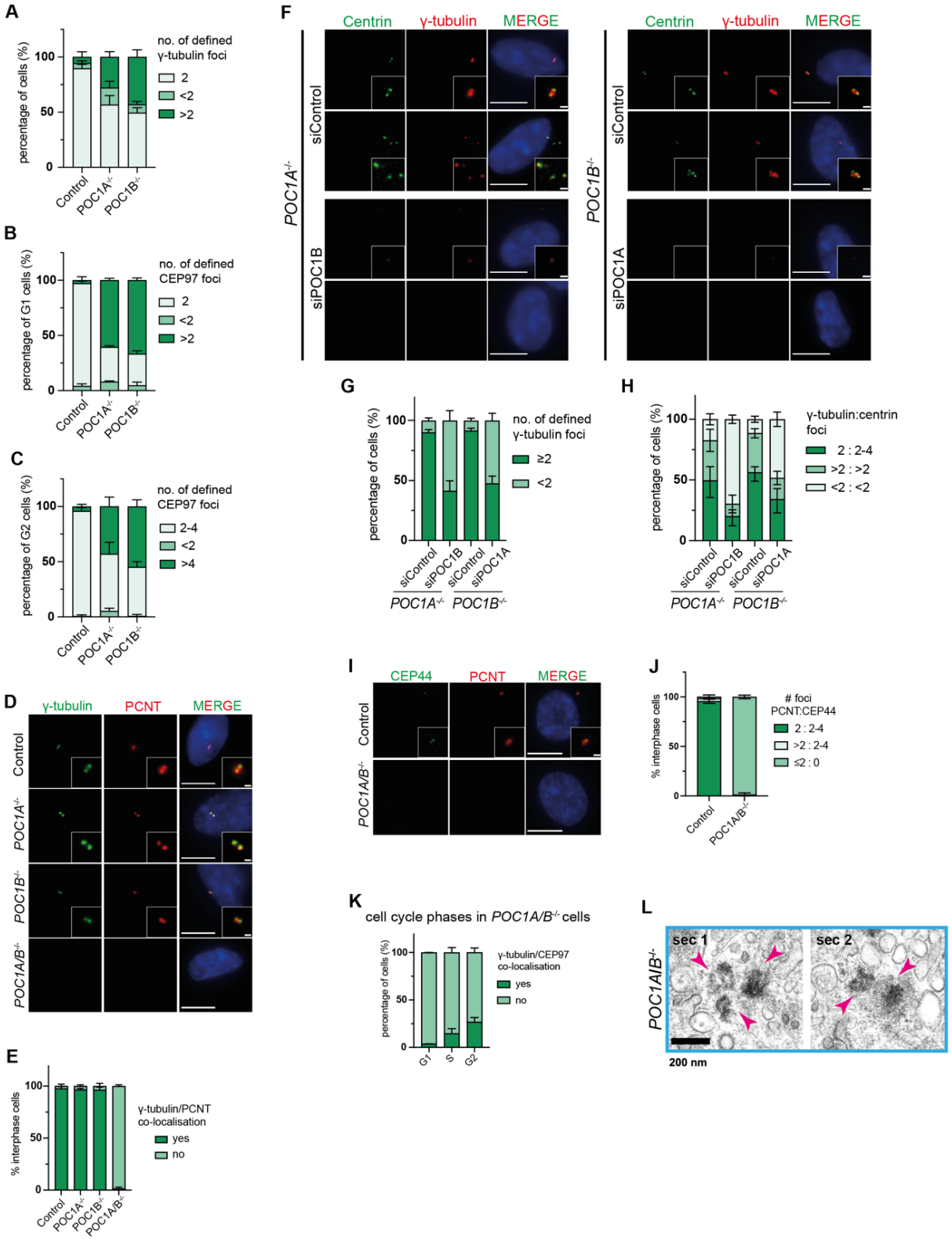

Figure 26: POC1A and POC1B act together in centriole biogenesis

(**A**) Quantification of the γ-tubulin signals as a proxy for centrosome number in interphase *POC1*$^{-/-}$ cells using γ-tubulin antibody by IF. An increase in γ-tubulin foci was observed, indicating centrosome amplification. (**B, C**) Quantification of the centriole numbers in G1 and G2 cells using the distal tip protein CEP97 as a centriolar marker. Centriole numbers were altered in the *POC1*$^{-/-}$ knockout cell lines, leading to an increase of overamplified centrioles in G2 phase. (**D**) IF images of interphase control, *POC1A*$^{-/-}$, *POC1B*$^{-/-}$ and *POC1A/B*$^{-/-}$ cell lines stained against γ-tubulin (green) and PCNT (red). In most of the double knockout cells the centrosomal signal was lost. Scale bars: 10 µm, magnification scale bars: 1 µm. (**E**) Quantification of (**D**). (**F**) IF images of *POC1*$^{-/-}$ cells treated with siRNAs targeting *POC1A* and *POC1B* and stained against Centrin (green) and γ-tubulin (red). Scale bars: 10

μm, magnification scale bars: 1 μm. (**G**, **H**) Quantification of (**F**). After siRNA depletion, centriole and centrosome numbers decreased. (**I**) IF images of interphase control and *POC1A/B*$^{-/-}$ cell lines stained against CEP44 (green) and PCNT (red). Scale bars: 10 μm, magnification scale bars: 1 μm. (**J**) Quantification of the percentage of cells from (**I**) showing CEP44 and PCNT co-localization. (**K**) Percentage of *POC1A/B*$^{-/-}$ cells showing centrosomal signal in different cell cycle phases. During S and G2 phase, the percentage of cells showing co-localization is increasing. Data are presented as mean ± SD. N=3 biologically independent experiments, $n > 80$ cells per cell cycle phase and per cell line in each experiment. (**L**) EM images of *POC1A/B*$^{-/-}$ cells. In the majority of *POC1A/B*$^{-/-}$ cells, no clear centriolar structure was observed. In rare cases, centriole fragments were detected by EM. Scale bar: 200 nm. (**B**, **C**, **E**, **J**) Data are presented as mean ± SD. N=2 biologically independent experiments, $n > 100$ cells per cell line for each experiment. *Figure modified and adapted from* (Sala et al., *Nat Comm* 2024)[133].

3.15 Loss of POC1A and POC1B causes mitotic defects

Structural defects in centrioles have direct consequences on the centrosome function which includes the formation of the mitotic spindle. In *POC1A*$^{-/-}$ and *POC1B*$^{-/-}$ cells, centriole integrity is defective and also numerical aberrations of centrosomes are frequently observed. This may translate directly into mitotic defects, showing improper spindle formation. To check this possibility, I analyzed in each knockout cell line metaphase cells stained against α-tubulin and the centrosomal markers γ-tubulin and CDK5RAP2 (Fig. 27A). Indeed, the majority of *POC1A*$^{-/-}$ and *POC1B*$^{-/-}$ cells showed various mitotic defects, including monopolar, multipolar and pseudobipolar spindles. Multipolar spindles were the most prominent phenotype in both cell lines (Fig. 27A, B). Compared to the single knockout cell lines, an increase in the percentage of cells showing defective spindles was observed in the *POC1A*/*B*$^{-/-}$ cell line (Fig. 27B), indicating an enhanced effect on centrosome function when both POC1 proteins are lost. This observation is in concordance with the severe centriole phenotype in the *POC1A*/*B*$^{-/-}$ cell line. Interestingly, the majority of *POC1A*/*B*$^{-/-}$ cells show a pseudobipolar spindle configuration with dispersed γ-tubulin signals at each site of the poles instead of the multipolar spindle observed in the single knockouts (Fig. 27A, B).

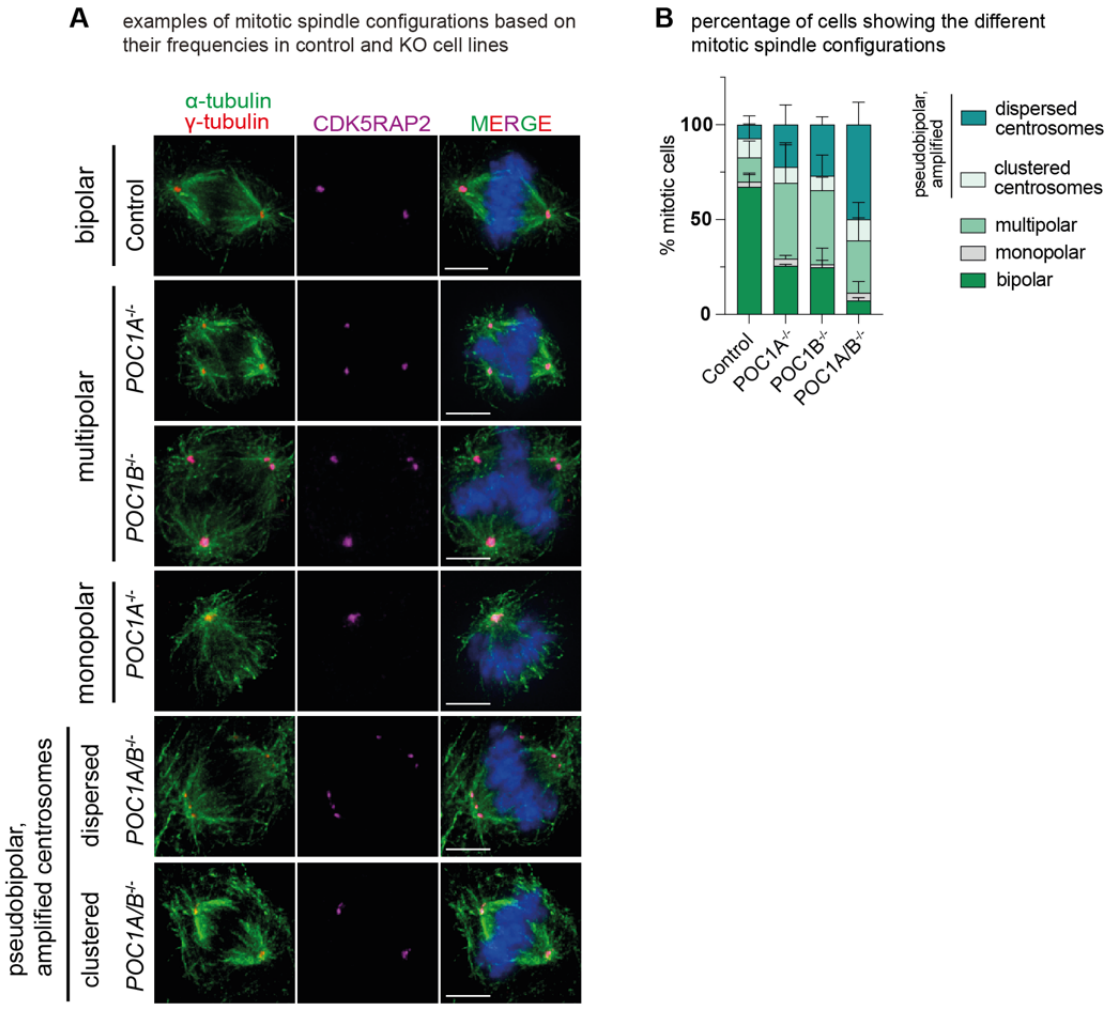

Figure 27: Mitotic defects in *POC1* knockout cell lines
(**A**) Mitotic spindle configurations based on their frequency observed in control and knockout cell lines. Green: α-tubulin, red: γ-tubulin, magenta: CDK5RAP2. Scale bars: 5 µm. (**B**) Quantification of the percentage of cells showing the different spindle configurations shown in (**A**). Data are presented as mean ± SD. N=2 biologically independent experiments, $n > 50$ cells per cell line for each experiment. *Figure modified and adapted from* (Sala et al., *Nat Comm* 2024)[133].

3.16 POC5 forms a tetramer and is an integral component of the inner scaffold

Within the centriole, the interaction between POC1A and POC5 may play an important role in centriole integrity, because it establishes the connection between the inner scaffold and the luminal pool of augmin-γTuRC that was shown to stabilize centrioles[159]. POC5 is a conserved protein and predicted to have coiled-coil regions and Centrin-binding domains[59]. AlphaFold2 predicts POC5 with a long coiled-coil helix flanked by disordered regions at both sites and further indicates the possibility of POC5 forming a tetramer in which two POC5 dimers interact with each other via their N-termini (residues 153-184) (Fig. 28A). To gain a deeper understanding about the structural properties of POC5, I, together with Dr. Martin Würtz, expressed and isolated via affinity purification and size-exclusion chromatography (SEC)

FLAG-tagged human POC5 in complex with Centrin2 from a recombinant insect cell expression system. Coomassie-stained SDS-PAGE and SEC confirmed successful purification of the POC5-Centrin2 complex (Fig. 28B, C). The purified complex was subsequently analyzed with negative stain EM coupled with 2D classification and single particle averaging for low-resolution 3D reconstruction. This revealed a ~50 nm elongated structure with two globular heads on each site that are in close proximity to the predicted Centrin-binding region (Fig. 28D). Further indication for a POC5 tetramer comes from mass photometry analysis, in which a pronounced peak at 418 kDa occurred, corresponding to four POC5 molecules with 6-8 molecules of Centrin2 molecules (Fig. 28E). To verify the predicted site required for tetramerization and that the elongated structure observed in the negative stain EM derives from a POC5 tetramer, a POC5 mutant lacking residues 153-184 (predicted site for tetramerization), was expressed in complex with Centrin2 and purified from insect cells, followed by negative stain EM analysis (Fig. 28F-H). The structures obtained after single particle averaging, displayed only half the length of the wild type POC5-Centrin2 complex and only one globular head, indicating that the mutant assembles only to a POC5 dimer with bound Centrin2 (Fig. 28H). Subsequent mass photometry analysis reflects this observation and shows a peak at 169 kDa, corresponding to two POC5 molecules and 1-2 attached Centrin2 molecules (Fig. 28I). This verifies that the elongated structures are formed by a POC5 tetramer and that the predicted site for tetramerization at amino acid residues 153-184 is indeed required to form the tetrameric formation (Fig. 28J).

Deletion of the C-terminal POC1-binding site reduced the centriolar recruitment of POC5 and was inefficient to rescue the loss of the luminal γ-tubulin in *POC5*$^{-/-}$ cells (Fig. 20). Therefore, I tested whether also the tetramerization is important for the function of POC5 by expressing HA-tagged *POC5*$^{\Delta 153-184}$ in *POC5*$^{-/-}$ cells. The mutant localized at centrosomes as seen by conventional IF (Fig. 28K), but u-ExM revealed that it did not show the proper inner centriole localization as observed with WT POC5 (Fig. 28L). In addition, *POC5*$^{\Delta 153-184}$ was not able to rescue the loss of the luminal γ-tubulin pool and centrioles still exhibit microtubule wall defects (Fig. 28L). These results collectively indicate that POC5 forms a tetramer, and while tetramerization itself is not required for centriolar localization, it is essential for fulfilling its function within the centriole.

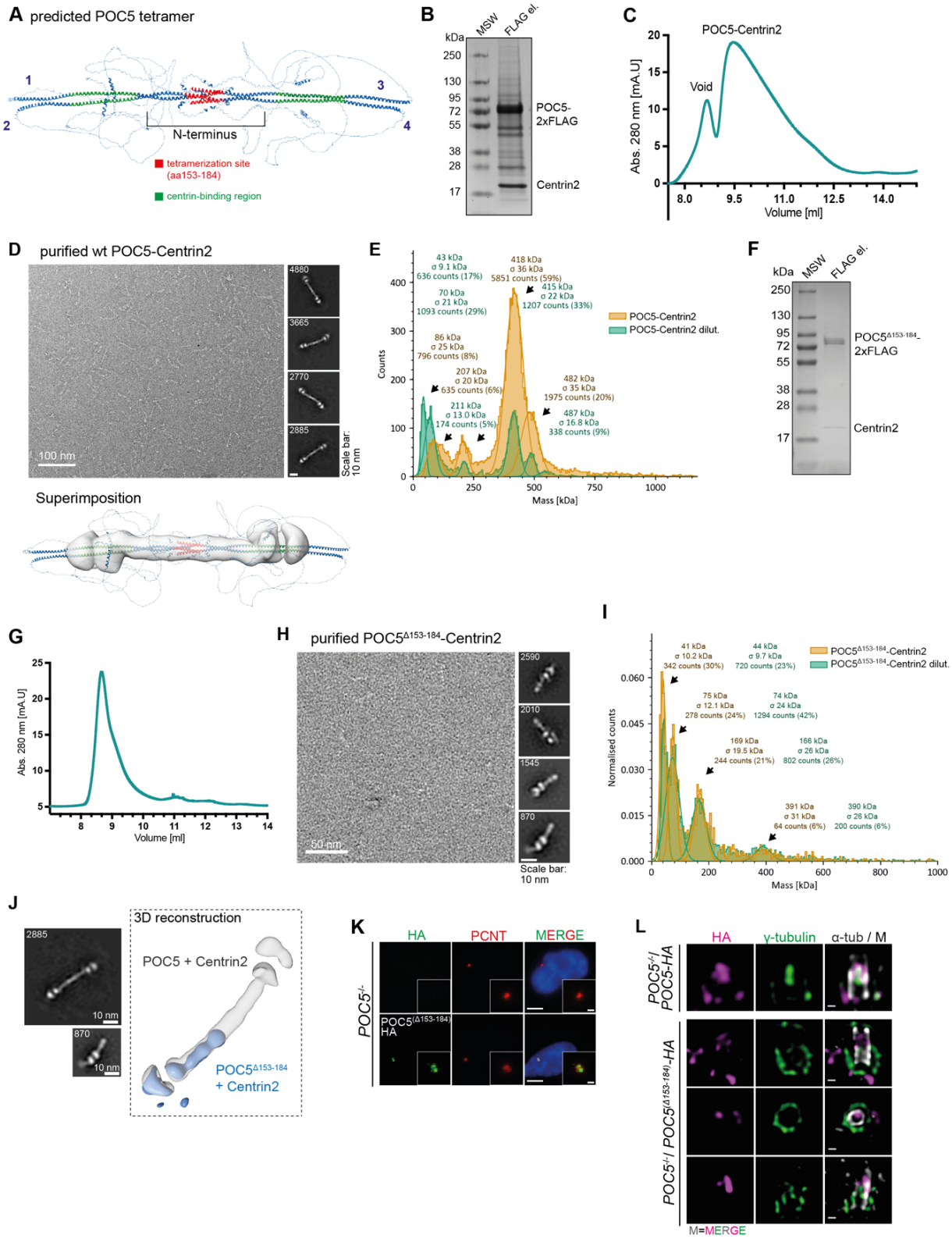

Figure 28: Structural analysis of the POC5 tetramer

(**A**) AlphaFold2 prediction of a POC5 tetramer. The site required for tetramerization is predicted to be at residues 153-184 (depicted in red). (**B, C**) Coomassie Blue stained SDS-PAGE and Chromatogram of the SEC purification (using Superdex 6 increase column) for the POC5-Centrin2 construct. N= 3 biologically independent experiments for protein expression and purification. (**D**) Representative negative stain EM micrograph from purified human wild type POC5-Centrin2. The numbers in the left upper corner of the 2D class averages indicate particle numbers. Superimposition of the negative stain EM 3D reconstruction with the AlphaFold prediction places the globular domains in proximity to the Centrin-binding region. Scale bars: 100 nm and 10 nm. N=1 biologically independent experiment. (**E**) Mass photometry histogram of the purified wild type POC5-Centrin2 sample shown in (**C**). A

distinct peak can be observed at 415-418 kDa for the undiluted (orange) and diluted (green) sample corresponding to the tetrameric formation of POC5 bound to multiple Centrin2 molecules. Experiment performed once. (**F, G**) Coomassie Blue stained SDS-PAGE and Chromatogram of the SEC purification (using Superdex 75 column) for the POC5$^{\Delta 153\text{-}184}$-Centrin2 construct. N=2 biologically independent experiments for protein expression and purification. (**H**) Representative negative stain Electron Microscopy (EM) micrograph from purified human POC5$^{\Delta 153\text{-}184}$-Centrin2. Scale bars: 100 nm and 10 nm. N=1 biologically independent experiment. (**I**) Mass photometry histogram of the purified POC5$^{\Delta 153\text{-}184}$-Centrin2 sample shown in (**G**). Experiment performed once. (**J**) Comparison of wild type POC5-Centrin2 and POC5$^{\Delta 153\text{-}184}$-Centrin2. Left: negative stain 2D classes, scale bars and particles numbers are given. Right: negative stain EM 3D reconstructions of wild type POC5-Centrin2 (grey) and POC5$^{\Delta 153\text{-}184}$-Centrin2 (blue). POC5$^{\Delta 153\text{-}184}$-Centrin2 particles show a structure shorter than the wild type. (**K**) Representative IF images of *POC5*$^{-/-}$ cells expressing HA-tagged *POC5*$^{\Delta 153\text{-}184}$ and stained against HA (green) and PCNT (red). The mutant localizes to centrosomes. Scale bars: 5 µm, magnification scale bars: 1 µm. (**L**) U-ExM images of *POC5*$^{-/-}$ cells expressing the HA-tagged mutant *POC5*$^{\Delta 153\text{-}184}$ and stained against HA (magenta), γ-tubulin (green) and α-tubulin (grey). Scale bar: 100 nm. N=2 biologically independent experiments. *(***A-H** *and* **J-L***) modified and adapted from* (Sala et al., *Nat Comm* 2024)[133].

3.17 Spatial organization of the POC1A-POC1B heterodimer within the inner scaffold

POC1A and POC1B have a similar domain architecture with an N-terminal WD40 domain and a C-terminal coiled-coil. Based on my previous results, the interaction between the two proteins is mediated by the C-terminal coiled-coil, leading to the WD40 domains exposed and available for interaction with other proteins. WD40 domains function as protein-protein interaction platforms and through different binding modes a single WD40 protein can interact with different substrates[161,162]. A recent study proposed POC1 of *Tetrahymena* as a triplet microtubule inner junction protein, sealing the junction between the A-B tubule and B-C tubule[140]. Within the centriole, POC1A and POC1B show differences in terms of MT wall distance, with the Middle/C-terminal (M/C) regions residing closer to the lumen in the case of POC1A or more towards the MT wall in the case of POC1B. This led me to the hypothesis, that inside the centriole the POC1A-POC1B heterodimer displays a certain orientation with the WD40 domains facing opposite directions. To test this, I tagged the N-terminal region of POC1A and POC1B with EGFP and expressed these constructs, hereafter EGFP-POC1A and EGFP-POC1B, in the control and *POC1A*/*B*$^{-/-}$ cell line. IF analysis verified that the N-terminally-tagged constructs localize to centrosomes and that they can rescue the loss of centrosomes in *POC1A*/*B*$^{-/-}$ cells as marked by the co-localization with γ-tubulin (Fig. 29A). Using u-ExM, I determined the distance of EGFP-POC1A and EGFP-POC1B and compared with the distance of the M/C region of the respective proteins (Fig. 29B, C). In control cells, EGFP-POC1A localizes closer towards the centriole lumen compared to the M/C region of POC1A, whereas for POC1B the opposite was observed: EGFP-POC1B resides closer to MT wall than the M/C region of POC1B (Fig. 29C). This is consistent with recent findings in *Tetrahymena*[140]. Intriguingly, in *POC1A*/*B*$^{-/-}$ cells the localization of EGFP-POC1A shifts towards the MT wall, whereas the localization of EGFP-POC1B remains unchanged (Fig. 29C),

indicating that POC1A may compensate to some extent for the absence of POC1B. Taken together, the POC1A-POC1B heterodimer displays a certain spatial organization within the centriole, in which the WD40 domain of POC1A is facing towards the centriole lumen, while the WD40 domain of POC1B is facing the MT wall (Fig. 29D).

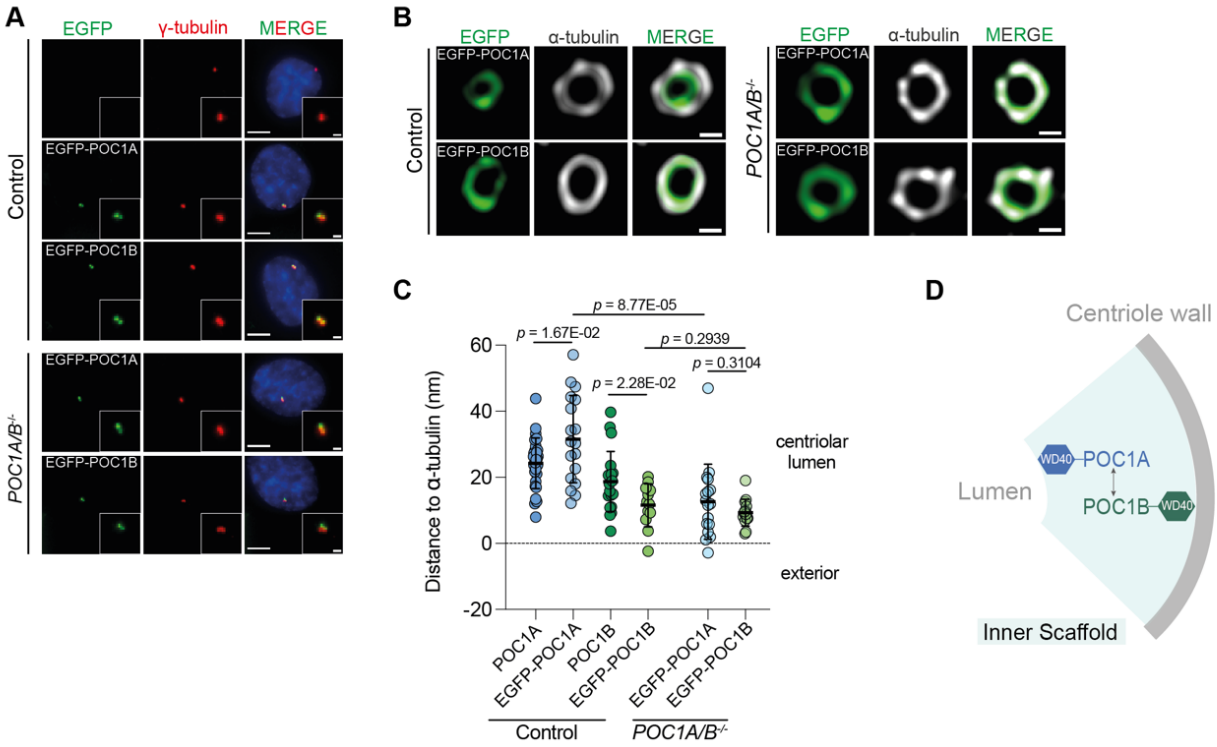

Figure 29: The POC1A-POC1B heterodimer orientation within the inner scaffold
(**A**) IF images of control and *POC1A/B*$^{-/-}$ cells expressing N-terminally EGFP-tagged versions of *POC1A* or *POC1B* and stained against EGFP (green) and γ-tubulin (red). Tagging of the N-terminus does not affect centrosomal localization. Scale bars: 5 µm, magnification scale bars: 1 µm. (**B**) U-ExM images of top view centrioles from cells shown in (**A**) stained against EGFP (green) and α-tubulin. Scale bar: 100 nm. (**C**) Quantification of centrioles shown in (**B**). The distance between the EGFP signal and α-tubulin was measured compared to the distance exhibited when stained with an antibody detecting epitopes at the C-terminus of the POC1 proteins (labelled as POC1A and POC1B, respectively). The data set for centrioles stained with the antibodies detecting the M/C-portions of the POC1 proteins was shown in **Fig. 10I** and is included for better comparison. (**D**) Model of the spatial organization of the POC1A-POC1B heterodimer. The WD40 domains are facing opposite directions, with POC1A's WD40 domain being closer towards the lumen and POC1B's closer to the centriole wall. *(**A-C**) modified and adapted from* (Sala et al., *Nat Comm* 2024)[133].

4. Discussion

4.1 POC1A and POC1B are early recruited centriolar lumen proteins and show overlapping localization

The centriole, as a central building block of the centrosome, that ensure integrity, duplication, and cilia formation, has a complex structure involving numerous proteins that define its polarity through the formation of substructures such as the cartwheel, the inner scaffold, the distal and subdistal appendages. One of these substructures, the inner scaffold, is a ring-like assembly in the centriole lumen and is suggested to function in centriole stability and integrity[85,132]. Based on localization studies, POC1B is proposed to be an inner scaffold component[85]. Humans, vertebrates in general, possess a paralogous form of POC1B called POC1A. Its function has not intensively been studied, primarily due to the assumption that it functions redundantly with POC1B[104,163]. Previous studies showed centrosomal localization for POC1A and indicate a synergistic role with POC1B3. Despite these studies, the exact centriolar localization and the role of POC1A has not been determined.

Based on the data presented in this study, I could show via u-ExM that allows for an in-depth analysis of centrioles, that POC1A, like POC1B, is a centriolar lumen protein that is localized in the central part of the centriole. Although both POC1 proteins have overlapping localization, two main differences were revealed during the study: First, while POC1A is restricted solely on the central part of centrioles, POC1B extends also towards the proximal centriole region. It has been shown, that POC1B interacts with the proximal centriole-to-centrosome conversion protein CEP44[63], which could explain the proximal extension of POC1B. Second, POC1A localizes closer towards the centriole lumen, whereas POC1B resides in the proximity of the centriole wall. These differences in localization indicate that both POC1 proteins may take over different functions within the centriole. POC1A and POC1B are both being recruited to the procentriole in S-phase, suggesting an important role in centriole biogenesis[133]. However, it is not known whether there are differences in the recruitment time between the POC1 proteins, as the temporal resolution of my study does not allow for the detection of smaller variations. Due to the proximal extension of POC1B and its interaction with CEP44, a possibility could be that POC1B´s recruitment precedes slightly ahead of POC1A´s. Additionally, an important aspect to investigate is which factors are the main recruiters of POC1A and POC1B to the centriole. The localization and function of the two POC1 proteins might help to narrow down potential candidates as recruitment factors. In the case of POC1B a function as a MT inner junction protein is proposed (see below in 4.5), thus, its recruitment could coincidence with the formation of B- and C- MTs and proteins involved in this could be tested.

4.2 POC1A and POC1B loss affects the centriolar distribution of inner scaffold components and leads to defective centrioles

In contrast to POC1B, POC1A has been not mentioned in the context of the inner scaffold. The localization pattern revealed in this study, however, made POC1A a likely candidate for an inner scaffold component. Interestingly, comparison of the distances to the microtubule wall between the previously proposed inner scaffold proteins POC5, FAM161A, CCDC15[85,90] and POC1A and POC1B, uncovered a similar localization between POC5 and POC1A, with both proteins being closer towards the centriole lumen than the other inner scaffold components[133]. POC1B and CCDC15 on the other hand shared a similar localization closer to the MT wall[133], indicating a possible relationship between these proteins. U-ExM analysis of centrioles from *POC1A*$^{-/-}$ and *POC1B*$^{-/-}$ cells, revealed that loss of POC1 proteins affect the protein composition at the central part of centrioles. While loss of POC1B primary affected the localization of CCDC15 and MDM1, loss of POC1A additionally affected the localization of POC5, FAM161A and Centrin as well as γ-tubulin and HAUS46. In support of this data, complementation experiments rescued the phenotypes and restored the localization of inner scaffold components. These observations point out two novel findings: POC1A plays a role in the inner scaffold and deletion of both *POC1* genes affect different subsets of proteins, indicating divergent functions between POC1A and POC1B. The impact on the inner scaffold upon loss of the POC1 proteins directly translated into structural defects in *POC1A*$^{-/-}$ and *POC1B*$^{-/-}$ centrioles as seen by EM and u-ExM data. In concordance with this, also *POC5*$^{-/-}$ cells showed broken centrioles, indicating the importance of the inner scaffold for centriole integrity. Interestingly, all knockout cell lines displayed defects at the central region of centrioles, while the proximal region appeared to be intact. Within the proximal region, two substructures can be found, the cartwheel (in procentrioles) and the A-C linker, and they might account together with the PCM for the centriole integrity in this region[81,83,85,165]. Centrioles from *POC1B*$^{-/-}$ cells exhibited defects more proximally compared to *POC1A*$^{-/-}$ and *POC5*$^{-/-}$ cells, fitting well with the more proximal localization of POC1B and might indicate a function of POC1B as a bridge between the proximal and central region of the centriole.

4.3 Localization of proximal proteins is extended to the distal region of centrioles upon loss of POC1A

The inner scaffold is affected by the loss of POC1A, therefore structurally defects in the central region can be observed in centrioles. Surprisingly, u-ExM analysis of the proximal proteins CEP44, CEP135 and CEP295 in *POC1A*$^{-/-}$ showed also an impact on these proteins. While in wild type conditions, these proteins are restricted to the proximal region, an extension towards

the distal half of the centriole occurred in *POC1A*$^{-/-}$ cells[133]. This led me to propose the hypothesis, that substructures within the centriole can restrict each other´s localization and can act therefore as internal rulers. Several substructures, like the A-C linker or the cartwheel, exist besides the inner scaffold, and each of these structures display a certain length and dimension in the centriole. Indications for this hypothesis came in addition from the experiment, where CEP44 was analyzed in *POC5*$^{-/-}$ cells, showing the same extension that was observed in *POC1A*$^{-/-}$, and in the *vice versa* experiment, where POC5 was checked in *CEP44*$^{-/-}$, with the result that POC5 extends now towards the proximal region. However, whether substructures inhibit each other simply by blocking binding sites within the centriole needs to be further investigated. Yet, this might be a possibility, since CEP44, CEP135 and CEP295 bind to MTs[63,166,167] and can bind to the MT centriole wall which is exposed when the inner scaffold is defective. In *POC1A*$^{-/-}$ cells the levels of the MT-binding proteins FAM161A and MDM1 at centrioles are reduced, leading potentially to exposed binding sites on the MT wall that could be then occupied by CEP44, CEP135 and CEP2956. In a recent study, a similar phenotype was observed in RPE1 *TUBD1*$^{-/-}$ and *TUBE1*$^{-/-}$ cells[77]. *TUBD1* and *TUBE1* encode for delta (δ-) and epsilon (ε-) tubulin that are belonging to the tubulin superfamily and are critical for the formation of the B- and C-tubule of the MT triplets[75,76,79,168]. *TUBD1*$^{-/-}$ and *TUBE1*$^{-/-}$ cells fail to recruit POC5 at centrioles and proximal proteins showed an extended localization[77]. However, contrary to *TUBD1*$^{-/-}$ and *TUBE1*$^{-/-}$ cells, the cartwheel component SAS-6 is not extended in *POC1A*$^{-/-}$, indicating different mechanisms responsible for restricting the cartwheel´s length. One factor, that could play a role, is the presence of MT triplets: while in *POC1A*$^{-/-}$ cells the MT triplet formation *per se* is not affected, *TUBD1*$^{-/-}$ and *TUBE*$^{-/-}$ cells fail to form B- and C-tubules, leading to a MT wall with only singlet MTs[77,79].

4.4 Structural differences between POC1A and POC1B shift preferred interactions towards one POC1 paralogue

POC1A and POC1B, although encoded by different genes, share a similar protein domain architecture with conserved features mainly found in the WD40 domain at the N-terminus and the coiled-coil at the C-terminus. The variable linker connecting these two domains, however, showed less conservation between the paralogues. Unlike *POC1B*$^{-/-}$ cells, *POC1A*$^{-/-}$ cells showed reduced POC5 levels at the centriole, altering its centriolar distribution and indicating that POC5 preferentially interacts with POC1A. AlphaFold2 predictions together with IP experiments confirmed an interaction between POC1A and POC5, mediated by the WD40 of POC1A and the POC1-binding region at the C-terminus of POC5. POC1B, based on AlphaFold2 predictions and IP experiments, also interacts with POC5, but less efficient

compared to POC1A. The predicted Intra beta strand provided by the linker region of POC1B, potentially weakens the POC5 binding to blade 1 of POC1B's WD40 domain. IP experiments with the chimeric version POC1Ab (WD40 domain of POC1A is fused with the C-terminus of POC1B, containing also POC1B's linker region) support this by showing less efficient binding of POC5 to POC1Ab, compared to POC1A. Intriguingly, contrary to the predictions, also the WD40 domain of POC1B binds less efficient to POC5, compared to the WD40 domain of POC1A, indicating that POC1B's overall efficiency to bind to POC5 is influenced by Intra as well as the WD40 domain. A possibility could be that post-translational modifications like phosphorylation, that are known to impact protein interactions, alter the structure of POC1B's WD40 domain. Phosphorylation of POC1B, but not POC1A, by Cdk1 has been described in mitotic cells[104] and it cannot be excluded that further phosphorylation events by other kinases occur during interphase. The structural differences (and potential modifications) between POC1A and POC1B leads to the preferred binding of POC5 to POC1A, explaining the shift of interaction towards one paralogue.

4.5 POC1A-POC1B heterodimers act as crosslinks within the inner scaffold and mediate different interactions

The inner scaffold is considered to play an important role in centriole stability and suggested proteins involved in this structure comprises POC1B, POC5, FAM161A and CCDC15[85,90]. Although certain aspects of the inner structure have been known, the interplay of the involved proteins and if there is a certain spatial organization within the inner scaffold still are poorly understood. The combined approach of AlphaFold2 predictions and the verification in the cellular context via IP experiments, revealed interactions between POC1A-POC1A, POC1B-POC1B and POC1A-POC1B, all mediated by their C-terminal coiled-coil. The interaction between POC1A-POC1B was further supported by FLIM-FRET in living cells. Following these data, it is plausible that a POC1A-POC1B heterodimer displays a certain internal organization mediated by the coiled-coil, and leaving the WD40 domains of the POC1 exposed for interactions with other scaffold proteins. In the u-ExM experiments presented in this study, POC1A exhibits a higher distance towards the MT wall compared to POC1B, when antibodies detecting the middle/C-terminal (M/C) region of these proteins were used. Tagging the N-terminus of both POC1 proteins and analysing how the distance changed, placed the WD40 domain of POC1A closer to the lumen, while the WD40 domain of POC1B resides closer to the MT wall in comparison to the M/C region of the respective proteins. This indicates indeed a specific orientation of the heterodimer with WD40 domains facing opposite directions in the inner scaffold. Due to this special configuration, the POC1A-POC1B heterodimer can act as

crosslinks, mediating interaction with different proteins e.g. to ensure anchoring of the inner scaffold via MT-binding proteins like FAM161A or MDM1. Data from *Tetrahymena* suggest POC1´s localization at the A-B inner junction of the core region from basal bodies based on a doughnut-shaped density found in this region that resembles a WD40 domain[140]. This would fit with the localization of POC1B's WD40 being closer to the MT wall, indicating that in vertebrates a splitting of function occurred and that the inner junction function is taken over rather by POC1B than POC1A.

4.6 Specialized and redundant function of POC1A and POC1B

POC1 proteins are conserved across various species, but while some species like *Chlamydomonas* and *Tetrahymena* have only one POC1 protein, vertebrates have two, POC1A and POC1B, that are encoded by different genes. It is likely that by the gene duplication event, functionality has been split to the two encoded paralogues, leading to a specialization of POC1A and POC1B. An initial indication of this is the distinct clinical phenotypes caused by mutations in the *POC1A* and *POC1B* genes. While mutations in *POC1A* lead to a specific disease called SOFT syndrome, mutations in *POC1B* are solely associated with retinal dystrophies[130,143,147,150]. In support of this, the localization analysis presented in this study, showed that POC1B extends to the proximal centriole region and is closer towards the MT wall, compared to POC1A. Furthermore, loss of POC1A or POC1B affect the centriolar distribution of different subsets of proteins, which in part is a result from the structural differences between the POC1 proteins, influencing thereby interactions as observed in the case of binding with POC5. Deletion of either *POC1* gene directly results in structurally defective centrioles, highlighting the crucial role each *POC1* gene plays in maintaining centriole stability. Despite the specialized functions of POC1A and POC1B, a certain degree of functional overlap can be observed, because the simultaneous inactivation of both *POC1* genes leads to a more severe phenotype with totally disintegrated centrioles and the overlapping binding of both POC1 proteins to some proteins. This is in line with published data, where co-depletion of both genes enhances centrosomal defects[104]. Additionally, centriolar distribution of CCDC15 and MDM1 are affected by both POC1 proteins, although it cannot be ruled out whether this is a direct consequence in the case of one POC1 protein and an indirect consequence in the case of its paralogue. Implications that one POC1 protein can to some extent take over the function of the other one come from the u-ExM analysis of *POC1A/B*$^{-/-}$ cells expressing N-terminally tagged *EGFG-POC1A*: the WD40 domain of POC1A shifts its localization towards the MT wall, potentially compensating for the absence of POC1B. Further investigation is needed to dissect further the roles of POC1A and POC1B and get a deeper knowledge at which point the specialization and redundancy occurs.

4.7 The POC5 tetramer via its interaction with POC1A is an integral part of the inner scaffold

POC5, a Centrin-binding protein and associated with centriole elongation[59], is a main interaction partner of POC1A identified in this study, backed up by AlphaFold2 predictions and IP experiments. Comparison between *POC1A*$^{-/-}$ and *POC5*$^{-/-}$ cells revealed similar phenotypes, comprising loss of the inner luminal augmin-γTuRC and Centrin pool, and broken centrioles. Due to the early recruitment of POC1A in S-phase and the reported recruitment of POC5 in G2[59], it is plausible to conclude that POC1A acts upstream of POC5. Furthermore, deletion of the POC1-binding region in POC5, dramatically reduced POC5's efficiency to be recruited to centrioles. This is supported by the notion that the centriolar localization of POC1A is not affected in *POC5*$^{-/-}$ cells. Based on these data, the focus was shifted on POC5 to gain more knowledge about its function as an inner scaffold component. AlphaFold2 predictions suggested a tetrameric formation of POC5 with two POC5-dimers interacting with each other through their N-terminal regions. Purification of human POC5-Centrin complex from a recombinant system and subsequent negative stain EM analysis revealed a symmetrical 50 nm long elongated structure. Deletion of the predicted tetramerization site (POC5$^{\Delta 153\text{-}184}$) resulted in an elongated structure that showed half of the length of the wild type POC5-Centrin complex. These data combined with mass photometry analysis, confirmed the presence of a POC5 tetramer and that the N-terminal region is important to facilitate this configuration. Functional analysis of the POC5$^{\Delta 153\text{-}184}$ mutant showed that this mutant is not able to rescue the inner luminal augmin-γTuRC pool and the broken centriole in *POC5*$^{-/-}$ cells, indicating an important role of the POC5 tetramer. Interestingly, electron tomography data from purified centrioles of *Paramecium tetraurelia* shows for the inner scaffold an elongated structure[85], resembling the purified POC5-Centrin from this study, that bridges neighbouring MT triplets. Through the interaction between POC1A's WD40 domain and the C-terminal POC1-binding region of POC5, the POC5 tetramer is anchored and might play an integral part of the inner scaffold structure. In addition, the POC5 tetramer might function as a bridge to the luminal augmin-γTuRC pool for which a centriole-stabilization function has been described[159], thus connecting different protein networks to ensure centriole integrity. The bound Centrin on the POC5 tetramer might contribute to the stacking of POC5-Centrin complexes along the longitudinal axis of the centriole, as Centrin-Centrin interactions were observed in the yeast Centrin (Cdc31)- Sfi1 complex[169], while POC1A-homodimers connect the complexes in a lateral manner.

4.8 The inner scaffold structure across species

Although the inner scaffold is a conserved feature across species, ranging from protists to vertebrates, tomography data revealed subtle differences in this structure between different organisms[85]. The question that arises is whether the proposed functions of proteins in other species are the same as those of their human orthologues. This is especially important in the light of the POC1 proteins, because the divergence to two POC1 paralogues happened in vertebrates. In *Tetrahymena* only one POC1 protein exists with a length of 634 amino acid (human POC1A: 407, human POC1B: 478 amino acids). Based on AlphaFold predictions, *Tetrahymena* POC1 shows a similar architecture like human POC1B, because it is predicted to have a beta-strand resembling POC1B's intra. Previously published papers, localized *Tetrahymena* POC1 in the proximal as well as in the central part of the basal body[134,140]. Further, it has been proposed that POC1 functions as a junction protein, localizing to the A-B and B-C inner junction at the proximal part and at the central part only to the A-B inner junction[140]. Consistent with these notions, the data in my study, places the WD40 domain of POC1B closer towards the centriole wall. However, there are differences regarding the phenotypes upon loss of the POC1 proteins. While loss of POC1 in *Tetrahymena*, clearly affects the stability of the basal body under mechanical forces[134,140], loss of both POC1 proteins in humans, lead to a much severe phenotype with complete disintegrated centrioles[133]. This indicates, that POC1 proteins in vertebrates might have a slightly different function or that in *Tetrahymena* these functions are fulfilled by a different protein. It would be interesting to investigate, whether other inner scaffold components known in vertebrates, have ortholog forms in other phyla and if their function within the inner scaffold equals the one in vertebrates. For POC5 and FAM161A, homologous were identified in *Tetrahymena* and *Paramecium*[140,170,171]. In *Tetrahymena* basal bodies, both proteins localize in the core region[140,171] and for FAM161A it was shown that it is dependent on POC1[140], consistent with the interaction between the POC1 proteins and FAM161A in humans. However, in contrast to humans, *Tetrahymena* POC5 (TtPoc5), is a transient component of assembling basal bodies[171], indicating a slightly different role of POC5 in *Tetrahymena*. The *Tetrahymena* POC5-like protein SFR1 could take over the function of TtPoc5 as a stable incorporated protein[171]. It is an interesting question whether a POC1-POC5 interaction is conserved and can be found in other species. In addition, investigating the function of MDM1 and CCDC15 in other species and, whether they are conserved or not, may help to gain knowledge about shared fundamental features of the inner scaffold among different species.

5. Conclusion

Centriole integrity is important to ensure proper centrosomal function. Defects in centriolar stability and integrity interfere with many centrosome-associated pathways and lead to mitotic defects, which can ultimately result in cancer. Within the centriole, many substructures like the cartwheel and A-C linker, together with the PCM, contribute to structural integrity. The inner scaffold, a ring-like structure in the centriolar lumen comprised of POC1B, POC5, FAM161A and CCDC15, is suggested to play a role as an additional stabilization factor. This study proposes the first structural model of how a complex protein network within the centriole forms the inner scaffold and unveils the drastic consequences if this network is disturbed. Here, I identified POC1A, a paralogue of POC1B, as a new inner scaffold component and investigated the specialized and overlapping functions between POC1A and POC1B. The data showed, that both POC1 proteins have an impact on the centriolar localization of different inner scaffold proteins and that loss of either POC1 protein results in defective centrioles. The proposed model of the structural organization of the inner scaffold involves the formation of a POC1A-POC1B heterodimer with POC1A residing towards the centriole lumen and POC1B closer to the centriole wall. The POC1A-POC1B heterodimer cross-links other proteins like POC5, FAM161A, CCDC15 and MDM1 and establishes not only a specific arrangement of the proteins within the centriole but also a connection of the inner scaffold with the centriole wall (see Fig. 30, 1). An important aspect is the interaction between POC1A and POC5, mediated by the POC1-binding-region in the C-terminus of POC5 and POC1A's WD40 domain (see Fig. 30, 2). The connection to the centriole wall is achieved by interactions of POC1A and POC1B with MT-binding proteins like MDM1 or FAM161A (see Fig. 30, 3). POC5, in complex with Centrin, forms a tetramer, leading to a symmetric elongated structure, showing resemblance with parts of the inner scaffold connecting adjacent MT triplets (see Fig. 30, 4). In my model, the elongated POC5-Centrin builds the centrepiece of the inner scaffold and multiple of these complexes are connected by POC1A homodimers to build the ring-like structure (see Fig. 30, 5). The formation and maintenance of the inner scaffold involves this complex protein network and is key for the integrity of centrioles.

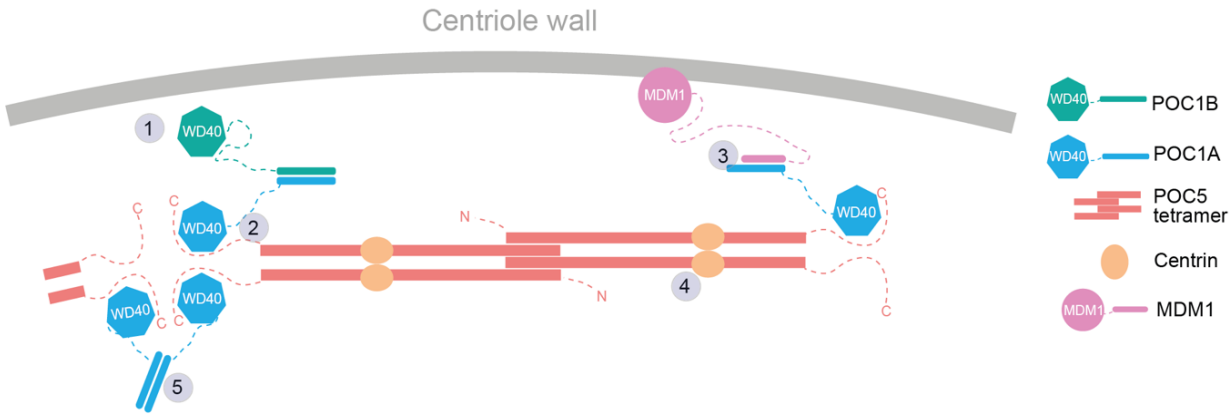

Figure 30: Model of the structural organization of the inner scaffold protein network
The elongated POC5-Centrin complex, anchored by the interaction with POC1A, is the centrepiece of the inner scaffold. POC1A-POC1B heterodimers display a certain spatial localization and act as organizer within the centriole to cross-link several proteins like MDM1A and FAM161A. This establishes a complex protein network and the connection of the inner scaffold with the centriole wall. *Figure modified and adapted from* (Sala et al., *Nat Comm* 2024)[1].

6. Perspectives

The data in this study showed that a complex protein network is necessary to build a structure like the inner scaffold and to ensure centriole integrity. The proposed model sheds light onto how a structure like the inner scaffold is organized. However, during the study, new questions arose and addressing them may help to gain more knowledge about centriole biogenesis.

POC1A-POC1B heterodimers play an important role in cross-linking various proteins within the inner scaffold, but AlphaFold predictions together with IP experiments showed that formation of POC1A and POC1B homodimers is also possible. It is interesting to investigate if in a centriole hetero- and homodimers co-exist in a specific ratio and what the conditions are that lead to either a homo- or a heterodimer and how this is regulated especially during the assembly of the inner scaffold or upon mechanical stress.

The structural differences between POC1A and POC1B could solely account for interactions with specific proteins. Nonetheless, it is plausible that also post-translational modifications enhance the structural differences and therefore shift preferred interactions towards one of the POC1 proteins. Previous studies indicated phosphorylation of POC1B by Cdk1. Further experiments are needed to test how these modifications alter the protein structure and what consequences these have on certain interactions. In addition, one could test if other kinases are involved and if also POC1A undergoes phosphorylation. Mutations in the *POC1* genes lead to different diseases specific to the affected paralogue: while *POC1A* mutations lead to a specific primordial dwarfism (SOFT syndrome), *POC1B* mutations are associated with retinal dystrophies and loss of vision[130,155]. In this regard, it would be interesting to test how mutations

found in patients affect the interactions with other proteins. Further, animal models can be utilised to understand the effect of mutations in inner scaffold proteins on certain tissues like the retina.

This study revealed functional differences between POC1A and POC1B, however, certain aspects need further investigation. How both POC1 proteins are recruited to the centriole is still not known and by identifying recruitment factors, new light on to the function of POC1A and POC1B could be shed. This might also help to identify new components of the inner scaffold.

Broken centrioles upon loss of POC1A, POC1B or POC5 indicate a stabilizing function of the inner scaffold, but the centriole assembly and elongation is *per se* not inhibited. It is known that centrioles are subjected to forces applied onto them during mitosis and that stabilization factors are necessary to withstand these forces. An interesting question that needs to be clarified is when the defects overserved in the knockouts occurs, taking a closer look onto procentrioles to check whether their structure already during formation shows defects.

7. Material

7.1 Equipment

Name	Manufacturer
Äkta Pure/ÄktaGO protein purification system	Cytiva
BD FACSAria III	BD Biosciences
Cellometer Luna FL	Logos Biosystems
Centrifuge 5810R, 5702R, 542R, 5417R	Eppendorf AG
DeltaVision RT widefield microscope	GE (Applied Precision)
Discovery 90SE ultracentrifuge	Sorvall
ImageQuant LAS-4000	GE Healthcare
KE76 sonicator tip	Bandelin
JEOL JEM1400 transmission electron microscope	Jeol
Orbitrap QE HF spectrometer	Thermo Fisher Scientific
Nanodrop ND-1000 spectrophotometer	Thermo Fisher Scientific
Refeyn TwoMP mass photometer	Refeyn
Superdex 6 Increased SEC column	Cytiva
Superdex 75 SEC column	Cytiva
Talos L120C transmission electron microscope	Thermo Fisher Scientific
TCS SP8 STED 3X-FALCON confocal microscope	Leica Microsystems
Thermocycler C1000	Bio-Rad
Ultimate 3000 liquid chromatography system	Thermo Fisher Scientific

7.2 Software

Name	Manufacturer
Adobe Illustrator 2024 (v28.5)	Adobe
AlphaFold-Multimer and AlphaFold3	EMBL's European Bioinformatics Institute and Google DeepMind

BD FACSDiva v8.0.1	BD Biosciences
FoldX	EMBL (Heidelberg) and Center for Genomic Regulation (Barcelona)
Fiji v.2.0.0-rc-69/1.52p and v.2.3.0/1.53q	ImageJ
Huygens' Deconvolution	Scientific Volume Imaging
Jalview 2.11.4.0	University of Oxford, EMBL-EBI and University of Dundee
LAS4000IR v2.1	FUJIFILM
Leica Falcon LAS X FLIM	Leica Microsystems
Perseus	Max Planck Institute of Biochemistry
Prism 10	GraphPad
Refeyn AcquireMP 2024 R1	Refeyn
Refeyn DiscoverMP 2024 R1	Refeyn
Relion 3.1	MRC Laboratory of Molecular Biology
SnapGene	Dotmatics
SoftWorx v6.1.1	GE (Applied Precision)
UCSF ChimeraX v. 1.6.1	Resource for Biocomputing, Visualization, and Informatics, University of California
Unicorn v.75/7.9	Cytiva

7.3 Cells

7.3.1 Human cell lines

RPE1 hTERT	AG Schiebel
RPE1 hTERT Tet3G	AG Schiebel
RPE1 hTERT Tet3G, TRE3G-CEP44-*TurboID-HA*	AG Schiebel
RPE1 hTERT Tet3G, TRE3G-*TurboID-HA*	AG Schiebel
RPE1 hTERT Tet3G *TP53*$^{-/-}$	AG Schiebel
RPE1 hTERT Tet3G *CEP44*$^{-/-}$	AG Schiebel
RPE1 hTERT Tet3G *TP53*$^{-/-}$, *POC1A*$^{-/-}$	AG Schiebel
RPE1 hTERT Tet3G *TP53*$^{-/-}$, *POC1B*$^{-/-}$	AG Schiebel
RPE1 hTERT Tet3G *TP53*$^{-/-}$, *POC1A*$^{-/-}$, *POC1B*$^{-/-}$ *(POC1A/POC1B double KO)*	AG Schiebel
HEK GP2-293	AG Schiebel
HEK T293 Tet3G	AG Schiebel
HEK T293 Tet3G, TRE3G-*POC1A-FLAG*	AG Schiebel
HEK T293 Tet3G, TRE3G-*POC1B-FLAG*	AG Schiebel
HEK T293 Tet3G, TRE3G-*WD40A-FLAG*	AG Schiebel
HEK T293 Tet3G, TRE3G-*WD40B-FLAG*	AG Schiebel
HEK T293 Tet3G, TRE3G-*POC1Ab-FLAG*	AG Schiebel
HEK T293 Tet3G, TRE3G-*POC1Ba-FLAG*	AG Schiebel
RPE1 hTERT Tet3G *TP53*$^{-/-}$, *CEP295*$^{-/-}$	This study
RPE1 hTERT Tet3G *TP53*$^{-/-}$, *POC5*$^{-/-}$	This study
RPE1 hTERT Tet3G *TP53*$^{-/-}$, *POC1A*$^{-/-}$, TRE3G-*POC1A-HA*	This study
RPE1 hTERT Tet3G *TP53*$^{-/-}$, *POC1A*$^{-/-}$, TRE3G-*WD40A-HA*	This study
RPE1 hTERT Tet3G *TP53*$^{-/-}$, *POC1A*$^{-/-}$, TRE3G-*C-TermA-HA*	This study
RPE1 hTERT Tet3G *TP53*$^{-/-}$, *POC1A*$^{-/-}$, TRE3G-*POC1Ab-HA*	This study
RPE1 hTERT Tet3G *TP53*$^{-/-}$, *POC1A*$^{-/-}$, TRE3G-*POC1Ba-HA*	This study
RPE1 hTERT Tet3G *TP53*$^{-/-}$, *POC1A*$^{-/-}$, TRE3G-*POC1B-HA*	This study

RPE1 hTERT Tet3G *TP53*$^{-/-}$, *POC1B*$^{-/-}$, TRE3G-*POC1B-HA*	This study
RPE1 hTERT Tet3G *TP53*$^{-/-}$, *POC1B*$^{-/-}$, TRE3G-*WD40B-HA*	This study
RPE1 hTERT Tet3G *TP53*$^{-/-}$, *POC1B*$^{-/-}$, TRE3G-*C-TermB-HA*	This study
RPE1 hTERT Tet3G *TP53*$^{-/-}$, *POC1B*$^{-/-}$, TRE3G-*POC1Ab-HA*	This study
RPE1 hTERT Tet3G *TP53*$^{-/-}$, *POC1B*$^{-/-}$, TRE3G-*POC1Ba-HA*	This study
RPE1 hTERT Tet3G *TP53*$^{-/-}$, *POC1B*$^{-/-}$, TRE3G-*POC1B*$^{\Delta 344\text{-}365}$*-HA*	This study
RPE1 hTERT Tet3G *TP53*$^{-/-}$, *POC1A/B* double KO, TRE3G-*POC1A-HA*	This study
RPE1 hTERT Tet3G *TP53*$^{-/-}$, *POC1A/B* double KO, TRE3G-*POC1B-HA*	This study
RPE1 hTERT Tet3G *TP53*$^{-/-}$, *POC1A/B* double KO, TRE3G-*POC1Ab-HA*	This study
RPE1 hTERT Tet3G *TP53*$^{-/-}$, *POC1A/B* double KO, TRE3G-*POC1Ba-HA*	This study
RPE1 hTERT Tet3G *TP53*$^{-/-}$, PGK-*EGFP-POC1A*	This study
RPE1 hTERT Tet3G *TP53*$^{-/-}$, PGK-*EGFP-POC1B*	This study
RPE1 hTERT Tet3G *TP53*$^{-/-}$, PGK-*EGFP-POC5*	This study
RPE1 hTERT Tet3G *TP53*$^{-/-}$, *POC1A*$^{-/-}$, PGK-*EGFP-POC1A*	This study
RPE1 hTERT Tet3G *TP53*$^{-/-}$, *POC1B*$^{-/-}$, PGK-*EGFP-POC1B*	This study
RPE1 hTERT Tet3G *TP53*$^{-/-}$, *POC1A/B* double KO, PGK-*EGFP-POC1A*	This study
RPE1 hTERT Tet3G *TP53*$^{-/-}$, *POC1A/B* double KO, PGK-*EGFP-POC1B*	This study
RPE1 hTERT Tet3G *TP53*$^{-/-}$, *POC5*$^{-/-}$, TRE3G-*POC5-HA*	This study
RPE1 hTERT Tet3G *TP53*$^{-/-}$, *POC5*$^{-/-}$, TRE3G-*POC5*$^{1\text{-}470}$*-HA*	This study
RPE1 hTERT Tet3G *TP53*$^{-/-}$, *POC5*$^{-/-}$, TRE3G-*POC5*$^{\Delta 472\text{-}532}$*-HA*	This study
RPE1 hTERT Tet3G *TP53*$^{-/-}$, *POC5*$^{-/-}$, TRE3G-*POC5*$^{\Delta 152\text{-}184}$*-HA*	This study
RPE1 hTERT Tet3G *TP53*$^{-/-}$, *POC5*$^{-/-}$, PGK-*EGFP-POC5*	This study

7.3.2 Bacterial and insect cell lines

E. coli DH5α	cloning
E. coli DH10MultiBac™	cloning
E. coli DH10EMBacY	cloning

Sf9 insect cells (*Spodoptera frugiperda*)	protein expression
Sf21 insect cells (*Spodoptera frugiperda*)	protein expression

7.4 Plasmids

Name	**Vector type**	**Source**	**Application**
pRetroX-TRE3G	retroviral, mammalian (dox-inducible) expression	Clontech	Retroviral integration, dox-inducible expression, empty vector
pVSV-G	mammalian	Clontech	Retroviral integration virus, plasmid encoding envelop proteins for virus production
px458	mammalian	AG Schiebel	sgRNA and Cas9 expression vector
POC1A_sgRNA_Exon2	mammalian	AG Schiebel	px458 with sgRNA targeting Exon2 of POC1A
POC1A_sgRNA_Exon7	mammalian	AG Schiebel	px458 with sgRNA targeting Exon7 of POC1A
POC1B_sgRNA_Intron4	mammalian	AG Schiebel	px458 with sgRNA targeting Intron4 of POC1B
POC1B_sgRNA_Exon10	mammalian	AG Schiebel	px458 with sgRNA targeting Exon10 of POC1B
POC5_sgRNA_Exon5	mammalian	This study	px458 with sgRNA targeting Exon5 of POC5
POC5_sgRNA_Exon10	mammalian	This study	px458 with sgRNA targeting Exon10 of POC5
pCMV3_POC5	mammalian	Sino Biological	cDNA of POC5, used as template for cloning
pCMV3_FAM161A	mammalian	Sino Biological	cDNA of FAM161A, used as template for cloning
pCMV3_MDM1	mammalian	Sino Biological	cDNA of MDM1, used as template for cloning

pCMV3_CCDC15	mammalian	Sino Biological	cDNA of CCDC15, used as template for cloning
pRetroX-TRE3G-POC1A-FLAG	retroviral, mammalian (dox-inducible) expression	AG Schiebel	Co-IP
pRetroX-TRE3G-WD40A-FLAG	retroviral, mammalian (dox-inducible) expression	AG Schiebel	Co-IP
pRetroX-TRE3G-C-TermA- FLAG	retroviral, mammalian (dox-inducible) expression	AG Schiebel	Co-IP
pRetroX-TRE3G-POC1B-FLAG	retroviral, mammalian (dox-inducible) expression	AG Schiebel	Co-IP
pRetroX-TRE3G-WD40B-FLAG	retroviral, mammalian (dox-inducible) expression	AG Schiebel	Co-IP
pRetroX-TRE3G-C-TermB- FLAG	retroviral, mammalian (dox-inducible) expression	AG Schiebel	Co-IP
pRetroX-TRE3G-POC1Ab-FLAG	retroviral, mammalian (dox-inducible) expression	AG Schiebel	Co-IP
pRetroX-TRE3G-POC1Ba-FLAG	retroviral, mammalian (dox-inducible) expression	AG Schiebel	Co-IP
pRetroX-TRE3G-POC1B$^{\Delta 344\text{-}365}$-FLAG	retroviral, mammalian (dox-inducible) expression	AG Schiebel	Co-IP
pRetroX-TRE3G-POC1A-HA	retroviral, mammalian (dox-inducible) expression	AG Schiebel	Rescue, Co-IP
pRetroX-TRE3G-WD40A-HA	retroviral, mammalian (dox-inducible) expression	AG Schiebel	Localization, Co-IP

pRetroX-TRE3G-C-TermA-HA	retroviral, mammalian (dox-inducible) expression	AG Schiebel	Localization, Co-IP
pRetroX-TRE3G-POC1B-HA	retroviral, mammalian (dox-inducible) expression	AG Schiebel	Rescue, Co-IP
pRetroX-TRE3G-WD40B-HA	retroviral, mammalian (dox-inducible) expression	AG Schiebel	Localization, Co-IP
pRetroX-TRE3G-C-TermB-HA	retroviral, mammalian (dox-inducible) expression	AG Schiebel	Localization, Co-IP
pRetroX-TRE3G-POC1Ab-HA	retroviral, mammalian (dox-inducible) expression	AG Schiebel	Rescue, Localization, Co-IP
pRetroX-TRE3G-POC1Ba-HA	retroviral, mammalian (dox-inducible) expression	AG Schiebel	Rescue, Localization, Co-IP
pRetroX-TRE3G-POC1B$^{\Delta 344\text{-}365}$-HA	retroviral, mammalian (dox-inducible) expression	This study	Rescue, Localization
pRetroX-TRE3G-WD40A-EGFP-HA	retroviral, mammalian (dox-inducible) expression	This study	GFP-Binder dimerization
pRetroX-TRE3G-WD40B-EGFP-HA	retroviral, mammalian (dox-inducible) expression	This study	GFP-Binder dimerization
pRetroX-TRE3G-GBP-C-TermA-mScarlet-I	retroviral, mammalian (dox-inducible) expression	This study	GFP-Binder dimerization
pRetroX-TRE3G-GBP-C-TermB-mScarlet-I	retroviral, mammalian (dox-inducible) expression	This study	GFP-Binder dimerization

pRetroX-TRE3G-mScarlet-I-WD40A-GBP	retroviral, mammalian (dox-inducible) expression	This study	GFP-Binder dimerization
pRetroX-TRE3G-mScarlet-I-WD40B-GBP	retroviral, mammalian (dox-inducible) expression	This study	GFP-Binder dimerization
pRetroX-TRE3G- WD40A-LinkerRegion-EGFP	retroviral, mammalian (dox-inducible) expression	This study	GFP-Binder dimerization
pRetroX-TRE3G- WD40B-LinkerRegion-EGFP	retroviral, mammalian (dox-inducible) expression	This study	GFP-Binder dimerization
pRetroX-TRE3G-mScarlet-I- WD40A-LinkerRegion-GBP	retroviral, mammalian (dox-inducible) expression	This study	GFP-Binder dimerization
pRetroX-TRE3G-mScarlet-I- WD40B-LinkerRegion-GBP	retroviral, mammalian (dox-inducible) expression	This study	GFP-Binder dimerization
pRetroX-TRE3G-POC1A-mNeonGreen	retroviral, mammalian (dox-inducible) expression	This study	FLIM-FRET
pRetroX-TRE3G-POC1B-mScarlet-I	retroviral, mammalian (dox-inducible) expression	This study	FLIM-FRET
pRetrox-TRE3G-POC5-HA	retroviral, mammalian (dox-inducible) expression	This study	Rescue, Co-IP
pRetrox-TRE3G-POC5$^{1-470}$-HA	retroviral, mammalian (dox-inducible) expression	This study	Rescue, Co-IP
pRetrox-TRE3G-POC5$^{266-575}$-HA	retroviral, mammalian (dox-inducible) expression	This study	Co-IP

pRetroX-TRE3G-POC5$^{\Delta 472\text{-}532}$-HA	retroviral, mammalian (dox-inducible) expression	This study	Localization, Co-IP
pRetroX-TRE3G-POC5$^{\Delta 152\text{-}184}$-HA	retroviral, mammalian (dox-inducible) expression	This study	Localization, Co-IP
pRetrox-TRE3G-FAM161A-HA	retroviral, mammalian (dox-inducible) expression	This study	Co-IP
pRetrox-TRE3G-MDM1-HA	retroviral, mammalian (dox-inducible) expression	This study	Co-IP
pRetrox-TRE3G-CCDC15-HA	retroviral, mammalian (dox-inducible) expression	This study	Co-IP
pQPXIP-PGK-EGFP-POC1A	retroviral, mammalian (constitutive) expression	This study	Localization in ExM
pQPXIP-PGK-EGFP-POC1B	retroviral, mammalian (constitutive) expression	This study	Localization in ExM
pQPXIP-PGK-EGFP-POC5	retroviral, mammalian (constitutive) expression	This study	Localization in ExM
pQPXIP-PGK-osTIR1-CEP44-mAID	retroviral, mammalian (constitutive) expression	This study	Auxin-inducible degron of CEP44

7.5 Primers

Name	**Sequence**
pRetroX-TRE3G-POC1B $^{\Delta 344\text{-}365}$-HA	I:ATCGATACGCGTGCGCCACCATGGCCTCAGCCACGGAG CTCAACTTTTTCCTCATGGGGATGTG B: CCCATGAGGAAAAAGTTGAGTCTTTTGATTCTACCACAACAACAGAAACCAG GGTGGCGCACGCGTATCG
pRetroX-TRE3G-GBP-C-TermA-mScarlet-I	GBP: ATCGATACGCGTGCGCCACCatggccgatgtgcagctg ggatccacttccagaaccggatccagaacctgaggagacggtgacctg CTA: ccggttctggaagtggatccATGATTGTTGATCATGGAGAAGTCACGA CTCGCCCTTGCTCACCATtgcaccagctcctgcac

	B: ATGGTGAGCAAGGGCGAG GGTGGCGCACGCGTATCG
pRetroX-TRE3G-GBP-C-TermB-mScarlet-I	GBP: TTGGATCCATCGATACGCGTGCGCCACCatggccgatgtgcagctg ggatccacttccagaaccggatccagaacctgaggagacggtgacctg B:ccggttctggaagtggatccGAATTGCATTGTAAAGGTCTTACC GCGTATCGATGGATCCAA
pRetroX-TRE3G-mScarlet-I-WD40A-GBP	mScarlet: TGGATCCATCGATAGCCACCATGGTGAGCAAGGGCGAG ggatccacttccagaaccggatccagaaccCTTGTACAGCTCGTCCATGC WDA: ggttctggaagtggatccGCTGCGCCCTGCGC actccaccagctgcacatcggctgcaccagctcctgcacc GBP: gccgatgtgcagctggtg tcatgaggagacggtgacc B:aggtcaccgtctcctcatgaGGCCCGAATTCTACCGGG GGTGGCTATCGATGGATCC
pRetroX-TRE3G-WD40B-LinkerRegion-EGFP	TGGATCCATCGATAGCCACCATGGCTGCGCCCTGCGCG CTCGCCCTTGCTCACCATTGATCCTGATCCTGATCCTGATCCTGATCCGGGCACACTCACGGGCTCC B: ATGGTGAGCAAGGGCGAG GGTGGCTATCGATGGATCCA
pRetroX-TRE3G-POC1A-mNeonGreen	I:TCATGCAGAGAGCAACACCAGGAGCTGGTGCAGGTGCAGGAGCTGGTGCAATGGTGAGCAAGGGCGAG TACCCGGTAGAATTCGGGCCttaCTTGTACAGCTCGTCCATGC B(POC1A):GGCCCGAATTCTACCGGG TGGTGTTGCTCTCTGCATG
pRetroX-TRE3G-POC1B-mScarlet-I	I (mScarlet):GTGCTGTCCAACAGAAAAGCGGAGCTGGTGCAGGTGCA TACCCGGTAGAATTCGGGCCTTACTTGTACAGCTCGTCCATGC BPOC1B): GGCCCGAATTCTACCGGG GCTTTTCTGTTGGACAGCAC
pRetrox-TRE3G-POC5-HA	ATCGATACGCGTGCGCCACCATGTCATCAGATGAGGAG CCTGCACCTGCACCAGCTCCGTCAACCACTTTTATGGAATG GGAGCTGGTGCAGGTGCAG GGTGGCGCACGCGTATCG
pRetrox-TRE3G-POC5$^{1-470}$-HA	ATCGATACGCGTGCGCCACCATGTCATCAGATGAGGAG CCTGCACCTGCACCAGCTCCCACATACATTTCTTCTGATGC GGAGCTGGTGCAGGTGCAG GGTGGCGCACGCGTATCG
pRetrox-TRE3G-POC5$^{266-575}$-HA	GATACGCGTGCGCCACCATGGTTTATGAAGGTAAACTAGCTG CCTGCACCTGCACCAGCTCCGTCAACCACTTTTATGGAATG GGAGCTGGTGCAGGTGCA CATGGTGGCGCACGCGTA
pRetroX-TRE3G-POC5$^{\Delta 472-532}$-HA	GATACGCGTGCGCCACCATGCCAAGAGTTGTAACCTCTG CCTGCACCTGCACCAGCTCCGTCAACCACTTTTATGGAATG GGAGCTGGTGCAGGTGCA CATGGTGGCGCACGCGTA

pRetrox-TRE3G-FAM161A-HA	ATCGATACGCGTGCGCCACCatggccacctcccaccga CCTGCACCTGCACCAGCTCCgtgtgattcttcaacagatttctcttcttcactttc GGAGCTGGTGCAGGTGCAG GGTGGCGCACGCGTATCG
pRetrox-TRE3G-MDM1-HA	ATCGATACGCGTGCGCCACCATGCCGGTGCGCTTCAAG CCTGCACCTGCACCAGCTCCTGTTTTACCCCAGAAATTCTCCTTC GGAGCTGGTGCAGGTGCAG GGTGGCGCACGCGTATCG
pRetrox-TRE3G-CCDC15-HA	ATCGATACGCGTGCGCCACCATGCTGGGAAGTATGGCC CCTGCACCTGCACCAGCTCCTAGATTTTTCAAAGTCCGCC GGAGCTGGTGCAGGTGCAG GGTGGCGCACGCGTATCG
pQPXIP-PGK-EGFP-POC1A	EGFP: AGTCTAGCGGCCGCGCCACCATGGTGAGCAAGGGCGAG CTTGTACAGCTCGTCCATGC POC1A: CATGGACGAGCTGTACAAGgcggccgcaGGAGCTGGTGCAGGTGCAGGAGCTGGTGCAGCTGCGCCCTGCGCGGAG TGGTGTTGCTCTCTGCATGATTAGCTGCTGG B: TCATGCAGAGAGCAACACCAtaaCTCGAGGAATTCCGCCCCCC GGTGGCGCGGCCGCTAGA
pQPXIP-PGK-EGFP-POC1B	CATGGACGAGCTGTACAAGgcggccgcaGGAGCTGGTGCAGGTGCAGGAGCTGGTGCAGCCTCAGCCACGGA GCTTTTCTGTTGGACAGCACTGAA B: TTCAGTGCTGTCCAACAGAAAAGCtaaCTCGAGGAATTCCGCCCCCC GGTGGCGCGGCCGCTAGA
pQPXIP-PGK-EGFP-POC5	CAGGTGCAGGAGCTGGTGCATCATCAGATGAGGAGAAATAC ttaGTCAACCACTTTTATGGAATG CATTCCATAAAAGTGGTTGACtaaCCACCGACTCTAGTCGAGG TGCACCAGCTCCTGCACC

7.6 sgRNA

Name	**Genomic target**	**sgRNA sequence 5'- 3'**
POC1A_sgRNA_Exon2	*POC1A* Exon 2	CCGAGATGCAGTTACCTGTG
POC1A_sgRNA_Exon7	*POC1A* Exon 7	TCAGGTAGTTTCCCGACGGG
POC1B_sgRNA_Intron4	*POC1B* Intron 4	ACTGCATGGGATGGTAACAG
POC1B_sgRNA_Exon10	*POC1B* Exon 10	GAAAGGATATCCATAACAGG
POC5_sgRNA_Exon5	*POC5* Exon 5	GGCTTCCTTGGCGATAACAC
POC5_sgRNA_Exon10	*POC5* Exon 10	GTAACTGGTAAGGGCATCGG

7.7 siRNA

Name	sgRNA sequence 5'- 3'	Manufacturer
siControl/ ON-TARGET plus non-targeting siRNA #1	UGGUUUACAUGUCGAC	Dharmacon
siPOC1A/ FlexiTube siRNA Hs_WDR51A_2	CUGGGUACCCAAUGUCAAA	Qiagen
siPOC1B/ FlexiTube siRNA Hs_WDR51B_4	GAUUCCGUUGGAUUUGCAA	Qiagen

7.8 Antibodies

Name	Host	Cat. #	Dilution
POC1A	rabbit	PA5-59217, ThermoFisher	1:300
POC1A	guinea pig	homemade	1:200
POC1B	rabbit	PA5-24495, ThermoFisher	1:250
POC1B	guinea pig	homemade	1:500
POC5	rabbit	Bethyl, A303-341A-T	1:1000
γ-tubulin	mouse	Abcam, ab27074	1:1000
γ-tubulin	guinea pig	homemade	1:50
PCNT	rabbit	Abcam, ab4448	1:2000
PCNT	guinea pig	homemade	1:800
CEP97	rabbit	Bethyl, A301-945A	1:300
CEP44	rabbit	homemade	1:200
CDK5RAP2	rabbit	Merck, 06-1398	1:500
Centrin	mouse	Millipore, MABC544	1:1000
Centrin	rabbit	Abcam, ab101332	1:500
α-tubulin	mouse	SigmaAldrich, DM1A	1:500
α-tubulin	mouse	Proteintech, 660311-1-Ig	1:500
α-tubulin	rabbit	Proteintech,11224-1-AP	1:500
HA	rat	Merck, 11867423001	1:1000
GFP	mouse	Roche, 11814460001	IF: 1:1000, ExM: 1:500

Mitosin	mouse	BD, 610768	1:100
FAM161A	rabbit	Sigma, HPA-032119	IF: 1:100, ExM: 1:250
WDR90	rabbit	NovusBio, NBP2-31888	1:250
MDM1	rabbit	ThermoFisher, PA5-59638	1:500
CCDC15	rabbit	ThermoFisher, PA5-59184	IF: 1:1000, ExM: 1:500
HAUS4	rabbit	Proteintech, 20104-1-AP	1:500
CEP295	rabbit	Abcam, Ab122490	1:500
CEP135	rabbit	homemade	1:200
CEP152	rabbit	homemade	1:1000
CEP192	rabbit	homemade	1:2000
FLAG	rabbit	Proteintech, 20543-1-AP	1:1000
HA	rabbit	Proteintech, 51064-2-AP	1:1000
GAPDH	mouse	Proteintech, 60004-1-lg	1:1000
Vinculin	mouse	Proteintech, 66305-1-lg	1:1000
Alexa Fluor 488/555/647 anti-mouse IgG	donkey	ThermoFisher	1:500
Alexa Fluor 488/555/647 anti-rabbit IgG	donkey	ThermoFisher	1:500
Alexa Fluor 488/555/647 anti-guinea pig IgG	goat	ThermoFisher	1:500
Alexa Fluor 488/647 anti-rat IgG	donkey	ThermoFisher	1:500
Abberior Start635P anti-mouse IgG	goat	Abberior, ST635P-1001-500UG	1:500
Abberior Start635P anti-rabbit IgG	goat	Abberior, ST635P-1002-500UG	1:500
HRP-conjugated anti-mouse IgG	donkey	Jackson Immunoresearch, 711-035-151	1:5000
HRP-conjugated anti-rabbit IgG	donkey	Jackson Immunoresearch, 711-035-152	1:5000

HRP-conjugated anti-rat IgG	goat	Jackson Immunoresearch, 112-035-003	1:5000

7.9 Buffers and solutions

7.9.1 DNA analysis and miniprep

Name	**Ingredients**
TAE (1x)	20 mM Tris-Cl, 1 mM EDTA, pH 7.5 adjusted with acetic acid
DNA loading dye (6x)	0.25% w/v bromophenol blue, 0.25% w/v xylene cynole, 30% v/v glycerol
Miniprep resuspension buffer S1	50 mM Tris-cl pH 8.0, 10 mM EDTA, 100 µg/ml RNase A
Miniprep lysis buffer S2	200 mM NaOH, 1% SDS
Miniprep neutralisation buffer S3	2.8 M K-Acetate, pH 5.1

7.9.2 Immunofluorescence

Name	**Ingredients**
PBS (1x)	50 mM $Na_2(PO_4)_3$, 150 mM NaCl, pH 7.5
Cytoskeleton (CSK) extraction buffer	10 mM K-PIPES pH 6.8, 100 mM NaCl, 300 mM sucrose, 1 mM EGTA, 1mM $MgCl_2$, 1% v/v Triton X-100
IF blocking buffer	10% v/v FBS, 0.1% Triton X-100, 0.03% w/v NaN_3 in 1xPBS
IF antibody incubation solution	3% w/v bovine serum albumin (BSA), 0.03% w/v NaN3 in 1x PBS
IF mounting medium	12 % w/v mowiol, 30% w/v glycerol, 120 mM Tris-Cl, pH 8.5

7.9.3 Ultrastructure Expansion Microscopy (U-ExM)

Name	**Ingredients**
U-ExM fixation buffer (for 1 ml)	19 µl formaldehyde (37% solution), 25 µl acrylamide (40% solution), 1x PBS
U-ExM monomer solution (for 900 µl)	500 µl Na-Acrylate (38% solution), 250 µl Acrylamide (40% solution), 50 µl *N*,*N*'-methylenbisacrylamide (BIS, 2% solution), 100 µl PBS (10x)
U-ExM denaturation buffer (for 50 ml)	28.57 ml SDS (10%), 2 ml NaCl (5 M), 0.3 g Tris-BASE; adjust to pH 9.0 with 37% HCl
U-ExM antibody inubation solution	1% w/v bovine serum albumin (BSA), 0.03% w/v NaN3 in 1x PBS
PBS-T (1x)	50 mM $Na_2(PO_4)_3$, 150 mM NaCl, pH 7.5, 0.1% (w/v) Tween-20

7.9.4 Immunoblotting

Name	**Ingredients**
Laemmli buffer (4x)	200 mM Tris-Cl, 40% v/v glycerol, 8% w/v SDS, 100 mM DTT, 0.08% w/v bromophenol blue
SDS-PAGE running buffer (1x)	25 mM Tris, 192 mM glycine, 0.1% w/v SDS
Coomassie staining solution	0.1% w/v Coomassie, 50% v/v methanol, 10% v/v acetic acid
Transfer buffer, Towbin buffer (1x)	25 mM Tris, 192 mM glycine, 0.25% w/v SDS, 20% v/v methanol
TBS (1x)	2.5 mM Tris-Cl, 15 mM NaCl, pH 7.5
TBS-T (1x)	2.5 mM Tris-Cl, 15 mM NaCl, pH 7.5, 0.05% v/v Tween-20
Immunoblot blocking buffer	5% w/v nonfat dry milk in TBS or TBS-T

7.9.5 IP and pulldown (mammalian cells)

Name	Ingredients
IP lysis buffer	10 mM Tris-Cl pH 7.5, 150 mM NaCl, 0.5 mM EDTA, 0.5% NP-40, 1 mM PMSF, 10 U/µl Benzonase
IP wash buffer	10 mM Tris-Cl pH 7.5, 300 mM NaCl, 0.5 mM EDTA
FLAG elution buffer	10 mM Tris-Cl pH 7.5, 150 mM NaCl, 0.5 mM EDTA, 0.2mg/ml 3xFLAG peptide (MERCK Cat. #F4799)

7.9.6 Protein purification, IP and pulldown from Sf21 insect cells

Name	Ingredients
lysis buffer (for 15 ml)	50 mM Tris-Cl pH 7.5, 200 mM NaCl, 1 mM $MgCl_2$, 1 mM EGTA, 0.5 mM DTT, 0.1% (v/v) Tween-20, 1x tablet of complete EDTA-free protease inhibitor cocktail, 5 µl Benzonase
wash buffer	50 mM Tris-Cl pH 7.5, 150 mM NaCl, 1 mM $MgCl_2$, 1 mM EGTA, 0.5 mM DTT
FLAG elution buffer	10 mM Tris-Cl pH 7.5, 150 mM NaCl, 0.5 mM EDTA, 0.2mg/ml 3xFLAG peptide (MERCK Cat. #F4799)
size exclusion chromatography (SEC) buffer	50 mM Tris, pH 7.5, 150 mM NaCl, 1mM MgCl2

7.9.7 Purchased kits, ready-to-use solutions and reagents

Name	Manufacturer	Application
Click-iT Plus EdU Alexa Fluor Imaging Kit	ThermoFisher, # C10638	S-phase cells detection
NucleoBond Xtra Midi Kit for plasmid DNA (transfection-grade)	Machery-Nagel, #740410	Plasmid isolation form *E. coli*

QuickExtract DNA Extraction Solution	Lucigen, #QE0905T	DNA extraction solution for mammalian cells (screening for CRISPR/Csas9 knockouts)
QIAquick Gel extraction kit	Qiagen, #28706	DNA extraction from agarose gel
Column PCR product purification Kit	Elite Biotech, # mB002	DNA extraction from PCR product
RNAiMAX siRNA transfection reagent	ThermoFisher, #13778075	siRNA depletion
Neon Transfection System	ThermoFisher, #MPK10096 and #MPK5000	Electroporation of mammalian cells
Retroviral system	Takarabio, #631188	Dox-inducible retrovirals ystem
NEBuilder Hifi DNA assembly master mix	NEB, #M5520AVIAL	cloning
Q5 High-Fidelity polymerase	NEB, #M0491S	PCR
T4 ligase	NEB, #M0202S	cloning of sgRNAs
T4 PNK	NEB, #M0201S	cloning of sgRNAs
Shrimp alkaline phosphatase (rSAP)	NEB, #M0371	cloning of sgRNAs
Trans-Blot TURBO Mini 0.2 µm PVDF Transfer kit	BioRad, #1704272	Western Blot (fast transfer)
Clarity Western ECL Substrate	BioRad #1705061	Western Blot (detection)

7.9.8 Human cell culture

Name	**Ingredients**
growth medium	DMEM/F-12 supplied with 10% v/v fetal bovine serum (FBS), 2mM L-glutamine, 20U/ml penicillin, 20U/ml streptomycin
transfection medium	Opti-MEM transfection medium
live cell imaging medium	DMEM/F-12 without phenolred, supplied with 10% v/v fetal bovine serum (FBS), 2mM L-glutamine, 20U/ml penicillin, 20U/ml streptomycin

Trypsinisation medium	Trypsin-EDTA (0.05%)

7.9.9 Bacterial cells

Name	**Ingredients**
growth medium	Lysogeny broth (LB) supplied with antibiotics (either ampicillin 100 µg/ml, kanamycin 50 µg/ml or chloramphenicol 30 µg/ml/spectinomycin 50 µg/ml)
growth medium	2x yeast extract tryptone (2xYT) medium supplied with antibiotics (either ampicillin 100 µg/ml, kanamycin 50 µg/ml or chloramphenicol 30 µg/ml/spectinomycin 50 µg/ml)
culture plates	LB-Agar: water (950 ml), tryptone (10 g), NaCl (10 g), yeast extract (5 g), agar (15%), supplied with antibiotics (either ampicillin 100 µg/ml, kanamycin 50 µg/ml or chloramphenicol 30 µg/ml/ spectinomycin 50 µg/ml)

7.9.10 Drugs

Name	**Application**
Doxycycline (dox)	inducible gene expression in mammalian cells
Palbociclib	Cdk4-6 inhibitor (arresting mammalian cells in G1)

8. Methods

8.1 Cell culture

8.1.1 Mammalian cell culture

Non-transformed RPE1 hTERT (human telomeres-immortalised retinal pigmented epithelial) cells, Human embryonic kidney 293 (T) (HEK T293) cells, HEK GP2-293 and all cell lines derived from these afore mentioned cell lines were cultured and passaged in phenol red-containing Dulbecco's Modified Eagle Medium/Nutrient Mixture F-12 (DMEM/F-12) medium supplied with 10 v/v fetal bovine serum (FBS), 2 mM L-glutamine, 20 U/ml penicillin and 20 µg/ml streptomycin at 37°C with 5% CO_2, and 95% rH. Fluorescence activated cell sorting (FACS) was performed with phenol red-free and HEPES-buffered DMEM/F-12. RPE1 hTERT stable cell lines with doxycycline (dox)-inducible expression of exogenous genes were under selection for 7 days with culture medium supplied with 10 µg/ml puromycin. All cells were regularly tested for mycoplasma.

8.1.2 Bacterial cell culture

E. coli- derived strains were grown either in LB or 2xYT medium supplied with antibiotics at 37°C for 12-16h while shaking.

8.1.3 Insect cell culture

Sf9 and Sf21 insect cells were cultured in Sf-900 III medium supplied 100 U/ml penicillin and 100 µg/ml streptomycin at 27°C.

8.2 DNA engineering

8.2.1 PCR amplification of insert and backbone for cloning

DNA fragments for cloning were prepared using PCR amplification with Q5® High-Fidelity DNA polymerase according to the manufacturer´s protocol. Annealing temperature and elongation time were adjusted according to the used primers and the length of the amplified region.

8.2.2 DNA gel extraction and PCR product purification

PCR products were run on 1-2% w/v agarose gel to confirm a successful PCR. For subsequent cloning, the correct bands (based on size) were cut out from the geld and purified using the QIAquick® Gel extraction kit (Qiagen) or the PCR products were directly purified using the Column PCR product purification Kit (Elite Biotech) following the manufacturer´s protocol. The DNA was eluted with ddH_20 and the concentration was measured on a NanoDrop® spectrophotometer.

8.2.3 Cloning via NEBuilder® HiFi DNA Assembly

Cloning was achieved using NEBuilder® HiFi DNA Assembly kit according to the manufacturer´s protocol. Briefly, DNA fragments (insert and backbone) were amplified via PCR, including at least 18 bp overhang regions, purified and then used for the assembly with the 2xHiFi DNA assembly master mix. To generate the overhangs NEBuilder assembly tool was used.

8.2.4 sgRNA cloning for CRISPR/Cas9

Cloning of the sgRNAs into the Cas9-containing px458 plasmid was done using T4 ligation. First, px458 was digested with the restriction enzyme *BbsI* and dephosphorylated with shrimp alkaline phosphatase (rSAP). Subsequently, sgRNAs oligo duplexes were generated and phosphorylated using following set up and thermocycler program:

1 ul	oligo 1 (100µM)
1 ul	oligo 2 (100µM)
1 ul	10X T4 Ligation Buffer (NI
6.5 ul	ddH_2O
0.5 ul	T4 PNK (NEB)
10 ul	total

Program:

37°C	30 min
95°C	5 min
25°C	ramp down 0.1°C/sec

The sgRNA oligo duplexes and the digested and dephosphorylated px458 were then used for T4 ligation using the following set up and incubation for 15-30 min at 37°C:

X	50 ng digested plasmid
1 ul	oligo duples
1 ul	10X T4 Ligation Buffer (NEB)
1 ul	T4 ligase
ad 10 µl	ddH_2O

Afterwards, 5 µl of the ligation product were directly used for bacterial transformation.

8.2.5 Miniprep and Midiprep plasmid isolation from bacteria

Bacteria colonies were picked from agar plates and inoculated in 4 ml of LB medium with antibiotics and incubated at 37°C for 12-16h while shaking for small scale plasmid isolation (miniprep). The following day, 2 ml of the culture were centrifuged and the pellet was resuspended with 350 µl S1 resuspension buffer. Then, 350 µl S2 lysis buffer was added, inverted 5x and incubated for 5 min at RT. Afterwards, 350 µl of S3 neutralisation buffer was added and inverted and then centrifuged for 5 min, max speed at 4°C. The supernatant was then resuspended with 900 µl isopropanol to precipitate the DNA and then centrifuged again for 5 min, max speed at 4°C. The supernatant was discarded and the DNA pellet was washed 1x with 70% ethanol and centrifuged for 1 min, max speed at RT. After air-evaporating the remaining ethanol, the DNA pellet was dissolved with ddH_20 and the concentration was measured on a NanoDrop® spectrophotometer.
For large scale plasmid isolation (midiprep), bacteria culture was inoculated in 120 ml 2xYT medium with antibiotics and incubated as described for miniprep. The overnight culture was then used for plasmid isolation using the NucleoBond Xtra Midi Kit from Machery-Nagel according to the manufacturer's protocol.

8.2.6 Genomic DNA extraction from mammalian cells and genomic PCR

DNA from mammalian cells (e.g. for CRISPR/Cas9 Knockout screen) was extracted using Quick DNA extraction solution from Lucigen. For a 96-well plate, cells were washed with 1x PBS and then 20 µl of the Quick extraction solution was added in each well and incubated on a thermoshaker for 15 min at 65°C and 550 rpm. Afterwards, the content of each well was transferred into a 96-well PCR plate and the following program was used to extract the DNA: 15min at 65°C, 15 min at 68°C and 10 min at 98°C. The DNA is ready to use for PCR using Q5® High-Fidelity DNA polymerase and the following PCR program:

1. Initial denaturation	98° C	5 min
35 Cycles **2. Denaturation** **3. Annealing** **4. Elongation**	 95° C variable 72° C	 30 sec 30 sec variable
5. Final elongation	72° C	2 min
6. Hold	12° C	∞

8.3 Transfection and transformation of cells

8.3.1 Transformation of chemically competent bacteria cells

Chemical competent DH5α cells (50 µl) were mixed with plasmid and incubated on ice for 30 min. Afterwards, cells were heat-shocked for 45 sec at 42°C and then placed directly on ice and incubated for 5 min. Then, 450 µl of LB medium was added to the cells and incubated on a thermoshaker for 30 min at 37°C and 300 rpm. 300 µl of the cell suspension was plated onto antibiotic containing LB-agar plates and incubated over night at 37°C.

8.3.2 Plasmid transfection and RNAi of mammalian cells

Transfection of HEK T293 and HEK GP2-293 was accomplished by using polyethyleneimine (PEI). Cells were seeded to reach at confluency between 40-60% at the time of the transfection. For co-IP experiments, cells were seeded onto 6 cm dishes (total volume 5 ml) and the transfection reagent was prepared with 5 ng of total DNA and 10 µl PEI in 500 µl Opti-MEM, mixed and incubated for 15 min. at RT. The transfection reagent was added drop-wise to the cells and for doxycycline (dox)-inducible cell lines, additionally dox was added at a final concentration of 1 µg/µl. Plasmid delivery into RPE1 cell lines was achieved by electroporation using the Neon™ Transfection system 100 µl Kit following the manufacturer's protocol. Briefly, for each transfection, $1.1x10^6$ were resuspended in 110 µl pre-warmed R buffer and mixed with 10-12 µg of DNA. 1050 V with 30 ms electro pulses (2 times) were applied to electroporate the cells. Afterwards, cells were seeded in pre-warmed fresh medium.
Transfection of synthetic siRNA oligos was performed using Lipofectamine® RNAiMAX Transfection Reagent from Life Technologies. Transfection reactions were prepared in Opti-MEM™ medium according to manufacturer's protocol. siRNA final concentration ranged between 50-100 nM.

8.3.3 Generation of stable cell lines (Transduction)

Stable cell lines were generated using the retroviral system. For dox-inducible expression, cell lines were generated by introducing first the Retro-X™ Tet-On® 3G Inducible Expression System (Takara Bio) into the parental cell line. The different constructs were then integrated under the TRE3G promotor via Retrovirus transfection. For this, HEK GP2-293 cell lines that express already the *gag* and *pol* gene were transfected with the respective construct containing the gene of interest and the pVSV-G vector (for the viral envelope protein). After harvesting of the virus, the target cell line was infected with the virus to generate the stable cell line. Constitutive expression cell lines were generated as the dox-inducible cell lines with the retroviral system.

8.4 Protein purification

8.4.1 Co-immunoprecipitation from mammalian cells

Co-immunoprecipitation experiments from mammalian cells were performed with transfected HEK293 cells. Cells were seeded onto 6 cm dishes so that they reach a confluency between 40% - 60% at the time of transfection. The following day, the medium was replaced with 4.5 ml fresh and the transfection reagent was prepared with 5 ng of total DNA and 10 µl PEI in 500 µl Opti-MEM, mixed and incubated for 15 min. at RT. The transfection reagent was added drop-wise to the cells and for doxycycline (dox)-inducible cell lines, additionally dox was added at a final concentration of 1 µg/µl. After 24h, cells were harvested, washed with PBS and then lysed with lysis buffer (150 – 250 µl depending on the confluency) for 45 min at 4°C while rotating. Afterwards, the lysate was pre-cleared via centrifugation for 30 min at 14000 x g and 4°C. Meanwhile, antibody-conjugated magnetic beads (Anti-FLAG M2 Magnetic Beads or Anti-HA Magnetic Beads) were equilibrated once with lysis buffer and then 2x with wash buffer. Per sample 20-30 µl of bead slurry was used. After pre-clearing of the cell lysate, 25 µl of the supernatant was taken as the input control sample and the remaining supernatant was added to the beads and incubated for 1h at 4°C while rotating. Beads were then washed 3x with wash buffer. For FLAG-IP experiments, beads were eluted with 35 µl elution buffer for 30 min at 4°C. After elution, 35 µl of Laemmli buffer was added onto the eluate and boiled for 10 min at 95°C. For HA-IP, beads were eluted directly with 70 µl Laemmli buffer and boiled as well for 10 min at 95°C.

8.4.2 Protein purification from insect cell

The MultiBac^{TM} system was used for protein expression in insect cells. First, POC5-Centrin2-2xFLAG or POC5$^{\Delta 153\text{-}184}$-Centrin2-2xFLAG construct was transformed in DH10MultiBac cells and then miniprep was performed to isolate the plasmid. Sf9 insect cells were then transfected with the plasmid to generate v0 baculoviruses using Cellfectin II (Invitrogen) according to the manufacturer's protocol. The v0 baculoviruses were then harvested after 72h to transfect 1x 10^6 cells/ml of Sf9 cells in a total volume of 30 ml. Afterwards, v1 baculovirus was diluted 1:50 in the cell suspension containing 1-2x 10^6 cells/ml of Sf21 cells and incubated 60h for protein expression. Cells were harvested, pelleted and then snap-frozen in liquid nitrogen and stored at -80°C until further use. For protein purification, the cell pellet was resuspended in cold lysis buffer and the lysate was pre-cleared via centrifugation at 20.000 x g for 30 min at 4°C. Meanwhile, anti-FLAG M2 Affinity Gel Beads were equilibrated once with lysis buffer and two times with wash buffer. Afterwards, the lysate was incubated with the beads for 1h at 4°C while rotating. The beads were then washed once with lysis buffer and twice with wash buffer

and eluted in elution buffer for 30 min at 4°C while rotating. The eluate was then either used for SDS-PAGE or loaded onto size exclusion chromatography (SEC) column and run in SEC buffer on a Äkta Pure/ÄktaGo device. For SEC of wild-type *POC5-Centrin2 sample,* the Superdex® 6 (Cytiva) Increase columns were used, whereas for POC5$^{\Delta 153\text{-}184}$-Centrin2 the Superdex® 75 column (Cytiva) was used. SEC samples were then analyzed via SDS-PAGE, Coomassie staining and were used also for Mass photometry.

8.5 SDS-PAGE and immunoblotting

Whole cell extracts or co-IP samples were loaded on a 4-20% gradient acrylamide gel and run for 90 min at 100 V. Afterwards, proteins were transferred on a ethanol-activated PVDF membrane using the optimised trans-blot turbo transfer kit and a semi-dry blotting system according to the manufacturer´s protocol. Alternatively, a wet tank transfer system with 1x transfer buffer was used and run with 110 V for 1h at 4°C. The membrane was then blocked for at least 1h at RT with blocking buffer (5% nonfat dry milk/TBS-T) while rotating. Primary antibodies were diluted in 3% BSA/TBS and the membrane was incubated in the antibody solution over night at 4°C while rotating. Afterwards, the membrane was washed three times for 5 min each with 1xTBS-T and then incubated with the secondary antibody (diluted in 5% nonfat dry milk/TBS-T) for 1h at RT while rotating. The membrane was washed three times for 5 min each with 1xTBS-T. Detection of the antibodies was done using the enhanced chemiluminescence (ECL) method and on a LAS4000IR imaging system.

8.6 Negative stain Electron Microscopy (EM)

Negative stain EM was performed by Dr. Annett Neuner. 5 µl of the sample was loaded on to glow-discharged copper-palladium 400 mesh grids that are covered with a 10 nm thick carbon layer (G2400D, Plano GmbH), incubated for 30 second at RT and then the grids were blotted with Whatman filter paper 50 (CAT N. 1450-070). After washing with three drops of water, the grids were stained 3% uranyl acetate in water. Image and data acquisition was done on a Talos Talos L120C transmission electron microscope (TEM) equipped with a 4k × 4k Ceta CMOS camera (Thermo Fisher Scientific) and the EPU software (v2.9, Thermo Fisher Scientific) at a nominal defocus of approximately −2 µm and an object pixel size of 0.2552 nm.
Image processing and 2D classification was performed by Dr. Martin Würtz using Relion 3.1. First, the contrast transfer function (CTF) of micrographs was estimated using Gctf and the approximately 500 particles were manually selected to create an initial 2D class for automated particle picking. During the automated particle picking, 20-200 classes were generated with a T-factor of 2, a translational search range of 20 pixels with a 2-pixel increment, and a mask diameter of 300−650 Å. For the wildtype POC5-Centrin2 sample, a total of 521 micrographs were acquired and from these 109.299 particles were automatically picked and then extracted at full pixel size. Two subsequent rounds of 2D classification were then performed to gain the best true positive classes. For the initial model that was later used as a template for the 3D classification, 50.652 particles were used and then (after one round of 3D classification), 31.687 particles were used for the 3D refinement and post-processing. For the POC5$^{\Delta 153\text{-}184}$-Centrin2 sample, 68.238 particles were picked automatically and then underwent three consecutive runs of 2D classification at full spatial resolution. To generate an initial model and for usage as a template for the 3D classification, 32.172 particles were selected. Afterwards, another round of 2D classification was performed to select the best classes. Ultimately, 19.021 particles were used for the 3D refinement and post-processing.

8.7 Mass Photometry

Mass Photometry analysis was performed by Dr. Karine Lapogue from the European Molecular Biology Laboratory (EMBL) Protein Expression and Purification Core Facility (PEPCF). High-precision microscope coverslips (24x50 mm) were prepared by washing with isopropanol and ddH_2O and dried under pressurised air stream. A silicone gasket containing six wells was positioned at the centre of the coverslip to create measurements wells. In each well, 19 µl of SEC buffer for both protein samples was added and then 1 µl of the protein sample with a concentration of 400 nM was mixed with the SEC buffer. All measurements were performed on a Refeyn TwoMP mass photometer and one-minute videos were recorded using the Refeyn AcquireMP 2024 R1 software and data was analyzed with the Refeyn DiscoverMP 2024 R1 software. To generate the standard contrast-to-mass calibration curve, bovine serum albumin (BSA, 66 kDa) and Immunoglobulin G (IgG, 150kDa and 300kDa) were used.

8.8 Immunofluorescence (IF)

Cells were grown on 12 mm #1.5 glass coverslips until desired confluence and were washed with 1x PBS before fixation with 100% ice-cold methanol at -20°C for 10 min. As an optional step to improve staining of certain antibodies, cells were treated with cytoskeleton extraction (CSK) buffer and washed once with 1x PBS before methanol fixation. After fixation, the coverslips were washed once with 1xPBS and incubated in blocking/permeabilisation buffer (10% FBS, 0.1% TritonX-100, 0.003% NaN_3, 1x PBS) for 30 min at RT. Then, coverslips were washed with 1x PBS and incubated with the primary antibody (diluted in 3% BSA in 1x PBS) for 1h at RT in a wet-chamber. Afterwards, the coverslips were washed three times with 1x PBS and then incubated with the secondary antibody and DAPI (diluted in 3% BSA in 1x PBS) for 30 min at RT in a wet chamber and protected from light. After washing three times with 1x PBS, the coverslips were mounted on microscope glass slides using Mowiol 4-88 and let dry over night at RT or for 1h at 37°C protected from light. All conventional IF images were acquired by the DeltaVision RT system (Applied Precision) with an Olympus IX71 microscope equipped with 60x/1.42 and 100x/1.40 oil objective lenses at RT temperature. Raw images were processed to generate maximum intensity projections using the softWoRx software provided by the DeltaVision microscope itself (Applied precision).

8.9 Detection of S- and G2-phase cells

To detect S-phase cells, cells were treated with 5-ethynyl-2-deoxyuridine (EdU) using the Click-iT Plus EdU Alexa Fluor Imaging Kit according to the manufacturer's protocol. Briefly, cells were treated incubated for 20-30 min with EdU prior fixation. Before primary antibody staining, coverslips were incubated with the EdU-detection solution for 30 min at RT in a wet-chamber and protected from light. Afterwards, the procedure follows the normal immunofluorescence protocol described in 8.6. To detect additionally G2-phase cells, cells were co-stained with Mitosin/CENP-F.

8.10 Analysis of conventional IF images

IF images acquired on the DeltaVision microscope were analyzed with Fiji. The quantification was performed on the maximum projected images using a semi-automated macro where the background signal was subtracted automatically:

```
macro "auto IF quantification [u]" {

s = selectionType();
if( s == -1 ) {
   exit("There was no selection.");
} else if( s != 10 ) {
   exit("The selection wasn't a point selection.");
} else {
   getSelectionCoordinates(xPoints,yPoints);
   x = xPoints[0];
   y = yPoints[0];

makeRectangle(x-10,y-10,20,20);
run("Measure");
ISm = getResult('IntDen', nResults-1);
ASm = getResult('Area', nResults-1);
makeRectangle(x-14,y-14,28,28);
run("Measure");
Ibig = getResult('IntDen', nResults-1);
Ab = getResult('Area', nResults-1);
A=Ibig-ISm;
B=(Ab-ASm);
C=ASm/B;
Intensity=ISm-(A*C);
print(d2s(Intensity,0));
}
```

8.11 Ultrastructure Expansion Microscopy (U-ExM)

Cells were grown on 12 mm #1.5 glass coverslips until desired confluence and were washed with 1x PBS and then treated with CSK buffer. Then, the coverslips were washed with 1x PBS and added into a 12-well plate containing the fixation solution and incubated for 3.5-5h at 37°C. Afterwards, gelation was performed in a pre-chilled wet-chamber with 35 µl monomer solution, including 0.5% TEMED and 0.5% APS to start the polymerisation and incubated for 10 min on ice and then for 1h at 37°C. After gelation, the coverslips were immersed in denaturation buffer and incubated for 15 at RT on a thermoshaker to detach the gel from the coverslip. Subsequently, the gel was added into an Eppendorf reaction tube (filled with denaturation buffer) and then boiled for 45 min at 95°C. The denatured gel was then expanded in water for 1h at RT with three times exchange of water. Afterwards, the gel shrank back in 1x PBS and then a small piece was cut out and added into a 12 well and incubated with 650 µl of primary antibody solution (diluted in 1% BSA/PBS) over night at 37°C while gently shaking. The next day, the gel was washed three times with 1x PBS-T for 5 min each and then incubated in 650 µl secondary antibody solution (diluted in 1% BSA/PBS) for 3h at 37°C while gently shaking. Afterwards, the gel was again washed three times with 1x PBS-T for 5 min each time and then expanded in water. For imaging, the gel was placed in a Ibidi µ-Dish 35 mm that was coated

with Poly-L-Lysine to prevent any moving of the gel. Acquisition of U-ExM images was performed on an inverted Leica TCS SP8 STED 3x with FALCON FLIM microscope using a HC PL APO 100x/1.40 STED White Oil objective. The z-interval was set to 0.15 µm. Raw images were deconvoluted by Huygens' Deconvolution software (SVI Inc.). The z-stack spanning the centrioles were z-projected by ImageJ/Fiji software.

8.12 Analysis of U-ExM images

U-ExM samples were co-stained with α-tubulin (as a centriolar reference) and the respective protein. The analysis was performed in Fiji on deconvoluted and then maximum projected images. For length measurements only longitudinal centrioles that were aligned nearly parallel to the x, y plane were considered. A line scan was drawn along the centriole and with the plot profile tool and plugin BAR the fluorescence intensity and the maxima values for the reference protein and the respective protein of interest was obtained. The length of a signal was determined as the distance between 50% of the signal from the most proximal maximum and 50% of the signal from the most distal maximum and was then corrected with the expansion factor to obtain the real distance. For diameter measurements, top view centrioles that were aligned vertically in the z axis were selected. Two lines that were perpendicular to each other were drawn through the centriole for each protein and the plot profile of each line was obtained and the maxima values were calculated by the BAR plugin. The average of the two measurements was used to define the diameter of the protein of interest and was then normalised to the average α-tubulin diameter.

8.13 FLIM-FRET microscopy

HEK293T cells were co-transfected with mNeonGreen-POC1A (donor) and mScarlet-I-POC1B (acceptor) or each plasmid alone using PEI. After 24h, cells were seeded into an ibidi µ-slide 8 well. 48h post-transfection, FLIM-FRET microscopy was performed on living cells on a Leica TCS SP8 STED 3× microscope with FALCON FLIM with white light laser (WLL) and a HC PL APO 100×/1.40 STED White Oil objective in room temperature. Images were acquired with an imaging repetition of at least 1000 photons/pixel. The data analysis of the fluorescence lifetime was measured using the FLIM option in the Leica LAS X software.

8.14 Electron microscopy

Electron Microscopy was performed by Dr. Annett Neuner. Cells, seeded onto coverslips and reached a confluency between 80-90%, were washed three times with 1x PBS and then pre-fixed in 2.5% glutaraldehyde, 1.6% paraformaldehyde, 2% sucrose in 50 mM cacodylate buffer for 30 min at RT. Afterwards, cells were rinsed with cacodylate buffer and post-fixed 2% OsO4 for approximal 45 min on ice protected from light. Then, the cells were washed with ddH_20 and incubated in 0.5% aqueous uranyl acetate overnight at 4°C. After incubation, the coverslips were washed with ddH_20, dehydrated stepwise with ethanol and then directly embedded on capsules filled with Spurr´s resin (Sigma-Aldrich) and polymerised at 60°C for 48h. The embedded samples were sectioned on a Reichert Ultracut S Microtome (Leica Instruments, Vienna, Austria) with a thickness of approximately 80 nm and then stained with 3% aqueous uranyl acetate and lead citrate. Serial-sections were acquired at a Jeol JE-1400 (Jeol Ltd., Tokyo, Japan), operating at 80 kV, equipped with a 4k x 4k digital camera (F416, TVIPS, Gauting, Germany). Data analysis was done using Fiji.

8.15 AlphaFold2 and AlphaFold3 predictions

For the prediction of a POC5 tetramer of *Paramecum tetraurelia*, the web-based AlphaFold Server (powered by AlphaFold3) was used.
Predictions with AlphaFold2 and the subsequent analysis of the interaction map were performed by Dr. Sebastian Eustermann and Dr. Thomas Hoffmann from EMBL. The Predictions were performed with a customised multimer pipeline of AlphaFold2 (AF2, release version 2.3.2) and each candidate sequence multiple sequence alignments (MSA) were computed separately. The MSAs were further processed using the AF2 multimer_v3 parameter set and the UniRef30 database version 2023_02. A total of 25 models were predicted per interaction, for the prediction of POC1A/POC1B and the POC1-binding region of POC5 (residues 472-532) a total of 125 models were predicted. The interaction maps were generated by taking into account of different factors (distance, hydrogen bonds etc.), leading to the score value.

8.16 Statistics and reproducibility

Graphs of the data analysis were plotted using Prism v.9/10 (GraphPad). All data are derived from at least three biologically independent experiments with triplicates, unless specified otherwise in the respective figure legend. All statistical tests (unpaired two-tailed t-test and one-way ANOVA) were performed in Prism v.9/10 (GraphPad): "n.s." stands for not significant: $P > 0.05$. Stars indicate the following levels of significance: *$P < 0.05$, **$P < 0.01$, ***$P < 0.001$, ****$P < 0.0001$. The exact p-values were calculated in Microsoft Excel. For the Graphs of the U-ExM analysis, data from independent experiments were pooled.

References

1. Bruce, A. *et al. Molecular Biology of the Cell*. (Garland Science, New York, 2015).
2. Salazar-Roa, M. & Malumbres, M. Fueling the Cell Division Cycle. *Trends Cell Biol* **27**, (2017).
3. Matthews, H. K., Bertoli, C. & M Bruin, R. A. Cell cycle control in cancer. doi:10.1038/s41580-021-00404-3.
4. Malumbres, M. Cyclin-dependent kinases. *Genome Biol* **15**, 122 (2014).
5. Lim, S. & Kaldis, P. Cdks, cyclins and CKIs: roles beyond cell cycle regulation. *Development* **140**, 3079–3093 (2013).
6. Glotzer, M., Murray, A. W. & Kirschner, M. W. Cyclin is degraded by the ubiquitin pathway. *Nature 1991 349:6305* **349**, 132–138 (1991).
7. Parker, L. L., Atherton-Fessler, S. & Piwnica-Worms, A. p107wee1 is a dual-specificity kinase that phosphorylates p34cdc2 on tyrosine 15. *Proc Natl Acad Sci U S A* **89**, 2917 (1992).
8. Dunphy, W. G. & Kumagai, A. The cdc25 protein contains an intrinsic phosphatase activity. *Cell* **67**, 189–196 (1991).
9. Nakayama, K. I. & Nakayama, K. Ubiquitin ligases: cell-cycle control and cancer. *Nature Reviews Cancer 2006 6:5* **6**, 369–381 (2006).
10. Schrock, M. S., Stromberg, B. R., Scarberry, L. & Summers, M. K. APC/C ubiquitin ligase: functions and mechanisms in tumorigenesis. *Semin Cancer Biol* **67**, 80 (2020).
11. Pennycook, B. R. & Barr, A. R. Restriction point regulation at the crossroads between quiescence and cell proliferation. *FEBS Lett* **594**, 2046–2060 (2020).
12. Pagano, M., Pepperkok, R., Verde, F., Ansorge, W. & Draetta, G. Cyclin A is required at two points in the human cell cycle. *EMBO J* **11**, 961–971 (1992).
13. Holder, J., Poser, E. & Barr, F. A. Getting out of mitosis: spatial and temporal control of mitotic exit and cytokinesis by PP1 and PP2A. *FEBS Lett* **593**, 2908–2924 (2019).
14. Gavet, O. & Pines, J. Progressive activation of CyclinB1-Cdk1 coordinates entry to mitosis. *Dev Cell* **18**, 533 (2010).
15. Bruinsma, W., Raaijmakers, J. A. & Medema, R. H. Switching Polo-like kinase-1 on and off in time and space. *Trends Biochem Sci* **37**, 534–542 (2012).
16. Lampson, M. A. & Cheeseman, I. M. Sensing centromere tension: Aurora B and the regulation of kinetochore function. *Trends Cell Biol* **21**, 133 (2011).
17. Magnaghi-Jaulin, L., Eot-Houllier, G., Gallaud, E. & Giet, R. Aurora A Protein Kinase: To the Centrosome and Beyond. *Biomolecules* **9**, (2019).
18. Prosser, S. L. & Pelletier, L. Mitotic spindle assembly in animal cells: a fine balancing act. *Nature Reviews Molecular Cell Biology 2017 18:3* **18**, 187–201 (2017).
19. Musacchio, A. The Molecular Biology of Spindle Assembly Checkpoint Signaling Dynamics. *Current Biology* **25**, R1002–R1018 (2015).
20. Akhmanova, A. & Steinmetz, M. O. Microtubule minus-end regulation at a glance. *J Cell Sci* **132**, (2019).
21. Tilney, L. G. *et al.* MICROTUBULES: EVIDENCE FOR 13 PROTOFILAMENTS. *J Cell Biol* **59**, 267 (1973).
22. Bergen, L. G., Kuriyama, R. & Borisy, G. G. Polarity of microtubules nucleated by centrosomes and chromosomes of Chinese hamster ovary cells in vitro. *J Cell Biol* **84**, 151–159 (1980).
23. Heidemann, S. R. & McIntosh, J. R. Visualization of the structural polarity of microtubules. *Nature* **286**, 517–519 (1980).
24. Howard, J. & Hyman, A. A. Dynamics and mechanics of the microtubule plus end. *Nature 2003 422:6933* **422**, 753–758 (2003).

25. Nigg, E. A. & Holland, A. J. Once and only once: mechanisms of centriole duplication and their deregulation in disease. *Nature Reviews Molecular Cell Biology 2018 19:5* **19**, 297–312 (2018).
26. Lawo, S., Hasegan, M., Gupta, G. D. & Pelletier, L. Subdiffraction imaging of centrosomes reveals higher-order organizational features of pericentriolar material. *Nature Cell Biology 2012 14:11* **14**, 1148–1158 (2012).
27. Woodruff, J. B., Wueseke, O. & Hyman, A. A. Pericentriolar material structure and dynamics. *Philosophical Transactions of the Royal Society B: Biological Sciences* **369**, 20130459 (2014).
28. Fu, J. & Glover, D. M. Structured illumination of the interface between centriole and peri-centriolar material. *Open Biol* **2**, (2012).
29. Azimzadeh, J. & Marshall, W. F. Building the centriole. *Curr Biol* **20**, (2010).
30. Murphy, S. M. *et al.* GCP5 and GCP6: two new members of the human gamma-tubulin complex. *Mol Biol Cell* **12**, 3340–3352 (2001).
31. Thawani, A., Kadzik, R. S. & Petry, S. XMAP215 is a microtubule nucleation factor that functions synergistically with the γ-tubulin ring complex. *Nature Cell Biology 2018 20:5* **20**, 575–585 (2018).
32. Rai, D. *et al.* CAMSAPs and nucleation-promoting factors control microtubule release from γ-TuRC. *Nat Cell Biol* **26**, 404–420 (2024).
33. Murphy, S. M., Urbani, L. & Stearns, T. The mammalian gamma-tubulin complex contains homologues of the yeast spindle pole body components spc97p and spc98p. *J Cell Biol* **141**, 663–674 (1998).
34. Stearns, T. & Kirschner, M. In vitro reconstitution of centrosome assembly and function: the central role of gamma-tubulin. *Cell* **76**, 623–637 (1994).
35. Zheng, Y., Jung, M. K. & Oakley, B. R. Gamma-tubulin is present in Drosophila melanogaster and Homo sapiens and is associated with the centrosome. *Cell* **65**, 817–823 (1991).
36. Zheng, Y., Wong, M. L., Alberts, B. & Mitchison, T. Nucleation of microtubule assembly by a γ-tubulin-containing ring complex. *Nature 1995 378:6557* **378**, 578–583 (1995).
37. Murphy, S. M. *et al.* GCP5 and GCP6: Two New Members of the Human γ-Tubulin Complex. *Mol Biol Cell* **12**, 3340 (2001).
38. Liu, P. *et al.* Insights into the assembly and activation of the microtubule nucleator γ-TuRC. *Nature* **578**, 467–471 (2020).
39. Letort, G., Nedelec, F., Blanchoin, L. & Théry, M. Centrosome centering and decentering by microtubule network rearrangement. *Mol Biol Cell* **27**, 2833 (2016).
40. Vlijm, R. *et al.* STED nanoscopy of the centrosome linker reveals a CEP68-organized, periodic rootletin network anchored to a C-Nap1 ring at centrioles. *Proc Natl Acad Sci U S A* **115**, E2246–E2253 (2018).
41. Panic, M., Hata, S., Neuner, A. & Schiebel, E. The Centrosomal Linker and Microtubules Provide Dual Levels of Spatial Coordination of Centrosomes. *PLoS Genet* **11**, e1005243 (2015).
42. Gönczy, P. Towards a molecular architecture of centriole assembly. *Nature Reviews Molecular Cell Biology 2012 13:7* **13**, 425–435 (2012).
43. Wei, Z. *et al.* Requirement of the Cep57-Cep63 Interaction for Proper Cep152 Recruitment and Centriole Duplication. *Mol Cell Biol* **40**, (2020).
44. Brown, N. J., Marjanović, M., Lüders, J., Stracker, T. H. & Costanzo, V. Cep63 and cep152 cooperate to ensure centriole duplication. *PLoS One* **8**, (2013).
45. Sonnen, K. F., Gabryjonczyk, A. M., Anselm, E., Nigg, E. A. & Stierhof, Y. D. Human Cep192 and Cep152 cooperate in Plk4 recruitment and centriole duplication. *J Cell Sci* **126**, 3223–3233 (2013).

46. Habedanck, R., Stierhof, Y. D., Wilkinson, C. J. & Nigg, E. A. The Polo kinase Plk4 functions in centriole duplication. *Nat Cell Biol* **7**, 1140–1146 (2005).
47. Bettencourt-Dias, M. *et al.* SAK/PLK4 is required for centriole duplication and flagella development. *Curr Biol* **15**, 2199–2207 (2005).
48. Kim, T. S. *et al.* Hierarchical recruitment of Plk4 and regulation of centriole biogenesis by two centrosomal scaffolds, Cep192 and Cep152. *Proc Natl Acad Sci U S A* **110**, E4849–E4857 (2013).
49. Martin, C. A. *et al.* Mutations in PLK4, encoding a master regulator of centriole biogenesis, cause microcephaly, growth failure and retinopathy. *Nat Genet* **46**, 1283–1292 (2014).
50. Kratz, A. S., Bärenz, F., Richter, K. T. & Hoffmann, I. Plk4-dependent phosphorylation of STIL is required for centriole duplication. *Biol Open* **4**, 370–377 (2015).
51. Vulprecht, J. *et al.* STIL is required for centriole duplication in human cells. *J Cell Sci* **125**, 1353–1362 (2012).
52. Leidel, S., Delattre, M., Cerutti, L., Baumer, K. & Gönczy, P. SAS-6 defines a protein family required for centrosome duplication in C. elegans and in human cells. *Nat Cell Biol* **7**, 115–125 (2005).
53. Comartin, D. *et al.* CEP120 and SPICE1 cooperate with CPAP in centriole elongation. *Curr Biol* **23**, 1360–1366 (2013).
54. Lin, Y. N. *et al.* CEP120 interacts with CPAP and positively regulates centriole elongation. *J Cell Biol* **202**, 211–219 (2013).
55. Lin, Y. C. *et al.* Human microcephaly protein CEP135 binds to hSAS-6 and CPAP, and is required for centriole assembly. *EMBO Journal* **32**, 1141–1154 (2013).
56. Gupta, H. *et al.* SAS-6 Association with γ-Tubulin Ring Complex Is Required for Centriole Duplication in Human Cells. *Curr Biol* **30**, 2395-2403.e4 (2020).
57. Gudi, R., Zou, C., Li, J. & Gao, Q. Centrobin–tubulin interaction is required for centriole elongation and stability. *J Cell Biol* **193**, 711 (2011).
58. Gudi, R., Haycraft, C. J., Bell, P. D., Li, Z. & Vasu, C. Centrobin-mediated Regulation of the Centrosomal Protein 4.1-associated Protein (CPAP) Level Limits Centriole Length during Elongation Stage. *Journal of Biological Chemistry* **290**, 6890–6902 (2015).
59. Azimzadeh, J. *et al.* hPOC5 is a centrin-binding protein required for assembly of full-length centrioles. *J Cell Biol* **185**, 101–114 (2009).
60. Fu, J. *et al.* Conserved molecular interactions in centriole-to-centrosome conversion. *Nature Cell Biology 2015 18:1* **18**, 87–99 (2015).
61. Fong, C. S., Ozaki, K. & Tsou, M. F. B. PPP1R35 ensures centriole homeostasis by promoting centriole-to-centrosome conversion. *Mol Biol Cell* **29**, 2801 (2018).
62. Wang, W. J., Soni, R. K., Uryu, K. & Tsou, M. F. B. The conversion of centrioles to centrosomes: essential coupling of duplication with segregation. *Journal of Cell Biology* **193**, 727–739 (2011).
63. Atorino, E. S., Hata, S., Funaya, C., Neuner, A. & Schiebel, E. CEP44 ensures the formation of bona fide centriole wall, a requirement for the centriole-to-centrosome conversion. *Nature Communications 2020 11:1* **11**, 1–15 (2020).
64. Tsou, M. F. B. & Stearns, T. Mechanism limiting centrosome duplication to once per cell cycle. *Nature* **442**, 947–951 (2006).
65. Nigg, E. A. & Holland, A. J. Once and only once: mechanisms of centriole duplication and their deregulation in disease. *Nat Rev Mol Cell Biol* **19**, 297–312 (2018).
66. Agircan, F. G., Schiebel, E. & Mardin, B. R. Separate to operate: control of centrosome positioning and separation. *Philosophical Transactions of the Royal Society B: Biological Sciences* **369**, (2014).

67. Mardin, B. R., Agircan, F. G., Lange, C. & Schiebel, E. Plk1 controls the Nek2A-PP1γ antagonism in centrosome disjunction. *Curr Biol* **21**, 1145–1151 (2011).
68. Chinen, T. *et al.* Centriole and PCM cooperatively recruit CEP192 to spindle poles to promote bipolar spindle assembly. *Journal of Cell Biology* **220**, (2021).
69. Tsou, M. F. B. *et al.* Polo kinase and separase regulate the mitotic licensing of centriole duplication in human cells. *Dev Cell* **17**, 344–354 (2009).
70. Kim, J., Lee, K. & Rhee, K. PLK1 regulation of PCNT cleavage ensures fidelity of centriole separation during mitotic exit. *Nature Communications 2015 6:1* **6**, 1–12 (2015).
71. LeGuennec, M., Klena, N., Aeschlimann, G., Hamel, V. & Guichard, P. Overview of the centriole architecture. *Curr Opin Struct Biol* **66**, 58–65 (2021).
72. Paintrand, M., Moudjou, M., Delacroix, H. & Bornens, M. Centrosome organization and centriole architecture: Their sensitivity to divalent cations. *J Struct Biol* **108**, 107–128 (1992).
73. Li, S., Fernandez, J. J., Marshall, W. F. & Agard, D. A. Electron cryo-tomography provides insight into procentriole architecture and assembly mechanism. *Elife* **8**, (2019).
74. Wang, J. T. & Stearns, T. The ABCs of Centriole Architecture: The Form and Function of Triplet Microtubules. *Cold Spring Harb Symp Quant Biol* **82**, 145 (2018).
75. Stathatos, G. G., Dunleavy, J. E. M., Zenker, J. & O'Bryan, M. K. Delta and epsilon tubulin in mammalian development. *Trends Cell Biol* **31**, 774–787 (2021).
76. Chang, P. & Stearns, T. δ-Tubulin and ε-tubulin: two new human centrosomal tubulins reveal new aspects of centrosome structure and function. *Nature Cell Biology 2000 2:1* **2**, 30–35 (1999).
77. Pudlowski, R. *et al.* A delta-tubulin/epsilon-tubulin/Ted protein complex is required for centriole architecture. *Elife* **13**, (2024).
78. Breslow, D. K. *et al.* A CRISPR-based screen for Hedgehog signaling provides insights into ciliary function and ciliopathies. *Nature Genetics 2018 50:3* **50**, 460–471 (2018).
79. Wang, J. T., Kong, D., Hoerner, C. R., Loncarek, J. & Stearns, T. Centriole triplet microtubules are required for stable centriole formation and inheritance in human cells. *Elife* **6**, (2017).
80. Guichard, P. *et al.* Native architecture of the centriole proximal region reveals features underlying its 9-fold radial symmetry. *Curr Biol* **23**, 1620–1628 (2013).
81. Klena, N. *et al.* Architecture of the centriole cartwheel-containing region revealed by cryo-electron tomography. *EMBO J* **39**, (2020).
82. Vorobjev, I. A. & Chentsov, Y. S. The ultrastructure of centriole in mammalian tissue culture cells. *Cell Biol Int Rep* **4**, 1037–1044 (1980).
83. Kitagawa, D. *et al.* Structural Basis of the 9-Fold Symmetry of Centrioles. *Cell* **144**, 364 (2011).
84. Van Breugel, M. *et al.* Structures of SAS-6 suggest its organization in centrioles. *Science* **331**, 1196–1199 (2011).
85. Le Guennec, M. *et al.* A helical inner scaffold provides a structural basis for centriole cohesion. *Sci Adv* **6**, eaaz4137 (2020).
86. Hiraki, M., Nakazawa, Y., Kamiya, R. & Hirono, M. Bld10p constitutes the cartwheel-spoke tip and stabilizes the 9-fold symmetry of the centriole. *Curr Biol* **17**, 1778–1783 (2007).
87. Hatzopoulos, G. N. *et al.* Structural Analysis of the G-Box Domain of the Microcephaly Protein CPAP Suggests a Role in Centriole Architecture. *Structure(London, England:1993)* **21**, 2069 (2013).

88. Bournonville, L., Laporte, Marine. H., Borgers, S., Guichard, P. & Hamel, V. The A-C Linker controls centriole cohesion and duplication. *bioRxiv* 2024.10.04.616628 (2024) doi:10.1101/2024.10.04.616628.
89. Greenan, G. A., Keszthelyi, B., Vale, R. D. & Agard, D. A. Insights into centriole geometry revealed by cryotomography of doublet and triplet centrioles. *Elife* **7**, (2018).
90. Arslanhan, M. D. *et al.* CCDC15 localizes to the centriole inner scaffold and controls centriole length and integrity. *J Cell Biol* **222**, e202305009 (2023).
91. Steib, E. *et al.* Wdr90 is a centriolar microtubule wall protein important for centriole architecture integrity. *Elife* **9**, 1–28 (2020).
92. Bowler, M. *et al.* High-resolution characterization of centriole distal appendage morphology and dynamics by correlative STORM and electron microscopy. *Nature Communications 2019 10:1* **10**, 1–15 (2019).
93. Yang, T. T. *et al.* Super-resolution architecture of mammalian centriole distal appendages reveals distinct blade and matrix functional components. *Nature Communications 2018 9:1* **9**, 1–11 (2018).
94. Ma, D., Wang, F., Teng, J., Huang, N. & Chen, J. Structure and function of distal and subdistal appendages of the mother centriole. *J Cell Sci* **136**, (2023).
95. Uzbekov, R. & Alieva, I. Who are you, subdistal appendages of centriole? *Open Biol* **8**, (2018).
96. Ma, D., Wang, F., Teng, J., Huang, N. & Chen, J. Structure and function of distal and subdistal appendages of the mother centriole. *J Cell Sci* **136**, (2023).
97. Bornens, M. & Gönczy, P. Centrosomes back in the limelight. *Philosophical Transactions of the Royal Society B: Biological Sciences* **369**, (2014).
98. Vorobjev, I. A. & Chentsov, Y. S. The ultrastructure of centriole in mammalian tissue culture cells. *Cell Biol Int Rep* **4**, 1037–1044 (1980).
99. Dippell, R. V. The development of basal bodies in paramecium. *Proc Natl Acad Sci U S A* **61**, 461 (1968).
100. Guichard, P. *et al.* Native architecture of the centriole proximal region reveals features underlying its 9-fold radial symmetry. *Curr Biol* **23**, 1620–1628 (2013).
101. Di gioia, S. A. *et al.* FAM161A, associated with retinitis pigmentosa, is a component of the cilia-basal body complex and interacts with proteins involved in ciliopathies. *Hum Mol Genet* **21**, 5174–5184 (2012).
102. Zach, F. *et al.* The retinitis pigmentosa 28 protein FAM161A is a novel ciliary protein involved in intermolecular protein interaction and microtubule association. *Hum Mol Genet* **21**, 4573–4586 (2012).
103. Pearson, C. G., Osborn, D. P. S., Giddings, T. H., Beales, P. L. & Winey, M. Basal body stability and ciliogenesis requires the conserved component Poc1. *Journal of Cell Biology* **187**, 905–920 (2009).
104. Venoux, M. *et al.* Poc1A and Poc1B act together in human cells to ensure centriole integrity. *J Cell Sci* **126**, 163–175 (2013).
105. Zhang, J. & Wang, Y. L. Centrosome defines the rear of cells during mesenchymal migration. *Mol Biol Cell* **28**, 3240 (2017).
106. Sumiyoshi, E. & Sugimoto, A. Cell Polarity: Centrosomes Release Signals for Polarization. *Current Biology* **22**, R281–R283 (2012).
107. Bettencourt-Dias, M. & Glover, D. M. Centrosome biogenesis and function: centrosomics brings new understanding. *Nature Reviews Molecular Cell Biology 2007 8:6* **8**, 451–463 (2007).
108. Arquint, C., Gabryjonczyk, A. M. & Nigg, E. A. Centrosomes as signalling centres. *Philosophical Transactions of the Royal Society B: Biological Sciences* **369**, 20130464 (2014).

109. Conduit, P. T., Wainman, A. & Raff, J. W. Centrosome function and assembly in animal cells. *Nature Reviews Molecular Cell Biology 2015 16:10* **16**, 611–624 (2015).
110. Bettencourt-Dias, M., Hildebrandt, F., Pellman, D., Woods, G. & Godinho, S. A. Centrosomes and cilia in human disease. *Trends Genet* **27**, 307–315 (2011).
111. Faheem, M. *et al.* Molecular genetics of human primary microcephaly: an overview. *BMC Med Genomics* **8**, S4 (2015).
112. Debec, A., Sullivan, W. & Bettencourt-Dias, M. Centrioles: active players or passengers during mitosis? *Cell Mol Life Sci* **67**, 2173 (2010).
113. Azimzadeh, J., Wong, M. L., Downhour, D. M., Alvarado, A. S. & Marshall, W. F. Centrosome Loss in the Evolution of Planarians. *Science* **335**, 461 (2012).
114. Fong, C. S. *et al.* 53BP1 and USP28 mediate p53- dependent cell cycle arrest in response to centrosome loss and prolonged mitosis. *Elife* **5**, (2016).
115. Lambrus, B. G. *et al.* A USP28–53BP1–p53–p21 signaling axis arrests growth after centrosome loss or prolonged mitosis. *Journal of Cell Biology* **214**, 143–153 (2016).
116. Meitinger, F. *et al.* 53BP1 and USP28 mediate p53 activation and G1 arrest after centrosome loss or extended mitotic duration. *Journal of Cell Biology* **214**, 155–166 (2016).
117. D'Assoro, A. B. *et al.* Impaired p53 function leads to centrosome amplification, acquired ERα phenotypic heterogeneity and distant metastases in breast cancer MCF-7 xenografts. *Oncogene 2008 27:28* **27**, 3901–3911 (2008).
118. Wang, W. J. *et al.* De novo centriole formation in human cells is error-prone and does not require SAS-6 self-assembly. *Elife* **4**, (2015).
119. Raff, J. W. & Basto, R. Centrosome Amplification and Cancer: A Question of Sufficiency. *Dev Cell* **40**, 217–218 (2017).
120. Karki, M., Keyhaninejad, N. & Shuster, C. B. Precocious centriole disengagement and centrosome fragmentation induced by mitotic delay. *Nat Commun* **8**, 15803 (2017).
121. Denu, R. A. *et al.* Centriole Overduplication is the Predominant Mechanism Leading to Centrosome Amplification in Melanoma. *Mol Cancer Res* **16**, 517 (2018).
122. Vitrea, B. *et al.* Chronic centrosome amplification without tumorigenesis. *Proc Natl Acad Sci U S A* **112**, E6321–E6330 (2015).
123. Serçin, Ö. *et al.* Transient PLK4 overexpression accelerates tumorigenesis in p53-deficient epidermis. *Nature Cell Biology 2015 18:1* **18**, 100–110 (2015).
124. LoMastro, G. M. & Holland, A. J. The emerging link between centrosome aberrations and metastasis. *Dev Cell* **49**, 325 (2019).
125. Godinho, S. A. *et al.* Oncogene-like induction of cellular invasion from centrosome amplification. *Nature* **510**, 167 (2014).
126. Durlu, Y. K., Köroɬlu, Ç. & Tolun, A. Novel Recessive Cone-Rod Dystrophy Caused by POC1B Mutation. *JAMA Ophthalmol* **132**, 1185–1191 (2014).
127. Hassan, A. *et al.* Adolescent idiopathic scoliosis associated POC5 mutation impairs cell cycle, cilia length and centrosome protein interactions. *PLoS One* **14**, e0213269 (2019).
128. Hassan, A. *et al.* Differential Regulation of POC5 by ERα in Human Normal and Scoliotic Cells. *Genes (Basel)* **14**, 1111 (2023).
129. Hubshman, M. W. *et al.* Whole-exome sequencing reveals POC5 as a novel gene associated with autosomal recessive retinitis pigmentosa. *Hum Mol Genet* **27**, 614–624 (2018).
130. Roosing, S. *et al.* Disruption of the Basal Body Protein POC1B Results in Autosomal-Recessive Cone-Rod Dystrophy. *The American Journal of Human Genetics* **95**, 131–142 (2014).
131. Ying, G., Frederick, J. M. & Baehr, W. Deletion of both centrin 2 (CETN2) and CETN3 destabilizes the distal connecting cilium of mouse photoreceptors. *J Biol Chem* **294**, 3957 (2019).

132. Mercey, O. *et al.* The connecting cilium inner scaffold provides a structural foundation that protects against retinal degeneration. *PLoS Biol* **20**, e3001649 (2022).
133. Sala, C. *et al.* An interaction network of inner centriole proteins organised by POC1A-POC1B heterodimer crosslinks ensures centriolar integrity. *Nature Communications 2024 15:1* **15**, 1–20 (2024).
134. Meehl, J. B., Bayless, B. A., Giddings, T. H., Pearson, C. G. & Winey, M. Tetrahymena Poc1 ensures proper intertriplet microtubule linkages to maintain basal body integrity. *Mol Biol Cell* **27**, 2394–2403 (2016).
135. Fourrage, C., Chevalier, S. & Houliston, E. A Highly Conserved Poc1 Protein Characterized in Embryos of the Hydrozoan Clytia hemisphaerica: Localization and Functional Studies. *PLoS One* **5**, e13994 (2010).
136. Pearson, C. G., Osborn, D. P. S., Giddings, T. H., Beales, P. L. & Winey, M. Basal body stability and ciliogenesis requires the conserved component Poc1. *Journal of Cell Biology* **187**, 905–920 (2009).
137. Keller, L. C. *et al.* Molecular architecture of the centriole proteome: the conserved WD40 domain protein POC1 is required for centriole duplication and length control. *Mol Biol Cell* **20**, 1150–1166 (2009).
138. Keller, L. C., Romijn, E. P., Zamora, I., Yates, J. R. & Marshall, W. F. Proteomic analysis of isolated chlamydomonas centrioles reveals orthologs of ciliary-disease genes. *Curr Biol* **15**, 1090–1098 (2005).
139. Kilburn, C. L. *et al.* New Tetrahymena basal body protein components identify basal body domain structure. *Journal of Cell Biology* **178**, 905–912 (2007).
140. Ruehle, M. D., Li, S., Agard, D. A. & Pearson, C. G. Poc1 bridges basal body inner junctions to promote triplet microtubule integrity and connections. *J Cell Biol* **223**, e202311104 (2024).
141. Junker, A. D. *et al.* Basal bodies bend in response to ciliary forces. *Mol Biol Cell* **33**, ar146 (2022).
142. Bayless, B. A. *et al.* Asymmetrically localized proteins stabilize basal bodies against ciliary beating forces. *Journal of Cell Biology* **215**, 457–466 (2016).
143. Min Ko, J. *et al.* SOFT syndrome caused by compound heterozygous mutations of POC1A and its skeletal manifestation. *Journal of Human Genetics 2016 61:6* **61**, 561–564 (2016).
144. Roosing, S. *et al.* Disruption of the basal body protein POC1B results in autosomal-recessive cone-rod dystrophy. *Am J Hum Genet* **95**, 131–142 (2014).
145. Gu, C., Li, J., Zhu, L., Lu, Z. & Huang, H. Analysis of catechol-O-methyltransferase gene mutation and identification of new pathogenic gene for paroxysmal kinesigenic dyskinesia. *Neurological Sciences* **37**, 377–383 (2016).
146. Jin, X. *et al.* Novel compound heterozygous mutation in the POC1B gene underlie peripheral cone dystrophy in a Chinese family. *Ophthalmic Genet* **39**, 300–306 (2018).
147. Yanık, Ö., Batıoğlu, F., Sahin, Y., Demirel, S. & Özmert, E. Seroreactivity against retinal proteins in a case of POC1B gene associated cone dystrophy with normal funduscopic appearance: a systematic approach to diagnosis. *Ophthalmic Genet* **44**, 389–395 (2023).
148. Kameya, S. *et al.* Phenotypical Characteristics of POC1B-Associated Retinopathy in Japanese Cohort: Cone Dystrophy With Normal Funduscopic Appearance. *Invest Ophthalmol Vis Sci* **60**, 3432–3446 (2019).
149. Saida, K. *et al.* SOFT syndrome in a patient from Chile. *Am J Med Genet A* **179**, 338–340 (2019).
150. Barraza-García, J. *et al.* Two novel POC1A mutations in the primordial dwarfism, SOFT syndrome: Clinical homogeneity but also unreported malformations. *Am J Med Genet A* **170**, 210–216 (2016).

151. Al-Kindi, A. *et al.* A novel POC1A variant in an alternatively spliced exon causes classic SOFT syndrome: clinical presentation of seven patients. *Journal of Human Genetics 2019 65:2* **65**, 193–197 (2019).
152. Shaheen, R. *et al.* POC1A Truncation Mutation Causes a Ciliopathy in Humans Characterized by Primordial Dwarfism. *Am J Hum Genet* **91**, 330 (2012).
153. Koparir, A. *et al.* Novel POC1A mutation in primordial dwarfism reveals new insights for centriole biogenesis. *Hum Mol Genet* **24**, 5378–5387 (2015).
154. LI, S., ZHONG, Y., YANG, Y., HE, S. & HE, W. Further phenotypic features and two novel POC1A variants in a patient with SOFT syndrome: A case report. *Mol Med Rep* **24**, 494 (2021).
155. Sarig, O. *et al.* Short stature, onychodysplasia, facial dysmorphism, and hypotrichosis syndrome is caused by a POC1A mutation. *Am J Hum Genet* **91**, 337–342 (2012).
156. Bazzi, H. & Anderson, K. V. Acentriolar mitosis activates a p53-dependent apoptosis pathway in the mouse embryo. *Proc Natl Acad Sci U S A* **111**, E1491 (2014).
157. Izquierdo, D., Wang, W. J., Uryu, K. & Tsou, M. F. B. Stabilization of Cartwheel-less Centrioles for Duplication Requires CEP295-Mediated Centriole-to-Centrosome Conversion. *Cell Rep* **8**, 957–965 (2014).
158. Laporte, M. H. *et al.* Human SFI1 and Centrin form a complex critical for centriole architecture and ciliogenesis . *EMBO J* **41**, (2022).
159. Schweizer, N. *et al.* Sub-centrosomal mapping identifies augmin-γTuRC as part of a centriole-stabilizing scaffold. *Nature Communications 2021 12:1* **12**, 1–16 (2021).
160. Izquierdo, D., Wang, W. J., Uryu, K. & Tsou, M. F. B. Stabilization of cartwheel-less centrioles for duplication requires CEP295-mediated centriole to centrosome conversion. *Cell Rep* **8**, 957 (2014).
161. CU, S., E, P., RB, R. & CW, M. WD40 proteins propel cellular networks. *Trends Biochem Sci* **35**, 531–538 (2010).
162. Xu, C. & Min, J. Structure and function of WD40 domain proteins. *Protein Cell* **2**, 202–214 (2011).
163. Hames, R. S. *et al.* Pix1 and Pix2 are novel WD40 microtubule-associated proteins that colocalize with mitochondria in Xenopus germ plasm and centrosomes in human cells. *Exp Cell Res* **314**, 574–589 (2008).
164. Venoux, M. *et al.* Poc1A and Poc1B act together in human cells to ensure centriole integrity. *J Cell Sci* **126**, 163–175 (2013).
165. Brito, D. A., Gouveia, S. M. & Bettencourt-Dias, M. Deconstructing the centriole: structure and number control. *Curr Opin Cell Biol* **24**, 4–13 (2012).
166. Kraatz, S. *et al.* The Human Centriolar Protein CEP135 Contains a Two-Stranded Coiled-Coil Domain Critical for Microtubule Binding. *Structure* **24**, 1358–1371 (2016).
167. Chang, C. W., Hsu, W. Bin, Tsai, J. J., Tang, C. J. C. & Tang, T. K. CEP295 interacts with microtubules and is required for centriole elongation. *J Cell Sci* **129**, 2501 (2016).
168. Turk, E. *et al.* Zeta-Tubulin Is a Member of a Conserved Tubulin Module and Is a Component of the Centriolar Basal Foot in Multiciliated Cells. *Current Biology* **25**, 2177–2183 (2015).
169. Li, S. *et al.* Structural role of Sfi1p–centrin filaments in budding yeast spindle pole body duplication. *J Cell Biol* **173**, 867 (2006).
170. Bouhouche, K. *et al.* Paramecium, a Model to Study Ciliary Beating and Ciliogenesis: Insights From Cutting-Edge Approaches. *Front Cell Dev Biol* **10**, 847908 (2022).
171. Heydeck, W. *et al.* Tetrahymena Poc5 is a transient basal body component that is important for basal body maturation. *J Cell Sci* **133**, jcs240838 (2020).

Publication during PhD

Research paper:

Sala, C., Würtz, M., Atorino, E.S. *et al.* An interaction network of inner centriole proteins organised by POC1A-POC1B heterodimer crosslinks ensures centriolar integrity. *Nat Commun* 15, 9857 (2024). https://doi.org/10.1038/s41467-024-54247-5

Acknowledgements

It´s been one hell of a ride this PhD, but I wouldn´t miss any moment of it.

I want to express my gratitude to Prof. Dr. Elmar Schiebel for giving me the opportunity to do my PhD in his lab and for his strong passion and great discussions during all these years.
Thank you, Elmar!

I would particularly like to thank Prof. Dr. Sylvia Erhardt, Dr. Anne-Lore Schlaitz and Dr. Ralph Grand for taking their time to be part of my thesis committee. My special thanks go to Dr. Gislene Pereira (and also Prof. Dr. Sylvia Erhardt) for their support and valuable input during my TAC meetings.

Many thanks to Dr. Sebastian Eustermann and Dr. Thomas Hoffmann from the EMBL for their great collaboration during our publication.

I want to thank with all of my heart the former and present members of the Schiebel Lab. Moving to another place and starting a new job in a new environment during corona crisis was hard, but you made me feel welcomed.
Thank you so much Azqa, Jlenia, Enrico, Onur, Martin and Patrick!

Spending a lot of time in the lab forms a bond that people outside science might not understand. With this I want to thank Laura Theile who not only supported me as a great colleague, but also as a great friend during the up´s and down´s of the crazy everyday lab life. In addition, I want to thank Aadyasha Mishra and Dilara Erdogdu for keeping up with me during the end phase of my PhD. I am lucky to have you as my dear friends.

Last but not least, I want to thank my family and my beloved ones.
Kilometers and sometimes even countries separate us, but you still managed to support me during these hard times with your love and trust in me.
Without you, I would not stand where I am now.
I love you.